Understanding Endothelial Cell Behaviors During Sprouting Angiogenesis

Part I

Endothelial cell division in angiogenic sprouts of differing cellular architecture

Part II

Characterizing the vascular lumen invagination process: Vesicle/membrane trafficking & subcellular events in sprouting angiogenesis

Inauguraldissertation

zur

Erlangung der Würde eines Doktors der Philosophie

vorgelegt der

Philosophisch-Naturwissenschaftlichen Fakultät

der Universität Basel

von

Vahap Aydogan

aus Malatya, Turkei

Basel, 2017

Genehmigt von der Philosophisch-Naturwissenschaftlichen Fakultät auf Antrag von

Prof. Dr. Markus Affolter

Prof. Dr. Anna Jazwinska

Basel, den 13. December 2016

Prof. Dr. Jörg Schibler
Dekan der Philosophisch-Naturwissenschaftliche Fakultät

Acknowledgments

First of all, I would like to thank Prof. Markus Affolter for giving me the opportunity to do my PhD in his lab in last 4 years. When I applied for the PhD fellowship at the Biozentrum, initially I did not plan to do a rotation in Affolter lab. However, I am very glad to meet with him during an interview week and asked to do the first rotation in his lab. After a second rotation, my final decision was to continue in Affolter lab. It turned out to be the most fruitful experience, giving me freedom to self explore in research, with extremely supportive and endless enthusiasm. He always supported me to attend many conferences and meetings in last 4 years. Furthermore, he is very good at simplifying scientific concepts and seeing the big picture. He can easily have an overall view on research projects, which is fascinating to zoom out and see the whole picture as well as going very deep. I am very much appreciated with all discussions and for all his advice and inspiration, strongly impacting my development as a scientist. I will always be grateful for his infallible support for critical discussions and helpful suggestions about my projects.

Another great source of support at the beginning of my PhD was Dr. Anna Lenard. She trained me for the most of the experimental parts. She was very passionate to my endless questions and I appreciated very much with many lively discussions, which helped me to shape my understanding in vascular development. At this point I also want to thank Henry Belting who shared his experience and contributed on interesting discussions.

I also want to thank Prof. Anna Jazwinska and Prof. Claudia Lengerke for volunteering to join my thesis committee and for all their inputs on my

projects.

I would like to thank all members of the Affolter lab for their encouragement, support, and help during my PhD especially, fish club: Etienne, Charles, Niels, Cora and Minkyoung for their support, and discussions and for a great lab atmosphere. Moreover, thanks to Dr. Loic Sauter for many discussions about experiments and his kind help, always being there to help. Additionally, I want to thank; Mario, Dimi, Shinya, Ilaria, Stefan who have provided incredible support and friendship throughout my graduate.

The Affolter Lab is fortunate to have the incredible Helen as our administrative, and I am quite respectful in all her work. She is always there when you need a help and many thanks for being such a great person. Special thanks to Angie Klarer for support and kind helps.

Most importantly, I need to thank my family: my parents, who taught me that I have the ability to do anything and who have always believed in me. Thanks to my girlfriend, Natalia, who was passionate and supportive along my work, giving me extremely valuable support in my difficult times and for sharing so many aspects of our lives, being my dearest friend.

I would like to dedicate this work to my grandparents, **Güllü** and **Ismail,** who gave me the great vision about importance of education and science.

“There is no science which does not spring from pre-existing knowledge.” William Harvey.

Summary

Here in the first part of this Thesis, I investigated endothelial cell division in differing vascular architecture during sprouting angiogenesis in zebrafish.

The vasculature of the zebrafish trunk is composed of tubes with different cellular architectures. Unicellular tubes form their lumen through membrane invagination and transcellular cell hollowing, whereas multicellular vessels become lumenized through a cord hollowing process. Endothelial cell proliferation is essential for the subsequent growth and maturation of the blood vessels. However, how cell division, lumen formation and cell rearrangement are coordinated during angiogenic sprouting has so far not been investigated at a detailed cellular level. We have analyzed and described the sequential steps of cell division (mitotic rounding, cytokinesis, actin re-distribution and adherence junction formation) in branches of differing cellular architectures during sprouting angiogenesis. In particular, we characterized mitosis and lumen dynamics within unicellular and multicellular tubes. Unicellular tubes constrict the lumen prior to mitosis and ultimately displace it from the division plane during mitosis, at which site a de-novo junction forms by the recruitment of junctional proteins at the division plane right after abscission. In contrast, the lumen of multicellular tubes remains intact throughout the cell division process and new junctions form from pre-existing junctions. Our findings illustrate that during the course of normal development, multiple tube architectures can accommodate the cell division machinery, thereby avoiding disruptions of the vascular network.

In the second part of this Thesis, I investigated the lumen invagination including the aspects of endosomal trafficking, as well as the distribution of cytoskeleton and subcellular organelles (e.g. golgi) during endothelial cell behavior changes.

During development, vascular networks form via vasculogenesis at early stages, followed by angiogenesis at later stages, a process in which new vessels grow from pre-existing vessels through coordinated cell division, migration, and cell rearrangements and eventually each sprout connects one with another to form vascular loops. The functionality of connected vascular networks depends on opening of luminal spaces allowing fluid flow. However, how vascular tubes establish continuous lumens within branches of endothelial cells *in vivo* to meet local metabolic needs remain obscure. In this study, we used a transgenic zebrafish line expressing the membrane marker CAAX-mCherry, to image apical membrane compartment with high spatial and temporal resolution. Our approach allows visualizing both the endothelial cell membrane and the apical lumen within the endothelial cells. Here we show that some vesicle-like structures, labeled with CAAX-mCherry, form and move in the cytoplasm and eventually dissolve on/fuse with the growing apical membrane. Based on these observations, our hypothesis is that the vesicular/membrane trafficking contributes to apical luminal membrane invagination. To investigate this phenomenon in more detail, we currently characterized localization and dynamics of Rab5c-early, Rab7-late, and Rab11a-recycling endosomal pathways during lumen invagination in sprouting angiogenesis. In addition, we also visualized the dynamics of the cytoskeleton (microtubules and actin) and the Golgi apparatus, which are linked to vesicle trafficking.

Contents

List of Figures

List of Movies

Movie S1

Movie S2

Movie S3

Movie S4

Movie S5

Movie S6

Movie S7

Movie S8

Movie S9

Movie S10

1 General Introduction

1.1 Cardiovascular system: research history and evolution

1.1.1 Circulatory system research throughout history

The circulatory or vascular system has fascinated many philosophers and researchers. Based on observations from animals and humans, a vast amount of knowledge has been acquired during the past centuries. Even though some of the early hypotheses have been disproved, it is interesting to have an overview over the origins of this field of research. The earliest writings about the circulatory system date back to the Ebers Papyrus, from the 16th century BC Egypt. The early Egyptians thought that air came in through the mouth and was distributed into the lungs and heart. They believed that from the heart, the air is delivered through the body by the arteries. In India during the 6th century BC, there was a notion of the circulation of vital fluids through the body however, there was no real proof of this concept. During the 4th century BC, Hippocrates discovered the valves of the heart without knowing their function. During this period, it was possible to examine and experiment on human cadavers. After death, blood accumulates in veins and arteries look empty. This observation led to the claim that arteries are filled with air instead of blood. At 335-280 BC, Herophilos, an anatomist, distinguished veins from arteries by pulse activity and claimed that pulse is the only property of arteries. He examined the human body for anatomical research, which had been banned a long time and then geared up with Leonardo Da Vinci later on in the 16th century. At 304-250 BC, Erasistratus

cut arteries on living bodies, and showed that air escapes from the arteries and is replaced by blood. Erasistratus was the first who described the circulatory system as an open system where arteries and veins are separate; the veins carrying blood, and arteries carrying air (Figure 1 (A)). He described that the digested food from the intestine was taken up by portal veins and transported to the liver where it was then transformed into blood, which was further delivered through the right ventricle (heart) by veins and then reaches pulmonary artery to feed the lungs. The air is taken up by the pulmonary arteries and then delivered to the left ventricle (heart) and is eventually distributed to the tissues by the arteries. The waste is removed through the pulmonary vein by retrograde flow (Aird, 2011).

During 2-3th century AD, Galen showed that arteries carry blood but not air. He claimed that arterial blood is derived from venous blood passing through invisible pores in the interventricular septum (interface of right-left ventricles in heart) (Figure 1 (B)). During 11th century AD, Avicenna provided first correct explanation of pulsation as 2 movements and 2 pauses: expansion-pause-contraction-pause. He explained the pulse occurs as a movement in the heart and arteries. At 13th century AD Ibn al-Nafis was the first person to accurately describe the process of pulmonary circulation. In addition, he stated that "it has to be some small pores or communications between the pulmonary artery and vein" and developed a theory of capillary circulation, which took another 400 years to confirm. In the early 16th century, Andreas Vesalius- an anatomist- was convinced that the porous interventricular septum theory from Galen was wrong based on his experimental observations. He believed that the cardiac systole synchronize with the arterial pulse. In addition, he also proved the presence of valves in

the veins and discovered the canal that goes into the fetus between the umbilical vein and vena cava. Later in the 16th century AD, Realdo Colombo described the pulmonary circuit, in which venous blood in the right ventricle passes through the lung and reaches the left ventricle in the heart and then the arteries. Until then, it was believed that blood flow in veins is centrifugal, meaning that blood goes away from liver towards other tissues. Colombo described a hybrid system; the pulmonary circuit represents the closed system and the open system represents blood flow from liver towards all tissues (Figure 1 (C)). At 16-17th century AD, Harvey discovered that blood circulates through the whole body (Figure 1 (D)), demonstrating direct connections between venous and arterial system throughout the body, not limited to the lungs. He also confirmed the presence of valves in the veins. The system was driven by the mechanical power of the heart; meaning that the heartbeat induces a continuous circulation. The blood transfer from arteries to the veins in the lung and periphery was shown by direct connections or anastomoses, but it was not yet known what these direct connections were. In 1661, 30 years after Harvey, Marcello Malpighi discovered the capillary system, which connects arteries with veins.

After all these centuries of research and development, we have gained a general understanding about the circulatory system. People had the common interest of observing curiosity and a search for the truth. They believed in the value of dissection and comparison of anatomy. The complexity of the circulatory system was explained with teleological causes in the early BC and towards the 19th century there was a demand of challenging dogma and authorities and more scientific explanations such as experimental reproducibility and quantification. However, there was little access to a

technology for example, microscopy was discovered in 17th century. In the present, we are in a more advance technological century with diverse research areas including molecular biology, genetics and biochemistry. However, we are still only at the beginning of understanding the mechanisms which drive the development of the vascular system (Aird, 2011). To obtain a cellular and molecular level understanding of the circulatory system, we have to keep developing new techniques and tools.

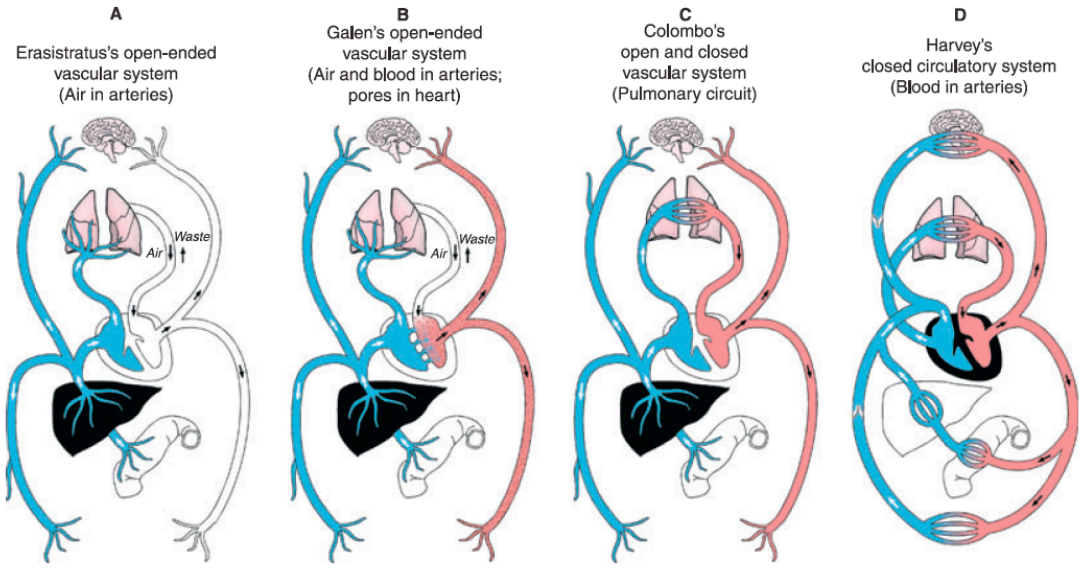

Figure 1: Demonstration of circulatory system throughout history.
(A) Erasistratus reported that arteries carry air (white color) and veins carry blood (blue color) and they are separate. Food was absorbed in intestine and transferred by portal veins to liver (black color), transformed into blood. (B) Galen reported that arteries carry blood (red color), not air. Arterial blood was derived from invisible pores in the interventricular septum. (C) Colombo reported pulmonary system in which venous blood in right ventricle passes through lungs and then reach left ventricle and arteries. (D) Harvey reported that blood circulates in whole body not only in lungs. Liver is not the source of veins anymore. The system is mechanically driven by heart-beat. Transfer of blood from arteries to veins occurs via direct connections, which was shown by Marcello Malpighi (Aird, 2011).

1.1.2 Evolutionary perspective on endothelium: the origin, the need and the diversity

First evidence of a prokaryotic life dates back 3.7 billion years and the first eukaryotic cells evolved 1.5 billion years ago. It took roughly 1 billion years for the first multicellular organism to appear.

All living organism evolved to survive, reproduce and grow. When a three dimensional (3D) body enlarges, surface area increases in proportion to radius squared (r^2), whereas volume develops more rapid by (r^3). Cells at the growing body need to proportionate its surface with volume. For example, early triplobastic animals- having a blastula stage with three layers; ectoderm, endoderm and mesoderm- such as flatworms, distribute their metabolites by diffusion, a movement from high to low concentration, which is energy-efficient but only effective at short distances (< 1mm). However, at some point, further growth leads to a disproportionate surface-to-volume ratio and more advanced strategies such as an internal exchange and transport system became necessary. Some indications suggest that the circulatory system (blood vascular system) first appeared in ancestor of the triploblasts over 600 million years ago. To overcome time-distance constraints of diffusion, optimize flow dynamics, deliver metabolites and immune cells through long distances, the endothelium, a layer of cells that line the interior surface of blood and lymphatic vessels, evolved in an ancestral vertebrate 540-510 million years ago (Monahan-Earley et al., 2013).

1.1.3 Endothelium acquirement: a transition from invertebrate to vertebrate

Throughout evolution, many drastic changes have occurred during the transition from invertebrate to vertebrate. One of the most important changes is the gain of the endothelium in vertebrates, which bring several advantages to vertebrates. First of all, it is important for immunological defense. The endothelium cooperates in the defensive task by exposing surface molecules or receptors in an inflammation area, which are then recognized by immune cells. This way, endothelial cells rapidly and precisely guide immune cells to the infection area. A second advantage is the regulation of blood flow. In invertebrates, regulation of flow is controlled by contraction and relaxation of the myoepithelial cells under neuoregenic stimuli (Shigei et al., 2001). Similarly, vertebrate blood flow is controlled by an interplay between smooth muscle cells, where endothelial cells produce nitric oxide to tightly regulate the local blood flow. The third advantage is angiogenesis, which is a process of new blood vessel formation. With this ability, the endothelium can invade tissues and control vascularization of embryonic areas such as head, tail, limbs, and other areas dynamically (Muñoz-Chápuli et al., 2005). As a summary, the gain of an endothelium provided many advantages in vertebrates including immunological defense, blood flow regulation and angiogenesis.

In the context of this thesis, the angiogenesis process is the most important and will be further described in the following chapters.

1.2 The cardiovascular system: development and associated diseases

1.2.1 Development of the vascular system

In all vertebrate species, the cardiovascular system is the first functional complex organ emerging in developing embryos and consists of four major components: heart, arteries, veins and blood. It provides tissues with nutrients, hormones, metabolites, gas-exchange, and removes waste products. During development, all organs need to form and connect to a proper vascular network as they form and grow. Endothelial cells (ECs), like many of our internal organs, derived from mesodermal progenitors and are the building blocks of the vasculature and their task is to form tubular structures surrounding a luminal space. Therefore it is critical for ECs to form and maintain the continuous hollow tubes (Risau and Flamme, 1995; Xu and Cleaver, 2011).

ECs line the interior surface of arteries and veins, which are additionally surrounded by smooth muscle cells, derived from mesoderm progenitors, as an elastic tissue and an additional layer of fibrous connective tissue. Depending on the size of vessels, muscle layer thickness can change to deal with blood pressure. In addition, larger veins contain valves, which are the specialized structures helping uni-directional blood transport towards the heart (reviewed in Torres-Vázquez et al., 2003).

The heartbeat induces the circulation of blood within the vessels. Blood flows through large arteries towards to smaller arterioles and eventually arrives at the capillaries, which infiltrate the tissues and where they are

involved in metabolite and gas exchange. Later, circulating blood returns back to the heart via venules and veins and finally reaches as the lungs, where the blood is replenished with oxygen (reviewed in: Adams and Alitalo, 2007; Carmeliet, 2005; Risau and Flamme, 1995).

Despite the variations in detailed blood vessel anatomy, the main vascular developmental plan is conserved among vertebrates. For example, similar cellular and molecular mechanisms play a role to build a blood vessel network.

During vascular network formation, ECs have to be able to execute many cellular activities such as cell migration, cell division, cell-cell contact formation (anastomosis), cellular re-arrangements and lumen formation in order to form a complete circulatory system (Herwig et al., 2011; Lenard et al., 2013). Therefore, it is critical to orchestrate cellular and molecular events to form intact vascular system.

1.2.2 Vascular development in disease

The circulation of blood via vascular system is vital to deliver oxygen and nutrients to each cell in our body. Homeostasis of such system has a fundamental role on health. After the circulatory system has been established, endothelial cells enter a quiescent phase. Intrinsic factors (e.g. genes) and extrinsic factors (e.g. microenvironment signaling) can induce a transition from quiescent state to the active state or vice versa. The balance and coordination between the intrinsic and the extrinsic factors provides a homeostasis in the vascular system and is involved in the control of the

location and degree of vascularization. Therefore, this balance is very critical to maintain the normal function of the vasculature. If the balance is broken, then the resulting vasculature can be either insufficient or extensive. Diabetes, multiple sclerosis, inflammation and cancer are diseases linked to extensive angiogenesis. Furthermore, many diseases occur due to inappropriate function of heart, vessels (arteries and veins) and fluid. Diseases such as coronary artery disease, atherosclerosis, stroke, hypertension, heart failure, cardiomyopathy, vasculitis are prominent examples. To understand the underlying mechanisms of how diseases affect the circulatory system is crucial to fight those diseases (Carmeliet, 2005; Potente et al., 2011).

In order to treat diseases, many drugs are developed based on the understanding of the cellular and molecular processes of the vasculature. However, most of the angiogenesis inhibitor drugs in cancer have not been successful individually, suggesting that our current understanding is still incomplete. Therefore, basic research has a fundamental role to provide know-how and deep understanding of vascular system principles, which can be used to develop better drugs and therapies. For this, we use zebrafish as a model organism to study vascular development.

1.3 Vascular development in zebrafish

1.3.1 Zebrafish

To study vascular development *in vivo*, model organisms such as quail, mouse, chicken, frog, and zebrafish are indispensible. Although the final vascular anatomy differs greatly between species, most cellular and molecular mechanisms involved in vascular development are similar between zebrafish and other vertebrates, including mammals (Howe et al., 2013). The zebrafish (*Danio rerio*) is a tropical freshwater fish, native to the region in India and Southeast Asia. Adult zebrafish size is 4-5 cm and their live span is 2-3 years (Gerhard et al., 2002). Female adult fish (> 3 months) can lay eggs every week, around 100 eggs at a time. Within 10-15 minutes, the laid eggs are fertilized externally when male fish spawn their sperm on eggs. After the fertilization, the first cell division starts in 45 minutes and following cell divisions occur in a synchronous manner in a shorter time (Kimmel et al., 2005).

Among the mentioned species, we use zebrafish as a model organism to study angiogenesis. Zebrafish is one of the most promising model organisms for the study of cardiovascular development for the following reasons: the embryos are transparent throughout their early development and develop externally, fish are easy to breed, and transgenic lines are available (e.g fli:EGFP), which enable us to visualize cellular and subcellular events dynamically during vascular development (Figure 2). The vasculature develops early in the embryo and at 24 hpf (hours post fertilization), heart-beat already starts and the blood cells can be seen traveling along the arteria and veins. Transparency of the vascular system and availability of transgenic zebrafish lines allow us to use high-resolution live imaging tools to observe

the entire process of vascular development, including angiogenesis (Lawson and Weinstein, 2002a).

In the recent years a considerable variety of genetic tools, indispensable for functional analyses, are getting more and more established for the fish. For example, the novel CRISPR/Cas9 system is being used for genetic modifications in zebrafish (Cong et al., 2013; Hwang et al., 2013; Wang et al., 2013). However, genome duplication in zebrafish (all teleost fish have a duplicated genome) creates additional complexity for functional studies. Additionally zebrafish embryos are suitable for large-scale drug screening (Parng et al., 2002). All those advantages make zebrafish an outstanding model organism to study vascular development.

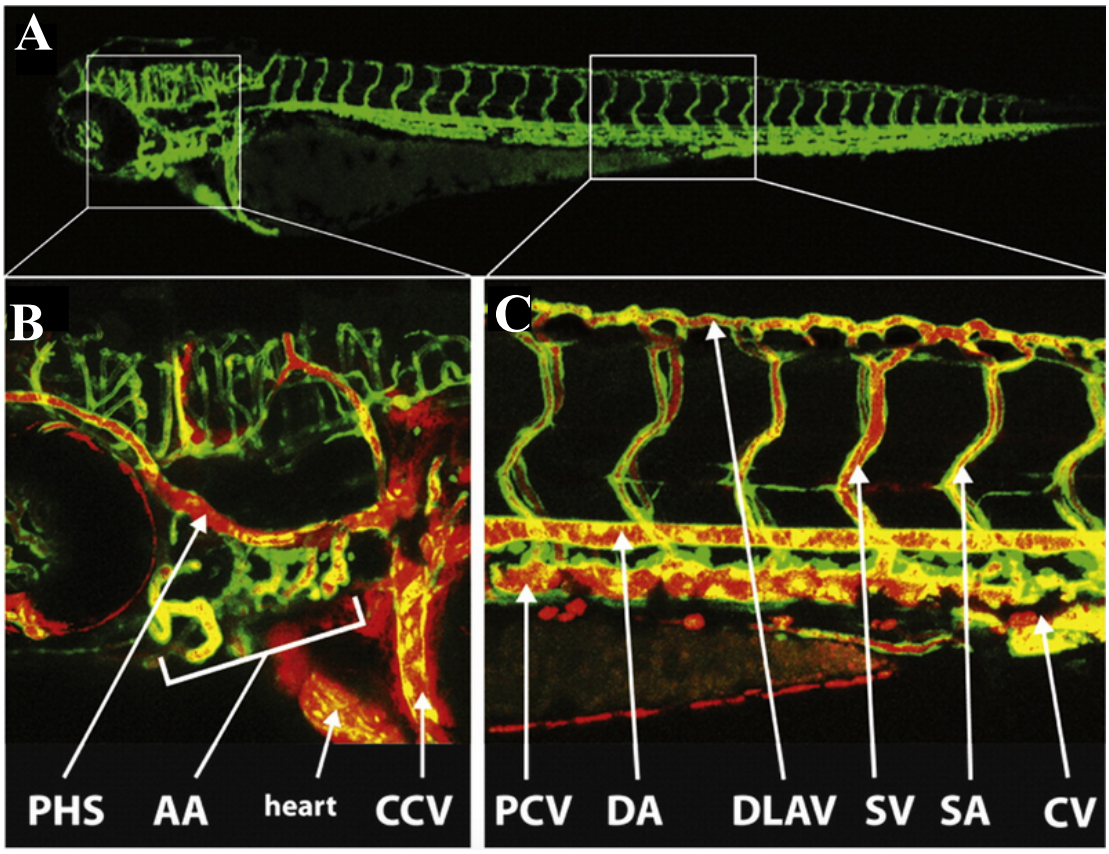

Figure 2: Zebrafish vascular network formation (~3 day embryo).
(A) Image shows the zebrafish blood vessel network formation visualized by *flk1*:EGFP (green) and (B-C) blood visualized by microangiography injecting quantum dots (red).
PHS: primary head sinus; AA: aortic arches; CCV: common cardinal vein.
PCV: posterior cardinal vein; DA: dorsal aorta; DLAV: dorsal longitudinal anastomotic vessel; SV segmental vein; SA: segmental artery; CV: caudal vein (Ellertsdottir et al., 2010). At these stages, we focus on SA and DLAV in our experiments.

1.3.2 Vascular network formation

Two distinct mechanisms, vasculogenesis and angiogenesis, contribute to blood vessel formation in zebrafish embryos. Two main vessels in the trunk, the dorsal aorta (DA) and the posterior cardinal vein (PCV), develop along the anterior- posterior axis through assembly of mesoderm-derived angioblasts in a guided manner (Figure 3 (A)). This process is also known as vasculogenesis, the *de novo* formation of blood vessels (Poole and Coffin, 1989).

During angiogenesis, new vessels sprout from pre-existing ones and eventually these sprouts fuse with each other to form new vascular loops. Sprouting vessels are made up of two distinct cell populations: tip cells and stalk cells (Figure 3 (B)). Tip cells are leading and guiding the sprout. The following stalk cells provide the connection between the tip cell and the parental vessel (reviewed in Siekmann et al., 2013). In the embryo trunk, new sprouts emerge from the dorsal aorta (DA) at ~22 hpf (hours post fertilization) and form intersegmental vessels (ISVs). Eventually, these sprouts fuse to each other to form the dorsal longitudinal anastomotic vessel (DLAV). At ~32 hpf, secondary sprouts emerge from the PCV. They

connect to the nearest primary segmental artery (SA) and transform it into a segmental vein (SV), which allows the formation of a closed blood circuit (Ellertsdottir et al., 2010; Isogai et al., 2001)

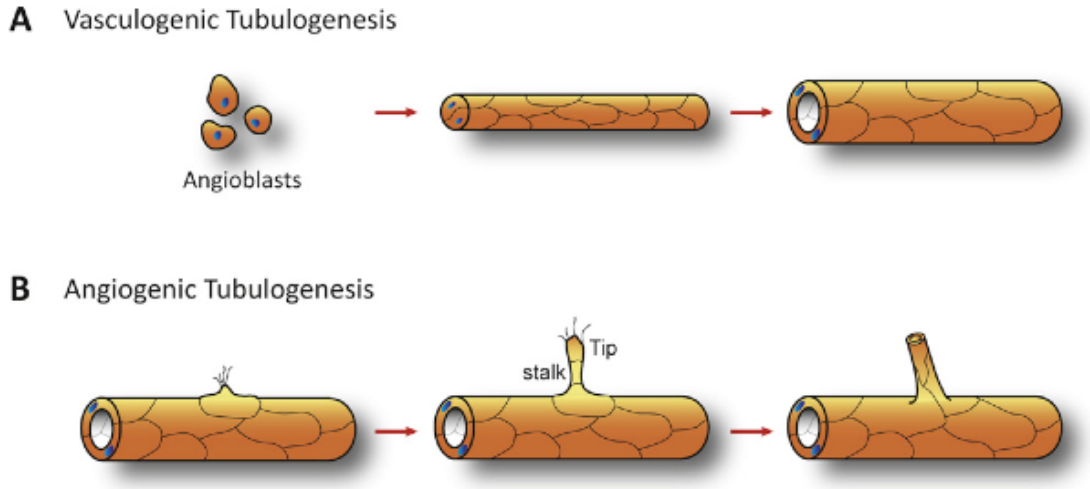

Figure 3: Vasculogenesis and angiogenesis
(**A**) Angioblast cells (> 1000 cells) come together in a guided manner and form a *de novo* vascular tube, which is known as vasculogenesis. (**B**) A sprout comes out from the pre-existing vessel to form a new vessel, which is known as angiogenesis process (Blasky et al., 2015)

1.3.2.1 Vasculogenesis

The cardiovascular system is the first organ system developing in the embryo because of its critical role in nutrient and oxygen delivery. The heart is one of the earliest developing organs. However, it does not start pumping until the first vascular loop has been formed. Da Vinci compared the vascular loop formation in an analogy to a sprouting seed, where the seed represents the heart and the roots are the vessels (Wener Risau, 1997). Now, we know that vascular sprouts form and eventually connect to the heart.

Early stages during development, a primitive network of blood vessel is formed and ramified into arteries, veins and capillaries through the migration and aggregation of mesoderm-derived angioblasts. This *de novo* blood vessel formation process is known as vasculogenesis. The circulatory system is different in their pattern formation from species to species. However, basic principles of mechanisms are commonly shared among vertebrates.

Unlike mammals in which a pair of dorsal aorta (DA) forms during embryogenesis, in zebrafish (Danio rerio) vasculogenesis produces only one DA. During the zebrafish embryonic development at 13 hours post fertilization (hpf), angioblasts come together in two stripes and give raise to dorsal aorta (DA) and posterior cardinal vein (PCV). Mesoderm derived angioblasts migrate towards the embryonic midline and coalesce and form a tube at 17 hpf (Lawson and Weinstein, 2002a). Initial cells give raise to arteria (DA) and shortly afterword, DA sprouts ventrally to form the PCV (Herbert and Stainier, 2011).

It has been identified that signaling pathways influence the formation of DA and PCV extensively. For example, growth factors, secreted by the ventral somites, determine the angioblast fate to give raise to DA. However, in the notochord, sonic hedgehog signaling regulates the secretion of vascular endothelial growth factor A (VEGFA) in the ventral somites. VEGFA signals attract the angioblasts towards the midline and promotes the angioblast arterial determination (Lawson and Weinstein, 2002b; Lawson et al., 2002). Therefore, angioblasts at the dorsal side start expressing the arterial marker EphrinB2a, downstream of Notch signaling. The expression of EphrinB2a represses the venous fates and promotes arterial fates.

However, Ephrin signaling in the ventral region might drive the angioblast sprouting which give rise to the PCV (Ellertsdottir et al., 2010; Herbert et al., 2009).

While vasculogenesis is critical for the early steps in vascular network formation, it is through angiogenesis that the majority of networks grow and adapt to the quickly changing environment of the developing embryo.

1.3.2.2 Angiogenesis

Angiogenesis is a process of new blood vessel formation from pre-existing ones. Eventually, these vessels fuse with one another to form new vascular loops. During angiogenesis, endothelial cells divide, migrate, re-arrange, contact one another, polarize and subsequently lumenize to fulfill their function, the carrying of metabolites in and the removal of waste away from cells. During development, the majority of vessels in a body are formed via the angiogenesis process. Furthermore, angiogenesis is not limited to early development or embryogenesis. It can occur in adults as results of physiological adaption such physical trainings, wound healing after an injury, organ lining regeneration (e.g. in stomach and intestine), menstrual cycle and tumor vascularization. Thus depending on the local needs, the system is flexible and adopts constantly.

There are two types of angiogenesis: sprouting angiogenesis and intussusception. The sprouting angiogenesis will be the main focus of my thesis and explained in more detail in the following paragraph.

1.3.2.2.1 Sprouting angiogenesis

Sprouting, tip cell activation, migration, and proliferation

Sprouting angiogenesis is a multistep branching morphogenesis process and represents the major part of angiogenesis. To start an angiogenic sprout, angiogenic growth factors (e.g. VEGFA) activate receptors on quiescent endothelial cells, which are located on pre-existing vessels. The one that gets the signal and responds quickly goes from a quiescent to an active state (Figure 4 (A)). For example, extending filopodia structure, which facilitates migration towards the source, is a characteristic of such cells called tip cells. The active endothelial cell secretes enzymes to degrade the basal membrane to allow cell migration away from the parental vessels (Figure 4 (B)). In parallel, the active endothelial cells repress neighboring cells via Notch-delta signaling in order not to get activated by angiogenic stimulus (Figure 4 (C)). Sprouting vessels are made up of two distinct cell populations: the first cell that comes out of a parental vessel represents the tip cell and the following cell(s) are stalk cell(s) that provide the connection between the tip cell and the parental vessel (Jakobsson et al., 2010; Siekmann et al., 2013). In the sprout, tip and stalk cells proliferate and migrate towards the source of an angiogenic stimulus, for example VEGF signals, which stimulate sprouting of ECs. It was thought that a single migratory cell at the tip guides the sprout and the stalk cells behind the tip cell, follow it with fixed fates (Gerhardt, 2003). However, during the migration, tip and stalk cell compete for their position and possibly change the leading position based on quick response towards stimulus. Cross-talk between VEGF-A and Notch signaling balance tip and stalk cell formation, revealing dynamic changes in cell behavior rather than fixed fates for endothelial cells (Arima et al., 2011; Jakobsson et

al., 2010). The tip cell experience high VEGF and low Delta4/Notch signaling and, tip cell selection is achieved by Dll4-Notch mediated lateral inhibition. The stalk cell reacts to tip cell DII4 by increasing Notch signaling activity, which downregulates VEGF signaling (Hellström et al., 2007; Siekmann and Lawson, 2007a).

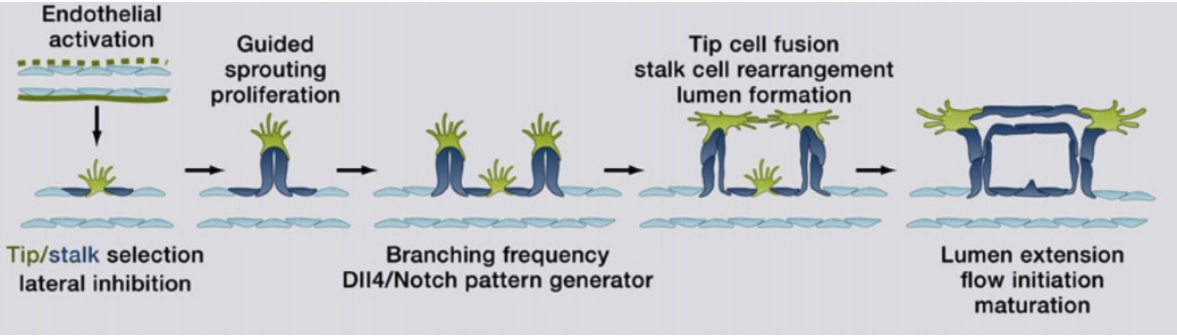

Figure 4: Steps of sprouting angiogenesis
(**A**) tip/stalk cell selection; (**B**) tip cell migration towards VEGF signals and tip and stalk cell division; (**C**) branching coordination; (**D**) stalk cell elongation, tip cell fusion (anastomosis), and lumen formation; and (**E**) perfusion and vessel maturation. (Potente et al., 2011)

Sprouts expand towards the source of the angiogenic stimulus as the lumen formation within the vessels takes place continuously. During the sprouting, vessel architecture is not homogenous and changes dynamically. Therefore, we describe the vascular architecture as unicellular and multicellular tube, based on junctional positioning. At the earlier stages of the sprouting process, in many cases the lumen goes through a single cell and junctions are not continuous, and cell-cell contacts are far from each other. This type of vessel is named a unicellular tube (Figure 5 (A)). However, in later stage of angiogenesis, sprouts consist of multiple cells with continuous junctions

along the cell-cell contact sides and lumen goes between the cells. Such a vessels is referred to as a multicellular tube (Figure 5 (B)).

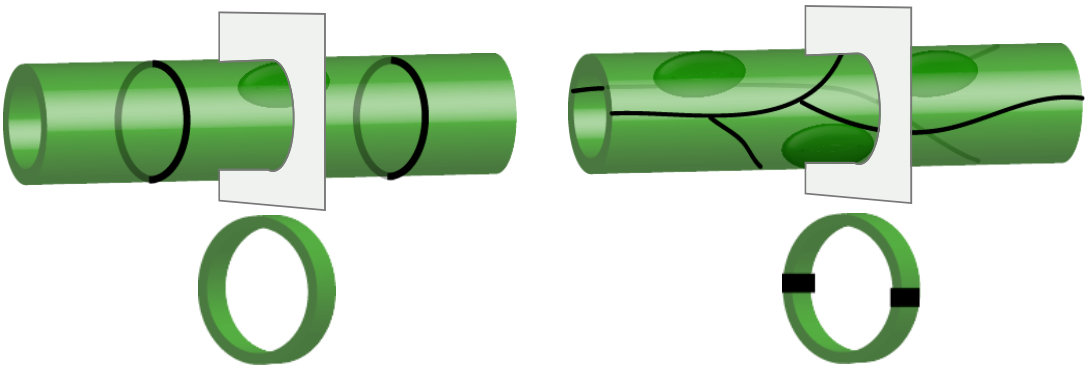

Figure 5: Unicellular and multicellular tube
(**A**) Unicellular tube: lumen goes trough a single cell and there are no continuous junctions (right). (**B**) Multicellular tube: lumen goes between multiple cells and there are continuous junctions (left).

Anastomosis and Vascular Polarization

Extending sprouts from parental vessels eventually come together and connect to one another, a process known as anastomosis or vessel fusion, in which sprouts form loops to become fully functional, lumenized vessel (Figure 4 (D-E)). As sprouting angiogenesis takes place, collectively migrating tip and stalk cells move towards each other in dorsal side and eventually tip cells contact with one another. Two cells make first contact with filopodial structures and deposit their adherens junctions at the contact sites. When two ECs make a first contact via filopodia, they deposit junctional materials at the contact side (Figure 6 (A)). Junctions are dispersed and localized in a small contact area at the beginning. Eventually, the junctional contact area enlarges and forms a ring shape. While the ring forms, apical domain material such as podocalyxin, an anti adhesive transmembrane protein, is carried by vesicles and deposited at the junctional

contact. By this way, two endothelial cells form apical compartments at the contact side and apical-basal polarity is established (Figure 6 (B)).

After ECs establish apical domains at the contact sites, they extent the junctional area by crawling over each other. Eventually, circuit loops need to be lumenized in order to complete and become functional to allow blood flow (Figure 6 (C)). Anastomosis is one of the important key steps in order to form circular loops. However, it is not yet understood, what molecules are involved in the regulation of the anastomosis process. How endothelial cells avoid connecting to other cell types and how they make a right cell connection still remain challenging questions.

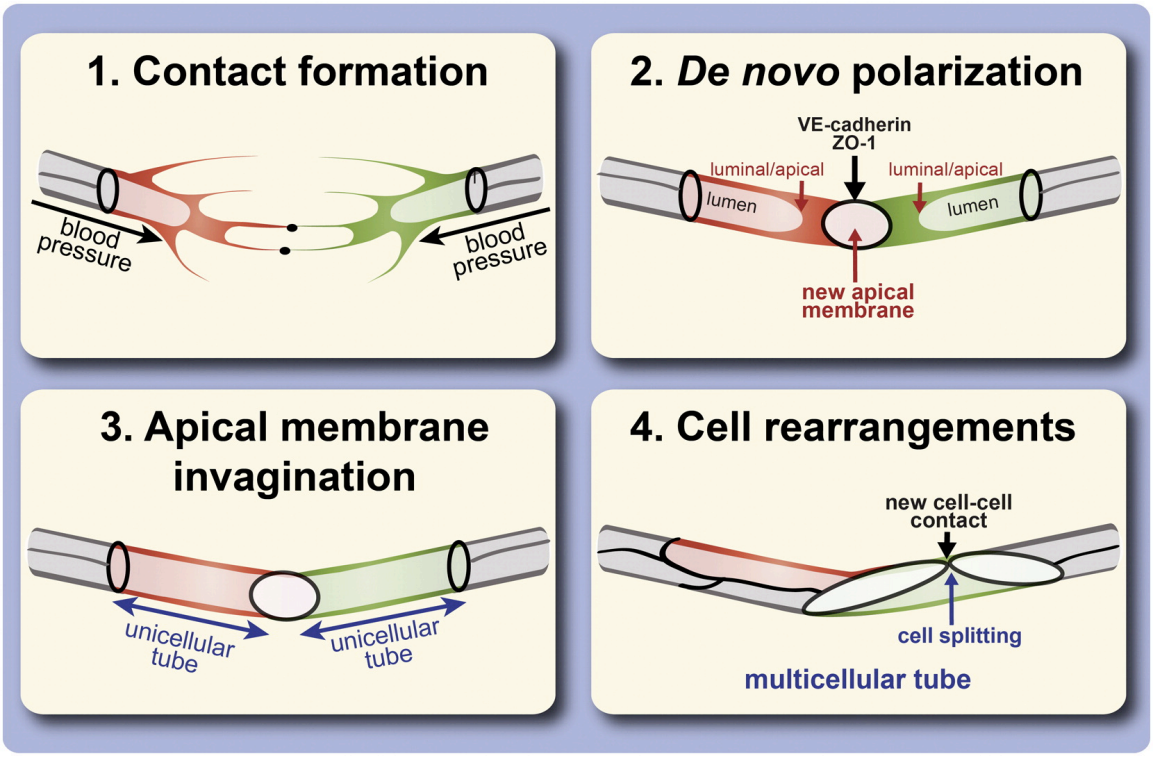

Figure 6: A multistep process in anastomosis
(**1**) Contact formation with filopodia structures. (**2**) *De novo* polarization of newly contacted cells. (**3**) Apical membrane invagination (lumen) in unicellular tubes. (**4**) Cell rearrangements: junctional rearrangements and transformation from unicellular to multicellular tube (Lenard et al., 2013)

1.4 Vascular remodeling

1.4.1 Intussusception

Intussusception angiogenesis is a process in which an existing vessel splits into two by pillar formation. In other words, vessels can sense blood flow changes and react towards those changes. Thereby, vascular tubes undergo rearrangements and split a vessel into smaller diameter vessels. Intussusception does not require cell division or drastic changes in the surrounding tissues, which sets the process apart from sprouting angiogenesis.

1.4.2 Pruning

Pruning is an adaptation process, removing vessels in order to optimize blood flow after functional vascular networks have been established. When there is less or no blood flow, endothelial cells migrate toward adjacent vessels from the pruning vessel to regulate the blood flow dynamics (reviewed in Betz et al., 2016). However, when there is an increased blood pressure, pruning vessel number decreases dramatically, which shows the relationship between blood pressure and pruning activity. VEGF signaling level is also associated with pruning activity. It has been demonstrated that due to hyperoxia (high oxygen), VEGF signaling suppresses pruning activity (Alon et al., 1995).

1.5 Endothelial cell-cell junctions

In order to maintain the integrity of the endothelium, junctional structures play critical roles such as promoting cell-cell adhesion, vascular homeostasis and functioning as signaling structures for cellular activities (reviewed in Dejana, 2004). Similar to epithelial cells, endothelial cells also have two types of junctions; adherens junctions (AJs) and tight junctions (TJs). However, in the endothelium TJs are merged with AJs along the intercellular cleft, rather than being concentrated more in the apical side of the cleft. In addition, the endothelium lacks desmosomes with some exceptions in the lymphatic system and veins, which have desmosomal-like structures, and which are associated with vascular endothelial cadherin (VE-cadherin) (Dejana, 2004; Dejana et al., 1995). Even though AJs and TJs are built from different components, they share the feature of mediating adhesion between cells. AJs, e.g. Cadherins and Catenins, play an important role for cell-cell adhesion. The most important cadherins are, for example, vascular endothelial cadherin (VE-cadherin), N-cadherin, PECAM-1 (platelet/endothelial cell adhesion molecule 1) and VCAM-1 (vascular cell adhesion molecule). TJs are adhesion molecules and Claudins, Occludins and JAMs (e.g. ESAM) are some of the examples. For example, Zona occludens 1 (ZO-1) is an intracellular molecule associated with TJs and localized at the cell-cell contacts (reviewed in Xu and Cleaver, 2011). Overall, in the lab we use VE-cadherin (AJs) and ZO-1 (as TJs) transgenic zebrafish lines to investigate the endothelial cell behaviors during sprouting angiogenesis (Figure 7).

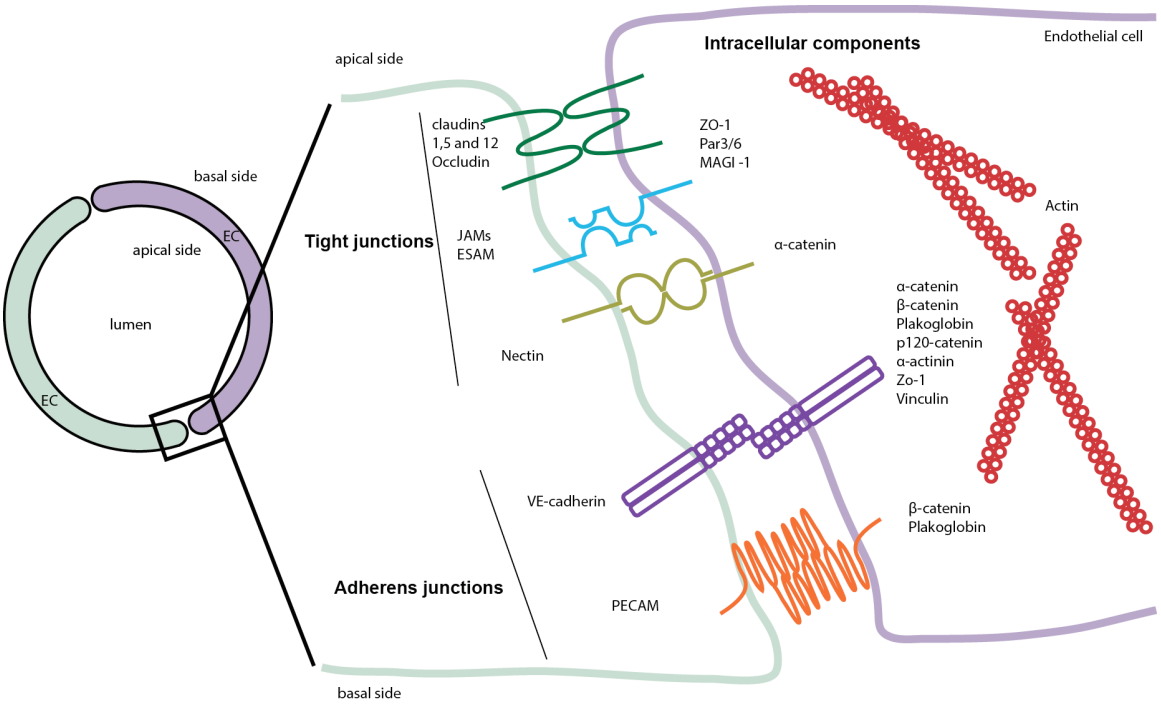

Figure 7: Junctions in endothelial cells
A cross-section of a vascular tube (left) and a magnification of the contact surface between two endothelial cells (right). TJ components were located apically and AJ components were located basolaterally. (Dejana et al., 2004 and PhD Thesis of Loic Sauteur)

In this thesis I want to focus on two projects:

1. Endothelial cell division in a differing vascular architecture, based on unicellular and multicellular patterns in sprouting angiogenesis.
The results of the first project have recently been published; in the first project, I analyzed how endothelial cells divide in differing cellular architectures during sprouting angiogenesis.

2. Lumen invagination process, investigating whether vesicular/membrane trafficking contributes to the formation of the apical membrane compartment in sprouting angiogenesis.
In the second project, an ongoing project, I characterized three distinguished vesicular/membrane trafficking pathways during the lumen invagination in angiogenic sprouts to investigate relationship between lumen growth and endosomal trafficking.

Part I: Endothelial cell division in angiogenic sprouts of differing cellular architecture

2 Introduction

2.1 Endothelial cell division

Cell division has been extensively investigated *in vitro*, and the cellular and molecular mechanisms of the mitotic machinery are well understood. The first step is mitotic rounding, a generic feature of cell division that is driven by changes in the shape and the rigidity of the cell cortex (reviewed in Cadart et al., 2014). It has been shown that this actomyosin-driven process is necessary for the proper assembly, maintenance and orientation of the central spindle (Kunda et al., 2008; Lancaster et al., 2013; Rosenblatt et al., 2004). Spindle orientation subsequently defines the plane of cell division through the accumulation of phosphorylated Myosin II at the plasma membrane, which drives the assembly of a contractile ring (reviewed in Fededa and Gerlich, 2012; Green et al., 2012; Levayer and Lecuit, 2012). The next step is the partitioning into two daughter cells, or cytokinesis, which takes place shortly after chromosome segregation. During cytokinesis, the actomyosin ring contracts and eventually collapses to a small intercellular bridge, the so called midbody. Finally, the severing of the constricted plasma membrane, a process known as abscission, marks the end of mitosis. This generally described process is also valid for ECs.

Within epithelial sheets or tubes, dividing cells maintain the adherens junctions (AJs), which confer tissue integrity (Nakajima et al., 2013; reviewed in Bourdages and Maddox, 2013). However, AJs are extensively reconstructed during mitotic rounding and cytokinesis (reviewed in Harris and Tepass, 2010; Herszterg et al., 2014). The neighboring ECs exert forces on the mitotic cell through cadherin proteins (the core of AJs) that are, in turn, linked to the actomyosin cortex (reviewed in Harris and Tepass, 2010). Morphogenetic movements such as cell intercalation and invagination require a degree of synchronization between junctional re-arrangement and mitosis (Kondo and Hayashi, 2013; reviwed in Levayer and Lecuit, 2012).

Because of their 3-dimensional structure, tubular networks have a more complex morphology than epithelial sheets. Therefore, the division of elongated and lumenized cells may require some adaptations of the mitotic machinery in order to accommodate their peculiar geometry as was recently shown in a study of the *Drosophila* larval trachea system (Denes et al., 2015). While the actomyosin rings that drive cytokinesis in the *Drosophila* epithelia are able to symmetrically deform the AJs of the two cells that flank the emerging junction (Founounou et al., 2013; Guillot and Lecuit, 2013; Herszterg et al., 2013), during cytokinesis in tracheal tubes, the membrane furrows asymmetrically on the side of the cell that is proximal to the nucleus, and the new junction then extends around the lumen until it connects and fuses with another membrane. It has been demonstrated that in the remodeling dorsal tracheal branches, such asymmetric *de novo* junction formation is the norm, presumably because the specific geometry and the rigidity of the tubes favor this outcome (Denes et al., 2015).

The vasculature of the zebrafish trunk consists of segmental arteries (SAs) that branch out of the dorsal aorta (Isogai et al., 2001). A vascular sprout contains several stalk cells and a leading tip cell (Blum et al., 2008a; Siekmann and Lawson, 2007b). SAs are arranged in a metameric pattern and their tip cells eventually contact each other, leading to vessel anastomosis and the formation of the dorsal longitudinal anastomotic vessel (DLAV) (Herwig et al., 2011; Lawson and Weinstein, 2002a). During the formation of the trunk vasculature, approximately from 20 and 50 hpf, the endothelial cells of the SAs and the DLAV undergo extensive proliferation (Blum et al., 2008a; Lawson and Weinstein, 2002a). Therefore, the interplay of the cellular mechanisms of junctional remodeling, lumen formation and EC division can be investigated through live imaging during this time window (Lawson and Weinstein, 2002a; reviewed in Ellertsdottir et al., 2010).

To form a proper vessel morphogenesis, the integration of proliferative and morphogenetic processes is critical (Zeng et al., 2007). However, it has not been investigated in detail how EC division proceeds in a dynamic environment, in which lumen formation and cell rearrangements occur concomitantly and vessel integrity has to be maintained.

2.2 Aim of Endothelial Cell Division Project

Here, we aimed to investigate the interplay between cell division, junctional rearrangement, actin distribution and lumen dynamics during SA morphogenesis in the zebrafish, using an array of fluorescently labeled markers and confocal live imaging. We aimed to demonstrate whether membrane furrowing during cytokinesis differs in unicellular tubes compared to multicellular tubes. In addition, we wanted to find out how ECs in a multicellular DLAV manage cytokinesis, depending on the orientation of the intercellular junctions relative to the plane of division. We also wanted to see that how the lumen of unicellular and multicellular vascular tubes overcome changes in cellular architecture during mitotic rounding and cytokinesis.

3 Materials and Methods

3.1 Preparation of electro-competent *E. coli* bacteria

Solutions:

Luria-Bertani (LB) without salt (10g tryptone, 5g yeast extract add water to 1l (ca. 980ml), autoclave)
10% Glycerol, sterile

Electro-competent cell preparation:

50 ml (LB) w/o salt medium was inoculated with TOP10 bacteria strain (Invitrogen) and incubated overnight at 37°C. As TOP10 has a Streptomycin-resistance cassette, Streptomycin (50 μg/ml) was added to the overnight culture. Next morning, the culture was diluted 1:100 in 1 L of LB w/o salt (without antibiotics) in 2x 3L Erlenmeyer flasks with baffles. Next, the culture was grown to an optical density (OD) of 0.6-0.8 (around 3-4h), and immediately cooled down on 4°C and kept cool from now on. Before use, collection bottles and centrifuge were precooled to 4°C. Then, 1L culture was distributed to 4 collection bottles for the SLA-3000 rotor and centrifuged for 10 min at 3300 rpm (It's normal when the supernatant is still a bit turbid after centrifugation). Next, the supernatant was discarded and each pellet was re-suspended in 5 ml 10% glycerol (sterile, cooled; do not vortex). Next, the suspension was redistributed to 2ml eppendorf tubes and centrifuged at 8000 rpm for 5 min in a cooled bench-top centrifuge. The supernatant was carefully discarded and the pellet was re-suspended in 1 ml

10% glycerol again (now the culture is 100x concentrated). As a last step, the suspension was distributed into 50-75ul aliquots and immediately frozen in liquid nitrogen. The aliquots were stored at -80°C until usage.

3.2 DNA preparation from a single fish

DNA sample was isolated from an adult fish fin. The DNA extraction was performed according to instructions, as described in (Meeker et al., 2007). The fish was anesthetized in 1 x tricaine solution in 1x E3 egg water and was transferred on a sterile plastic dish to cut the tip of the tail by sterilized razor blades (blades were sterilized by ethanol 70 %). The fin tip was transferred in 50 µl of DNA extraction buffer A (alkaline lysis, 50mM NaOH) and incubated at 95°C by shaking at 800rpm for ~ 30 min. After anesthesia, the fish was put in egg water with methylene blue for recovery. To extract DNA after shaking, the sample was put on ice and 5 µl Extraction Buffer B (neutralization, 1M Tris HCl, pH 8) was added, mixed and centrifuged down to the bottom of the tube and kept at -20°C for storage. 1 µl of the sample was used as a template for polymerase chain reaction (PCR).

3.3 Polymerase Chain Reaction (PCR)

PCR reaction mix:

5x Phusion® HF Reaction Buffer (Finnzymes)/ or 10x ThermoPol Reaction Buffer (NEB) or GC Buffer	10 µl/ or 5 µl
10mM dNTP mix	5 µl
10µM forward primer	2.5 µl
10µM reverse primer	2.5 µl
template (gDNA), usually 50 ng	1 µl
Phusion® Polymerase (Finnzymes)/ Taq DNA Polymerase (NEB)	(1.25 units/50 µl) 0.5 µl
H_2O	28.5 µl
	Total= 50 µl

Standard PCR program:

Initial denaturation	98°C 30sec	
Denaturation	98°C 10sec	30 cycles
Annealing	57°C 30sec	
Extension	72°C time alters with product length	
Final extension	72°C 5min	
Pause	4°C ∞	

T3 Thermocycler (Biometra) was used for the PCR reactions. For Phusion® Polymerase the elongation time was set to 30 sec per 1000 bp fragment size. For Taq DNA Polymerase the elongation time was set to 1 min per 1000 bp. If unspecific, spurious PCR products appeared on the agarose gel the annealing temperature was increased by 1-2 °C

After PCR reaction, the products were purified from Agarose gels using the NucleoSpin® Gel and PCR Clean-up Kit (Macherey-Nagel) following the provided protocol by the company.

To clone a DNA fragment, the region of interest was amplified from the genomic DNA by PCR. Primers were designed as 20-22 nucleotides (nt) complementary to the template DNA with a GC content between 40 % and 60 %. In order to further clone or manipulate the DNA, restriction sites were introduced at the 5' ends. To improve cleavage efficiency of these restriction sites, additional four nucleotides, usually an ATTA sequence, were added to the designed primers at the 5' end (Sambrook and Russell, 2006a). The oligonucleotides were ordered from and synthesized by Sigma-Aldrich Corp. (United Kingdom). pT2_4xUAS:EGFP-*rab*35 plasmid was generated by this way and will be explained in the cloning of the EGFP-*rab*35 plasmid section.

3.4 Restriction digestion

DNA backbone (1.5 µg)	1 µl
10x Buffer	2.5 µl
10x BSA	2.5 µl
Enzyme X	0.5 µl

H_2O	x µl to Total= 25 µl

Plasmids and the PCR products were digested by the corresponding restriction enzymes at the special temperature, which depends on enzyme working condition, for 2h in a volume of 25 µl in the corresponding buffers (NEB or Roche). Depending on the experiment design, if a sequential digestion by restriction enzymes was necessary, after incubation of the first enzyme for 2h, the fragment was cut and purified with the NucleoSpin® Gel and PCR Clean-up Kit (Macherey-Nagel). Further digestion was continued with a next enzyme.

3.4.1 Dephosphorylation

Arctic phosphate buffer (10x)	2.5 µl
Vector backbone	25 µl
Enzyme phosphotase	1 µl

In order to prevent the binding of sticky ends created by digestion enzymes, the vector backbone was dephosphorylated by Shrimp Alkaline Phosphatase (Promega) at 37°C for 30-60 min. Later on, the temperature was raised to 60 °C to deactivate the phosphatase.

Afterwards the digested DNA vector was run on an agarose gel electrophoresis to separate mixed DNA fragments (Sambrook and Russell, 2006b), and then purified with the NucleoSpin® Gel and PCR Clean-up Kit (Macherey-Nagel) according to the provided protocol. Finally, the purified DNA concentration was measured by spectrophotometry (NanoDrop spectrophotometer, Thermo Fischer Scientific).

3.5 Ligation

T4 DNA Ligase Buffer (10x)	2 µl
Vector DNA (4kb)	50 ng (0.020 pmol)
Insert DNA (1kb)	37.5 ng (0.060 pmol)
T4 DNA Ligase	1 µl
H_2O	to 20 µl

The plasmid of interest, together with the digested inserts was ligated in a volume of 20 µl in the presence of T4 DNA ligase and the corresponding buffer (T4 Ligase Buffer). The insert/plasmid ratio was shown in the above. The ligation was incubated at 18°C overnight (Sambrook and Russell, 2006c).

3.6 Transformation

Gene Pulser (Biorad) and cuvette
Electro-competent E.coli TOP10
Ligated plasmid of interest

Solution:

• Luria-Bertani (LB) medium (10g Bacto-tryptone; 5g yeast extract; 10g NaCl in 1l H2O, adjust to pH 7.5, autoclave)
• LB Agar plates (add 15 g Agar to 1l of LB, autoclave, added corresponding antibiotics, pourchot liquid LB Agar into plates (20ml in 10cm diameter plates) and let the Agar harden by cooling down to RT and kept in 4°C

Protocol:

Electro-competent Top10 E. coli bacteria were used for transformation. Frozen electrocompetent E. coli (50/ or 75 µl in Eppendorf tubes) were thawn on ice. Next, 1µl of the DNA ligation was added on the thawn bacteria. Then the bacteria were transferred into a 1 mm precooled Gene Pulser cuvette (Biorad). The electro-transformation was performed with a Gen Pulser (Biorad) at 1.8 mV, 200 Ω and 25 µF. After transformation, the bacteria were propagated in 1 ml LB medium without antibiotics on a shaker at 37°C for one hour. The bacteria were spread on LB Agar plates supplemented with corresponding antibiotics and grown over night in a 37°C incubator.

3.7 Minipreps

Single colonies were picked and incubated at 37°C overnight in 5 ml LB medium with corresponding antibiotics on a shaker. The plasmid DNA was further isolated with the NucleoSpin® Plasmid kit according to the provided protocol.

3.8 Gel electrophoresis

To assess the correct plasmid selection, the isolated DNA plasmids were digested by the corresponding enzymes and then run on the gel electrophoresis to separate the DNA fragments.

3.9 Sequencing

To confirm the positive candidates from the miniprep and PCR output, the products were sequenced. 0.8-1.2 µg of the plasmid were mixed with the

primer (either with Standard primers or self-designed primers were added) in a final volume of 15 µl. The sequencing was operated by Microsnyth AG (Balgach, Switzerland) and the result was sent on the following day via email. ApE© and SnapGene DNA softwares were applied to analyze sequencing results.

3.10 Midiprep

To purify high quality and large amount of DNA plasmid, midiprep was performed. A positive clone was picked and grown in100 ml LB medium with the corresponding antibiotics at 37°C on a shaker overnight.

At the following day, plasmid DNA was purified by applying a NucleoBond® Xtra Midi EF (Macherey-Nagel) protocol. After the purification, the plasmid DNA concentration was measured with the NanoDrop spectrophotometer (Thermo Fischer Scientific) and the plasmids were stored at -20°C.

3.11 Injection

Depending on experimental interests, appropriate fish lines were set up in mouse or small cages, replenished by stones or artificial plants to stimulate egg laying (set up 3 male and 3 female adult fish per cage) overnight. Next day around 8 a.m., the water in the cages were replaced by fresh water and internal grid was tilted around 30 degree. Fish began to the lay sufficient amounts of eggs for the injection.

Eggs were collected and transferred to a block of LB Agar channels (injection plates) and aligned with a coarse needle under the binocular. The plasmid solution (30-100 ng/µl plasmid in5 mM KCl, 100µM Na2HPO4 and 100µM NaH2PO4) was injected at single cell stage under the binocular. Injected eggs were then incubated at 28°C. In the afternoon, dead or unfertilized eggs were discarded. In the following day, the embryos were dechorionized manually or by proanase solution (0.1-0.5 mg/ml) for 10-20 min. After dechorionation, the embryos were washed with fresh 1x E3 egg water and transferred into a new dish. To assess the result of injection, embryos were screened for a fluorescent signal under a fluorescent binocular (Leica M205 FA). Selected positive embryos were either further imaged by confocal microscopy or grown up to generate transgenic lines.

3.12 Zebrafish Maintenance and Strains

Zebrafish (*Danio rerio*) were maintained at standard conditions (Westerfield, 2007) and embryos were raised and staged at 28.5 °C, as previously described (Kimmel et al., 2005). The following transgenic lines were used in this study: Tg(BAC:*kdrl*:mKate2-CAAX)^{UBS16} or Tg(BAC:*kdrl*:mcherry-CAAX) (Lenard et al., 2013). Tg(*kdrl*:NLSEGFP); Tg(*fli1a*:B4GALT1-mCherry) (Kwon et al., 2016); Tg(*kdrl*:eGFP:EB3) and Tg(*kdrl*:eGFP:tuba) (Asakawa and Kawakami, 2010); Tg(*fli1ep*:GAL4FF)^{UBS3}; (UAS:mRFP); Tg(UAS:EGFP-UCHD)^{UBS18} (Sauteur et al., 2014).

3.13 Immunohistochemistry

Embryos were grown in egg water (1x E3) until desired experimental age (in this case 24-48 hours) and then decorionated manually. If later stages needed, then embryos were incubated in 1x E3 containing 1x PTU (1-phenyl-2-thiourea) solution to prevent pigmentation.

Fixation solution

Embryos were fixed in 2% PFA o/n at 4°C. Next day, embryos were washed several times.

Permeabilization

Tissue permeabilization was done with 0.5% Triton X-100 in PBST (Sigma) for 2h at RT

Blocking solution

Next, embryos were incubated in "Bovine serum albumin (BSA)" o/n at 4°C.

Primary antibody

In the following day, embryos were incubated in primary antibody solution (diluted in blocking solution 1:500/1000) o/n at 4°C. Primary antibody solution was collected to reuse in future experiments and samples were washed 4-5 times in PBST for 6-8 hours at RT.

Secondary antibody

Next, embryos were incubated in secondary antibody (diluted in Blocking solution 1:1000/2000) o/n at 4°C. The following day, secondary antibody solution was preserved to reuse in future experiments and samples were washed at least 6 times with PBST during 6-8 hours at RT. Finally, embryos were ready to image.

3.14 Image acquisition and analysis

Sample mounting

Embryos were selected for fluorescent expression under a fluorescent binocular (Leica M205 FA). Then, staged embryos that exhibited fluorescence were anesthetized in 1x E3 with 1x tricaine (0.08 %). In mean while, 0.7% low melting agarose (Sigma, dissolved in 1x E3) was melted in microwave and supplemented with 1x tricaine and 1x PTU (0.003 %, Sigma) and was kept at 55°C during mounting. 4-6 embryos were put on a 35 mm glass bottom petri dish (0.17 mm, MatTek) and covered with pre-warmed low melting agarose. Life embryos or tail of fixed samples were oriented and aligned with a piece of soft material like hair, which attached on painting brush. After the agarose solidified, the glass dish was covered with 1x E3 egg water and supplemented with 1x tricaine and 1x PTU.

3.15 Confocal imaging

3.15.1 Point scanning confocal imaging

Leica SP5 II Matrix microscopy was used for over night time-lapse recordings with 40x water immersion objective (NA=1.1) and incubation chamber was always set to 28.5°C during the experiments. The point scanner was set to 400Hz. Over night time-lapse recordings were performed with multiple positions and z-stacks with a 0.5-0.75 µm step size were acquired every 8 or 10 minutes.

3.15.2 Spinning disk confocal imaging

Most of the movies were recorded by spinning disk confocal microscopy for

high spatial-temporal resolution (with $\Delta t<1$min). Here, endothelial cell division movies were recorded with 63x water immersion objective (NA=1.2) and z-stacks with a 0.2 µm step size were acquired every 30 seconds. Later on, vesicular/membrane trafficking movies were recorded every 10 second to improve spatial-temporal resolution. To obtain best resolution and the least photo-bleaching, laser intensities and exposure times were adjusted to get best signal to noise ratio.

3.16 Image processing and deconvolution

Images with 0.2µm z-stacks and high-resolution (>1024x1024pixel) were de-convolved. Raw data was divided to < 4gb parts and uploaded on to the server (HRM: smb://131.152.25.73/hrm_data/) and processed over the online interface (https://huygens.bc2.unibas.ch/hrm/) with pre-determined setup of parameters. Results were retrieved from the server and further processed by FIJI.

Imaris (Bitplane), Volocity (PerkinElmer) and ImageJ/ FIJI (http://imagej.nih.gov/ij/) were used for additional data processing and image analysis. All images are maximum intensity projections. Adobe Illustrator was used for figure preparation.

4 Results

4.1 Publication

© 2015. Published by The Company of Biologists Ltd | Biology Open (2015) 4, 1259-1269 doi:10.1242/bio.012740

RESEARCH ARTICLE

Endothelial cell division in angiogenic sprouts of differing cellular architecture

Vahap Aydogan, Anna Lenard, Alexandru Stefan Denes, Loic Sauteur, Heinz-Georg Belting and Markus Affolter*

ABSTRACT

The vasculature of the zebrafish trunk is composed of tubes with different cellular architectures. Unicellular tubes form their lumen through membrane invagination and transcellular cell hollowing, whereas multicellular vessels become lumenized through a chord hollowing process. Endothelial cell proliferation is essential for the subsequent growth and maturation of the blood vessels. However, how cell division, lumen formation and cell rearrangement are coordinated during angiogenic sprouting has so far not been investigated at detailed cellular level. Reasoning that different tubular architectures may impose discrete mechanistic constraints on endothelial cell division, we analyzed and compared the sequential steps of cell division, namely mitotic rounding, cytokinesis, actin re-distribution and adherence junction formation, in different blood vessels. In particular, we characterized the interplay between cell rearrangement, mitosis and lumen dynamics within unicellular and multicellular tubes. The lumen of unicellular tubes becomes constricted and is ultimately displaced from the plane of cell division, where a *de novo* junction forms through the recruitment of junctional proteins at the site of abscission. By contrast, the new junctions separating the daughter cells within multicellular tubes form through the alteration of pre-existing junctions, and the lumen is retained throughout mitosis. We also describe variations in the progression of cytokinesis: while membrane furrowing between daughter cells is symmetric in unicellular tubes, we found that it is asymmetric in those multicellular tubes that contained a taut intercellular junction close to the plane of division. Our findings illustrate that during the course of normal development, the cell division machinery can accommodate multiple tube architectures, thereby avoiding disruptions to the vascular network.

KEY WORDS: Junctional dynamics, Cytokinesis, Endothelial cell division, Multicellular tube, Unicellular tube, Lumen, Live-cell imaging, Actin distribution

INTRODUCTION

Embryonic organogenesis requires nutrient delivery, gas exchange and metabolic waste removal, and these processes depend upon the presence of a functional cardiovascular system. Therefore, the vascular network assembles early during development from endothelial cells (ECs) and grows into a dynamic network of hollow tubes that directs blood flow to the developing organs. Most of the later born blood vessels are the product of angiogenesis, a process in which new branches sprout from pre-existing blood vessels. During development, the vascular network becomes more elaborate through the opening of new circulatory pathways, a process known as anastomosis (Adams and Alitalo, 2007; Wacker and Gerhardt, 2011). As we have recently shown (Herwig et al., 2011; Lenard et al., 2013) anastomosis entails a stereotypic set of cell behaviors and can occur either between two sprouts that contact each other, or through the fusion of a sprout with a pre-existing, perfused blood vessel.

The vasculature of the zebrafish trunk consists of segmental arteries (SAs) that branch out of the dorsal aorta (Isogai et al., 2001). A vascular sprout contains several stalk cells and a leading tip cell (Blum et al., 2008; Siekmann and Lawson, 2007). SAs are arranged in a metameric pattern and their tip cells eventually contact each other, leading to vessel anastomosis and the formation of the dorsal longitudinal anastomotic vessel (DLAV) (Herwig et al., 2011; Lawson and Weinstein, 2002). During the formation of the trunk vasculature, approximately from 20 and 50 hpf, the endothelial cells of the SAs and the DLAV undergo extensive proliferation (Blum et al., 2008; Lawson and Weinstein, 2002). Therefore, the interplay of the cellular mechanisms of junctional remodeling, lumen formation and EC division can be investigated through live imaging during this time window (Ellertsdottir et al., 2010; Lawson and Weinstein, 2002). It has been shown that the ECs within the SAs can reorganize their intercellular junctions and apical domains, through a cell-autonomous process that does not require blood pressure (Herwig et al., 2011). Neighboring cells were observed to crawl over each other, expanding their shared subapical contacts and their apical surface until the vascular lumen was stabilized by multiple cells (Blum et al., 2008; Herwig et al., 2011; Lenard et al., 2013; Phng et al., 2015).

In terms of morphology and cellular plasticity, SA cells fall somewhere in-between migrating cells (at the tip) and cells that are tightly built into epithelial sheets (in the stalk). Tip cells are characterized by abundant filopodia at the leading edge, befitting their migratory nature and are followed by the trailing stalk cell (Gerhardt and Betsholtz, 2003; Siekmann and Lawson, 2007). By contrast, stalk cells undergo an extension of their cell surface and junctional contacts and are mostly arranged into multicellular tubes (Herwig et al., 2011; Sauteur et al., 2014).

Cell division has been extensively investigated using *in vitro* culture, and the cellular and molecular mechanisms of the mitotic machinery are well understood. The first step is mitotic rounding, a generic feature of cell division that is driven by changes in the shape and the rigidity of the cell cortex (Cadart et al., 2014). It has been shown that this actomyosin-driven process is necessary for the proper assembly, maintenance and orientation of the central spindle (Kunda et al., 2008; Lancaster et al., 2013; Rosenblatt et al., 2004). Spindle orientation subsequently defines the plane of cell division through the accumulation of phosphorylated Myosin II at the plasma

Biozentrum der Universität Basel, Klingelbergstrasse 70, Basel CH-4056, Switzerland.

*Author for correspondence (markus.affolter@unibas.ch)

Received 20 May 2015; Accepted 31 July 2015

Biology Open (2015) 4, 1259-1269 doi:10.1242/bio.012740

membrane, which drives the assembly of a contractile ring (reviewed in Fededa and Gerlich, 2012; Green et al., 2012; Levayer and Lecuit, 2012). The next step is the partitioning into two daughter cells, or cytokinesis, which takes place shortly after chromosome segregation. During cytokinesis, the actomyosin ring contracts and eventually collapses to a small intercellular bridge, the so called midbody (Green et al., 2012). Finally, the severing of the constricted plasma membrane, a process known as abscission, marks the end of mitosis.

Within epithelial sheets or tubes, dividing cells maintain the adherens junctions (AJs), which confer tissue integrity (Bourdages and Maddox, 2013; Nakajima et al., 2013). However AJs are extensively reconstructed during mitotic rounding and cytokinesis (Harris and Tepass, 2010; Herszterg et al., 2014). The neighboring ECs exert forces on the mitotic cell through cadherin proteins (the core of AJs) that are, in turn, linked to the actomyosin cortex (Harris and Tepass, 2010). Morphogenetic movements such as cell intercalation and invagination require a degree of synchronization between junctional re-arrangement and mitosis (Kondo and Hayashi, 2013; Levayer and Lecuit, 2012).

Because of their three-dimensional structure, tubular networks have a more complex morphology than epithelial sheets. Therefore, the division of elongated and lumenized cells may require some adaptations of the mitotic machinery in order to accommodate their peculiar geometry as was recently shown in a study of the *Drosophila* larval trachea system (Denes et al., 2015). While the actomyosin rings that drive cytokinesis in the *Drosophila* epithelia are able to symmetrically deform the AJs of the two cells that flank the emerging junction (Founounou et al., 2013; Guillot and Lecuit, 2013; Herszterg et al., 2013), during cytokinesis in tracheal tubes, the membrane furrows asymmetrically on the side of the cell that is proximal to the nucleus, and the new junction then extends around the lumen until it connects and fuses with another membrane. We found that in the remodeling dorsal tracheal branches, such asymmetric *de novo* junction formation is the norm, presumably because the specific geometry and the rigidity of the tubes favor this outcome (Denes et al., 2015).

The integration of proliferative and morphogenetic processes is therefore critical for proper vessel morphogenesis (Zeng et al., 2007). However, it has not been investigated in detail how EC division proceeds in a dynamic environment, in which lumen formation and cell rearrangements occur concomitantly and vessel integrity has to be maintained. Here, we investigated the interplay between cell division, junctional rearrangement, actin distribution and lumen dynamics during SA morphogenesis in the zebrafish, using an array of fluorescently labeled markers and confocal live imaging. We find that membrane furrowing during cytokinesis is symmetric in unicellular tubes and in those multicellular tubes with a cylindrical symmetry. ECs in a multicellular DLAV may undergo either symmetric or asymmetric cytokinesis, depending on the orientation of the intercellular junctions relative to the plane of division. We also found that, unlike the chitin-reinforced lumen of *Drosophila* trachea (Denes et al., 2015), the flexible lumen of unicellular vascular tubes can collapse during mitotic rounding and cytokinesis.

RESULTS

The cellular organization of SA branches and of the DLAV

The ECs that are part of the segmental arteries (SAs) divide in a stochastic fashion. SAs are dynamic structures, which contain anywhere between three and seven cells (Blum et al., 2008). Therefore, ECs, which undergo mitosis, may find themselves in quite different environments (Fig. 1). Tip cells sprout from the dorsal aorta (Childs et al., 2002; Siekmann and Lawson, 2007) and extend filopodia that will eventually contact those from neighboring branches, leading to anastomosis and giving rise to the DLAV (Blum et al., 2008; Herwig et al., 2011). During early phases of SAs formation the angiogenic sprout is not lumenized. Here, the tip cell is connected to the stalk cells by intercellular junctions (Fig. 1A). While the stalk is not lumenized at the onset of SAs sprouting, the stalk cells are surrounded by several neighbors – to each other, the tip cells and ventrally to ECs in the dorsal aorta (Fig. 1B). The formation of the lumen (through perfusion from the dorsal aorta) alters the shape of the stalk cells, as well as the relative positions of their nuclei and intercellular junctions (Fig. 1C). Subsequent junctional re-arrangements achieve the transition from a unicellular to a multicellular tube (Fig. 1D; Herwig et al., 2011; Lenard et al., 2013). Finally, the DLAV contains former tip cells that now possess a lumen and a T-shaped structure, and form intercellular junctions with the two neighboring tip cells and a stalk cell (Fig. 1E).

Cell division in migrating tip cells

In order to document different aspects of EC proliferation in the ISVs, we imaged 30-50 hpf embryos of the following genotypes: (1) Tg(*fli1ep*:GAL4FF)^{UBS3}, (UAS:RFP), (UAS:EGFP-ZO-1)^{UBS5}; (2) Tg(*fli1ep*:GAL4FF)$^{UBS2-4}$, (UAS:mRFP), (UAS:VE-cadherinΔC-EGFP)^{ubs12} (Herwig et al., 2011; Lenard et al., 2013); and (3) Tg(fli1ep:GAL4FF)^{ubs3}; (UAS:mRFP); Tg(UAS:EGFP-UCHD)^{ubs18} (Sauteur et al., 2014). The EGFP-labeled ZO-1 (zona occludens 1) and VE-cadherinΔC-EGFP proteins localize to the cell junctions, EGFP-tagged UCHD (utrophin calponin homology domain) localizes to the stable F-actin, while cytoplasmic RFP labels the entire cell. The presence and extent of the lumen was ascertained by subtracting the volume occupied by the cytoplasm in the Z-axis, or through the localization of the membrane marker mKate2-CAAX (Lenard et al., 2013). Condensed chromatin was identified either as a zone of low RFP accumulation, or directly through the localization of labeled histones (H2B-GFP; Kochhan et al., 2013).

During the early stages of SA formation, tip cells extend filopodia structures can undergo rapid shape changes. We observed that dividing tip cells (n=15; where n represents the number of the examined vessels) underwent mitotic rounding (Fig. 2B,B′,F,F′). At anaphase, cell furrowing started symmetrically (Fig. 2C,C′,G,G′, wedges) from both sides and was accompanied by actin accumulation. Following anaphase (Fig. 2C,C′), the cell was pinched the cell body at the plane of division (Fig. 2D,D′; supplementary material Movie S1a) and the two daughter cells remained attached through a thin cytoplasmic bridge (Fig. 2H,H′; supplementary material Movie S1b). We observed the deposition of new junctional material in the region of the division plane, followed by its expansion as the two daughter cells established a *de novo* junction along the mitotic interface. Blebs (Fig. 2D,G, arrowheads), which are dynamic membrane protrusions generated through actomyosin contractions (Bergert et al., 2012), were present at the interface between the daughter cells during cytokinesis. Interestingly, the filopodial dynamics at the front of the tip cells was not markedly changed during cell division, despite the mitotic rounding of the cell body (supplementary material Movie S1c).

De novo junctional formation in dividing stalk cells without a lumen

We next investigated those stalk cells, which divided before acquiring a lumen. We observed that dividing stalk cells (n=10; Fig. 3F,F′) also underwent mitotic cell rounding. Although lacking the extended filopodia of tip cells, these stalk cells also produced

Biology Open (2015) 4, 1259-1269 doi:10.1242/bio.012740

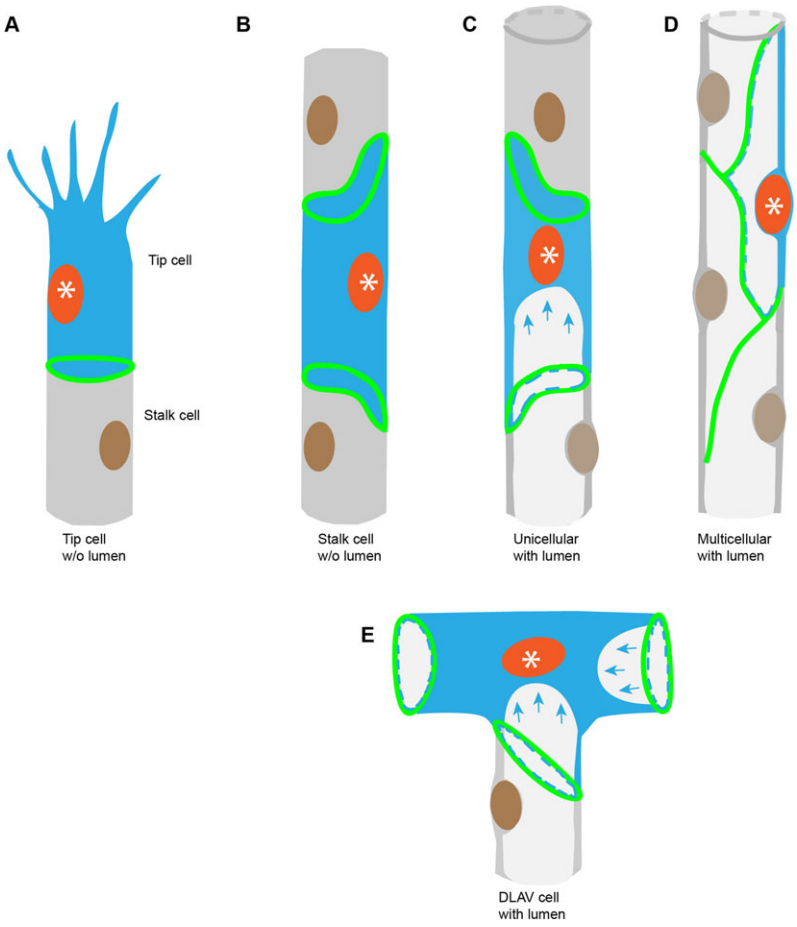

Fig. 1. Schematic representation of cell types in the SA and DLAV. (A) Early sprout from the dorsal aorta, showing the shape of a tip cell, highlighted by blue cytoplasm and an orange nucleus. (B) Stalk cell with elliptical intercellular junctions, highlighted by blue cytoplasm and an orange nucleus, before lumen and DLAV formation. (C) Highlighted stalk cell (blue cytoplasm and orange nucleus) showing a partial transcellular lumen (blue arrows). (D) Fully lumenized multicellular SA, with one highlighted cell (blue cytoplasm and orange nucleus). (E) Cell within the DLAV shows the three-way connection with the neighboring cells and two partial transcellular lumens (blue arrows). (Green represents cell-cell junctions.)

numerous blebs during mitosis (Fig. 3A,G, white/black arrowheads). Cytokinesis took place symmetrically and perpendicularly to the long axis of the sprout (Fig. 3A,G). Subsequently, and similar to tip cells, the two daughter cells formed a *de novo* junction (Fig. 3C,C′,D,D′; supplementary material Movie S2a) and actin accumulated at the plane of division (Fig. 3I,I′,J,J′; supplementary material Movie S2b).

Dividing unicellular stalk cells collapse the lumen in the plane of mitosis

We also investigated unicellular tubes made up of stalk cells that contain a lumen and entered mitosis (n=10). Such unicellular stalk cells form a transcellular lumen through a process of apical membrane invagination, during which the luminal compartment is extended and inflated from one or both sides of the cell under the pressure of incoming blood plasma. This type of lumen is not very stable and can easily collapse, upon a local drop in pressure (Herwig et al., 2011; Lenard et al., 2013). We observed that – in many cases – the inflated lumen did not penetrate the region of the cell where the prophase nucleus was located (Fig. 4A′; n=10). In those instances, in which comprised regions on either side of the nucleus, and where a pressure differential developed between the two sides, the nucleus was in some cases shifted to a new location within the cell (Fig. 4A, B; supplementary material Movie S3a). We also followed cell division in the presence of a fully inflated transcellular lumen (Fig. 4F,G; supplementary material Movies S3b, S8). The section of the lumen adjacent to the nucleus shrank during mitotic rounding (Fig. 4C,C′,H,H′). Subsequently, the lumen was entirely excluded from that region for the duration of cytokinesis (Fig. 4D,D′, I,I′), only to return immediately after the completion of mitosis (Fig. 4J,J′) and thereby inflating the ring-like *de novo* junction (Fig. 4E,E′,J,J′).

Mitosis in multicellular SAs does not collapse the lumen

During the later stages of SA formation, when the DLAV has formed and blood flow has been established, most ECs are part of multicellular tubes. In these vessels, we observed that dividing stalk cells (Fig. 5A,A′) clearly undergo mitotic rounding as well. However, and in contrast to cell division in a unicellular, lumenized tube, the lumen was kept intact during the entire process of cytokinesis (Fig. 5B,B′, n=25). The behavior of the intercellular junctions in such tubes closely resembled those described in epithelial tissues (Bourdages and Maddox, 2013). We observed that during anaphase, actin accumulated in the division plane, at a spot where two adjacent junctions were pulled towards the prospective location of the midbody, halfway between the two daughter nuclei (Fig. 5C,C′,H,H′). The previously straight junctions of the dividing cell were bent and brought into close proximity during cytokinesis (Fig. 5D,D′,I,I′; supplementary material Movie S4a,b), and shortly thereafter, the new intercellular junction began to form. Therefore, the new junctions only needed to extend halfway around the lumen in multicellular tubes (Fig. 5E,E′). Cytokinesis took place symmetrically, as the division plane that contained the collapsing actomyosin ring was equally distant to the two sides of the cell.

ECs within the DLAV can undergo asymmetric cytokinesis

During anastomosis, tip cells establish junctions with their anterior and posterior counterparts along the DLAV, while

Biology Open (2015) 4, 1259-1269 doi:10.1242/bio.012740

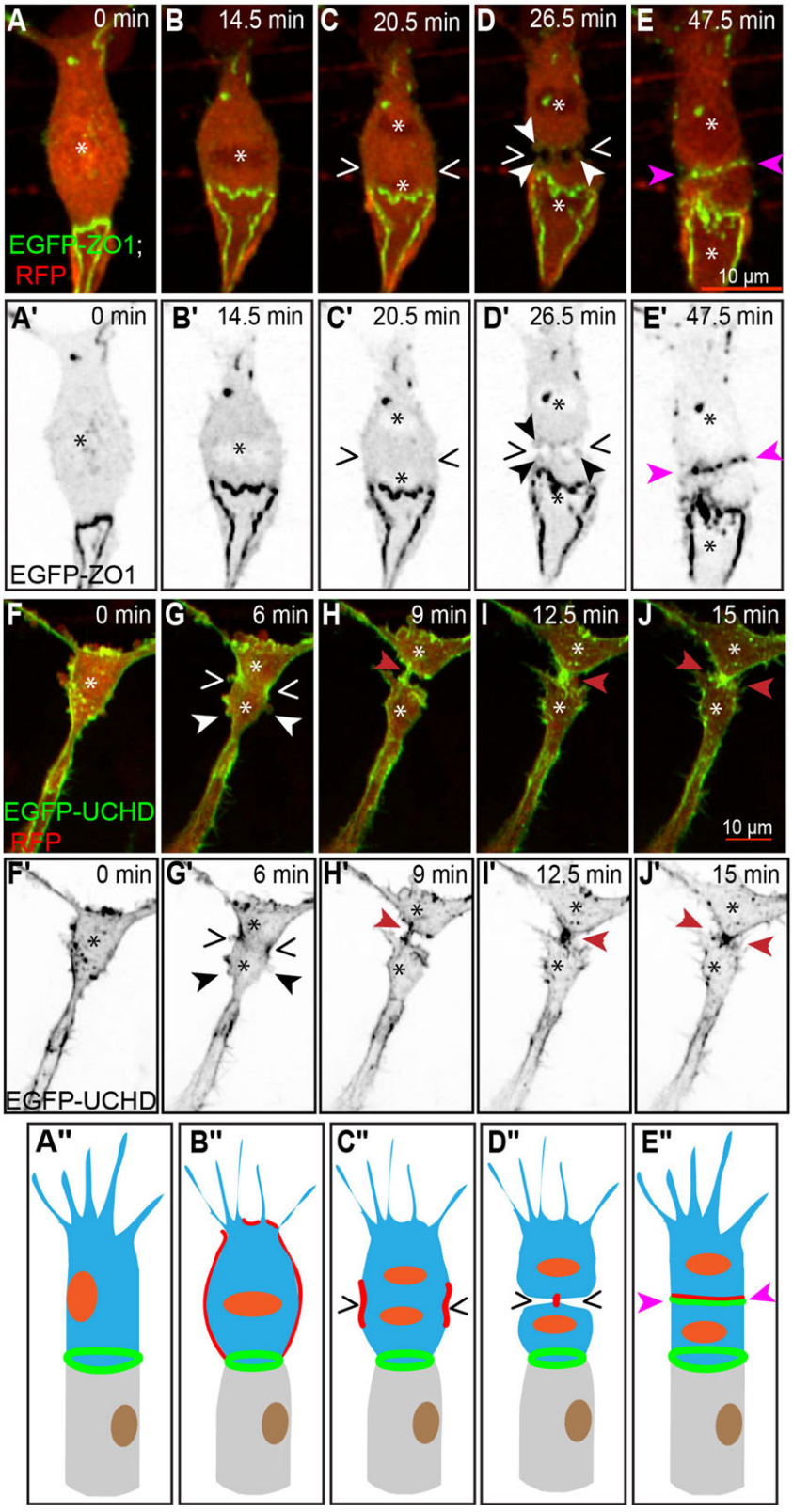

Fig. 2. Mitosis in a tip cell. (A-E) Still pictures from time-lapse supplementary material Movie S1a, with highlighted intercellular junctions (EGFP- ZO1) and cytoplasm (RFP); (F-J) time-lapse supplementary material Movie S1b, with actin cytoskeleton (EGFP-UCHD) and cytoplasm (RFP). The location of condensed chromatin is apparent as a zone of decreased red signal (asterisks). (A) Partially rounded tip cell, with the approximate position of the nucleus indicated by the asterisk. (B) Fully rounded tip cell with a metaphase plate (asterisk). (C) Tip cell during anaphase, showing the separation of the daughter chromosomes (asterisks) and the beginning of membrane furrowing (wedges). (D) Late stage cytokinesis, with a narrow intercellular bridge in the plane of division (wedges). Blebs are visible at the interface between the daughter cells (white/black arrowheads). (E) Established *de novo* junction between the two daughter cells (pink arrowheads). (A′-E′) Still pictures corresponding to those from panels A-E, showing only the green channel (grayscale). (F) Partially rounded tip cell, with the approximate position of the nucleus indicated by the asterisk. (G) Tip cell during anaphase, showing the separation of the daughter chromosomes (asterisks) and the beginning of membrane furrowing with actin accumulation (wedges) and blebs are visible at the cell surface (white/black arrowheads). (H) Late stage cytokinesis, with a narrow connection bridge in the plane of division (red arrowheads). (I) Thickening of the connection bridge between the daughter cells (red arrowheads). (J) Connection formed between the two daughters cells (red arrowheads). (F′-J′) Still pictures corresponding to those from panels F-J, showing only the green channel (grayscale). (A″-E″) Schematic representation corresponding to the five stages from panels A-E. (B″-E″) Schematic representation corresponding to from panels F-J. (In the schematic: red, actin; green, junctions; orange, nucleus; blue, cell body.)

retaining their initial junction with the most distal stalk cell of the corresponding sprout giving rise to T-shaped ECs. These ECs have 3 junctional rings and underwent asymmetrical cytokinesis, depending on the location of the prophase nucleus relative to the junctional rings. The DLAV was shown to transition from a unicellular to a multicellular tube through junctional re-arrangement (Herwig et al., 2011). Before this transition occurs, cells within the DLAV may be partially or completely perfused by a lumen, which in turn may be connected to the SA stalk, the neighboring tip cells, or both (Fig. 6A-A‴). The expansion of lumen (derived from the SA) into the dividing cell was apparent during metaphase and anaphase (Fig. 6A‴,B‴).

Biology Open (2015) 4, 1259-1269 doi:10.1242/bio.012740

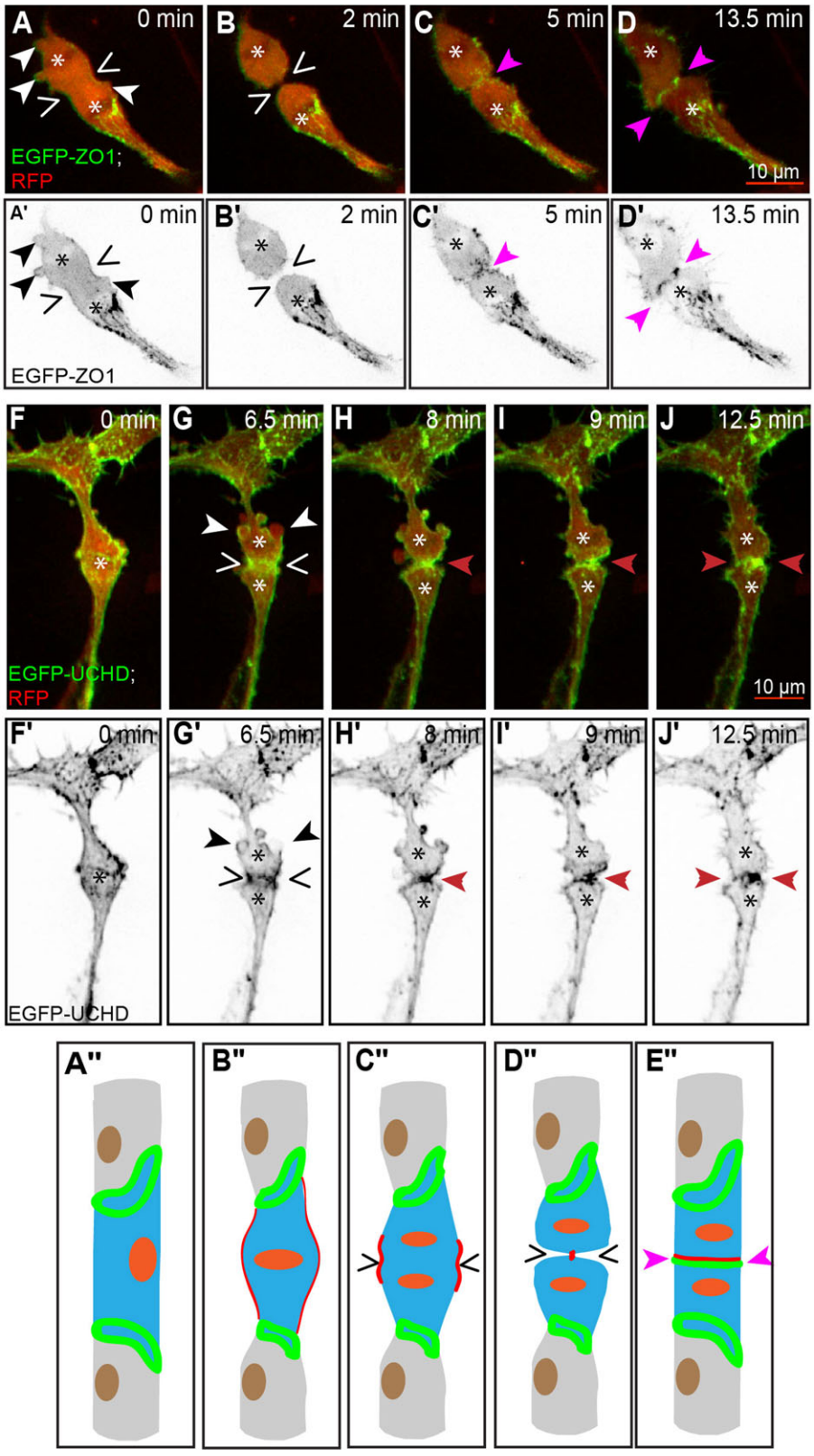

Fig. 3. Mitosis in a stalk cell without a lumen. (A-E) Still pictures from time-lapse supplementary material Movie S2a, with highlighted intercellular junctions (EGFP- ZO1) and cytoplasm (RFP); (F-J) time-lapse supplementary material Movie S2b, with actin cytoskeleton (EGFP-UCHD) and cytoplasm (RFP). The location of condensed chromatin is apparent as a zone of decreased red signal (asterisks). (A) Stalk cell during anaphase, showing the separation of the daughter chromosomes (asterisks) and the beginning of membrane furrowing (wedges). Blebs are visible at several locations around the cell (white/black arrowheads). (B) Late stage cytokinesis, with a narrow intercellular bridge in the plane of division (wedges). (C) Established *de novo* junction between the two daughter cells (pink arrowheads), as the two daughter cells start to reconnect. (D) Wide intercellular junction between the two daughter cells. (A′-D′) Still pictures corresponding to those from panels A-D, showing only the green channel (grayscale). (F) Partially rounded stalk cell, with the approximate position of the nucleus indicated by the asterisk. (G) Stalk cell during anaphase, showing the separation of the daughter chromosomes (asterisks) followed by blebs formation (white/black arrowheads) and the beginning of membrane furrowing with actin accumulation (wedges). (H) Late stage cytokinesis, with a narrow connection bridge in the plane of division (red arrowheads). (I) Thickening of the connection bridge between the daughter cells. (J) Connection formed between the two daughters cells (red arrowheads). (F′-J′) Still pictures corresponding to those from panels F-J, showing only the green channel (grayscale). (A″,B″) Schematic representation of the stalk cell during prophase and metaphase, not part of the movie (A-D). (C″-E″) Schematic representation corresponding to panels A-D. (A″-E″) Schematic representation corresponding to panels F-J. (In the schematic; red: actin, green: junctions, orange: nucleus, blue: cell body).

Subsequently, the progression of cytokinesis was associated with the shrinkage of the lumen in the plane of division (Fig. 6C,D,C‴, D‴). We observed the preferential deformation of the intercellular junction closest to the mitotic nucleus during the early stages of cytokinesis (Fig. 6B-B″). The emerging new junction first appeared as a pair of cellular processes, derived from the top right junctional ring (Fig. 6C-C″; supplementary material Movie S5). After the growing junction spanned almost the entire width of the cell, a complementary deformation of the bottom junctional ring became apparent as well (Fig. 6D-D″), shortly before the completion of the new junction between the daughter cells (Fig. 6E-E″). The cell within the DLAV divided

Biology Open (2015) 4, 1259-1269 doi:10.1242/bio.012740

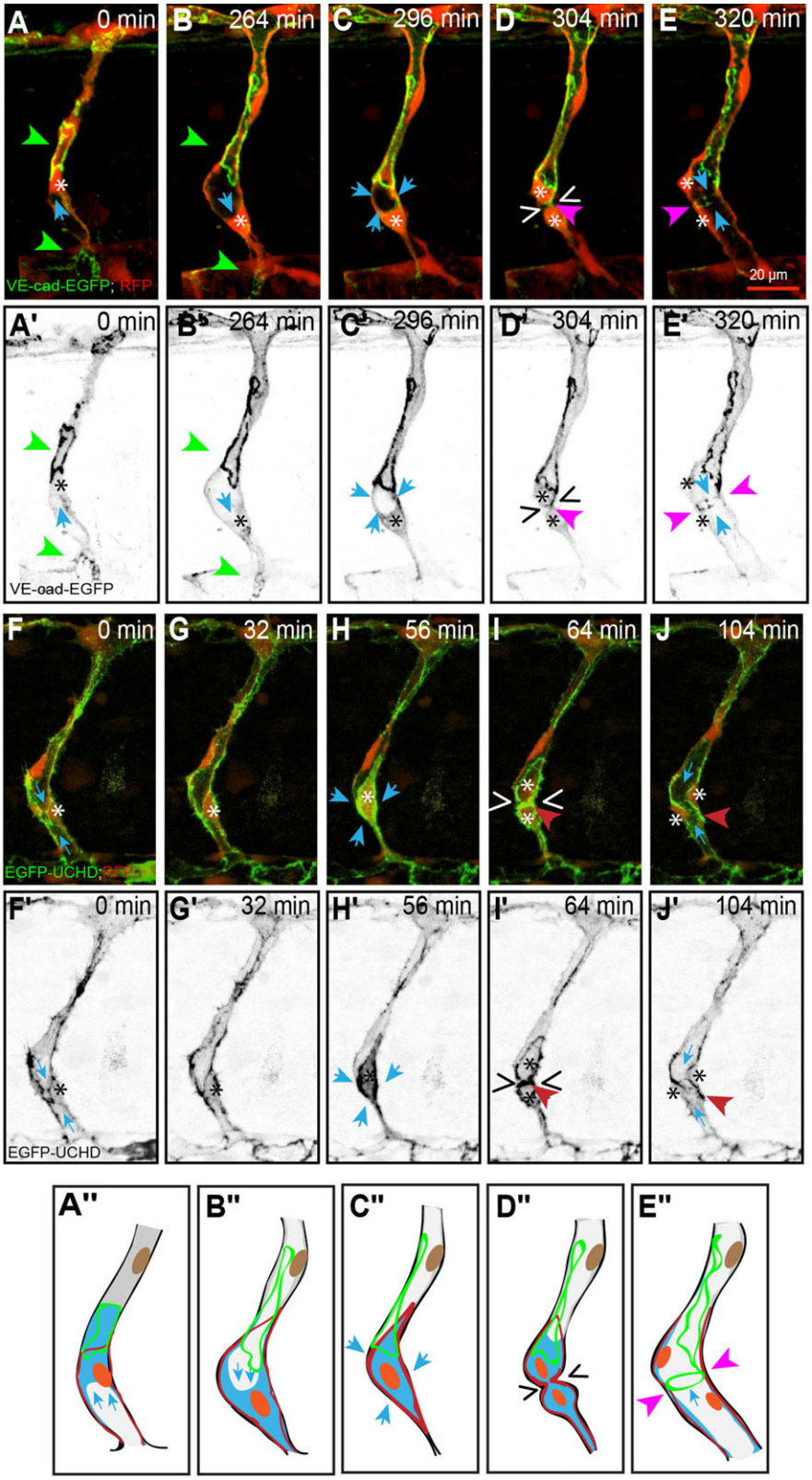

Fig. 4. Mitosis in a stalk cell with a partial transcellular lumen. (A-E) Still pictures from time-lapse supplementary material Movie S3a, with highlighted intercellular junctions (VE-cadherinΔC-GFP) and cytoplasm (RFP); (F-J) time-lapse supplementary material Movie S3b, with actin cytoskeleton (EGFP-UCHD) and cytoplasm (RFP). The location of the lumen is apparent as an empty zone bounded by red cytoplasm (blue arrows), and the approximate position of the nuclei is indicated by asterisks. (A) Stalk cell with a partial transcellular lumen (blue arrow) that extends from the aorta to the nucleus (asterisk). The cell is bounded by ring-like intercellular junctions (green arrowheads). (B) Retraction of the lumen from the bottom side of the cell and expansion of the transcellular lumen from the top (blue arrow). Elongation of the top ring and contraction of the bottom ring (green arrowheads). (C) Rounding of the stalk cell pushes out the lumen from the nuclear region (blue arrows). (D) Late stage cytokinesis, with a narrow intercellular bridge in the plane of division (wedges). The *de novo* junction between the two daughter cells is apparent as a dot (pink arrowheads) close to the intercellular bridge that contains the midbody. (E) The lumen re-inflates after mitosis is complete (blue arrows), expanding the *de novo* junction between the two daughter cells into a ring (pink arrowheads). (A′-E′) Still pictures corresponding to those from panels A-E, showing only the GFP channel (grayscale). (F) Stalk cell with a transcellular lumen (blue arrows) that extends from the aorta to the nucleus (asterisk). The cell is bounded by actin cytoskeleton. (G) Narrowing of the lumen from the bottom side of the cell prior to division. (H) Rounding of the stalk cell collapses the lumen from the bottom side of the cell (blue arrows). (I) After cytokinesis (wedges), the actin cytoskeleton accumulated at the plane of division (red arrowhead). (J) The lumen re-inflates after mitosis is complete (blue arrows), expanding the actin cytoskeleton between the two daughter cells (red arrowheads). (F′-J′) Still pictures corresponding to those from panels F-J, showing only the green channel (grayscale). (A″-E″) Schematic representation corresponding to the five stages from panels A-E and F-J. (In the schematic: red, actin; green, junctions; orange, nucleus; blue, cell body.)

without completely collapsing the lumen, in a manner reminiscent of the ECs in multicellular vessels. However, the repositioning of the nucleus close to one of the intercellular junctions favored asymmetrical cytokinesis. Our analysis (n=5) indicates that the actomyosin ring preferentially deforms those junctions that are close to it during cytokinesis (Fig. 6C-C″).

New junctions form through the zipping of furrowed membranes and the lumen does not impede cytokinesis

In order to better understand how the new junctions are formed during asymmetrical cytokinesis, we investigated the dynamics of the cell membrane on the apical and basolateral side, using the Tg(BAC:*kdrl*:mKate2-CAAX)^{UBS16} marker (Lenard et al.,

Biology Open (2015) 4, 1259-1269 doi:10.1242/bio.012740

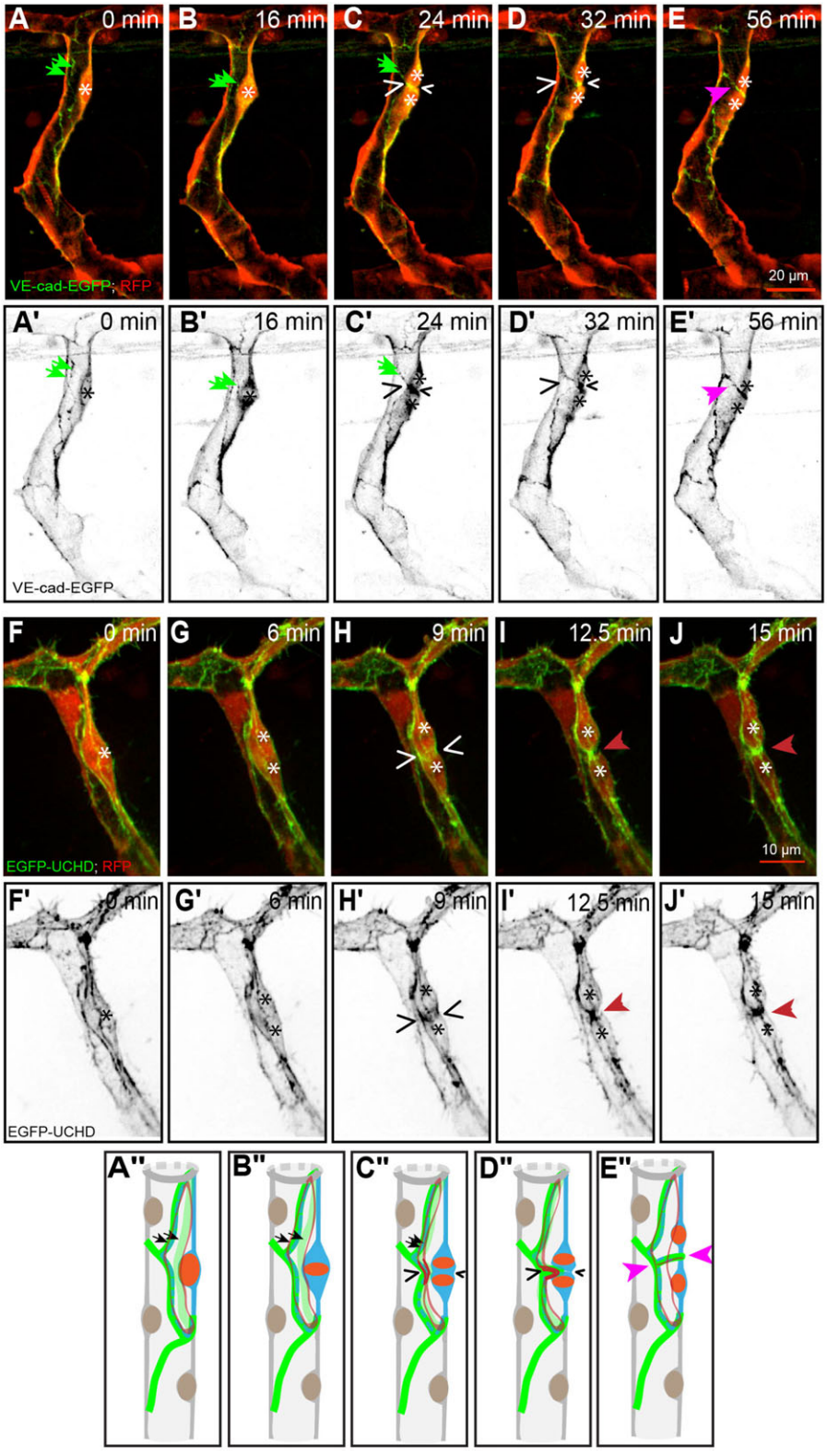

Fig. 5. Mitosis in a stalk cell with an extracellular lumen. (A-E) Still pictures from time-lapse supplementary material Movie S4a, with highlighted intercellular junctions (VE-cadherinΔC-GFP) and cytoplasm (RFP); (F-J) time-lapse supplementary material Movie S4b, with actin cytoskeleton (EGFP-UCHD) and cytoplasm (RFP). The location of the lumen is apparent as an empty zone bounded by red cytoplasm, and asterisks indicate the approximate position of the nuclei. (A) Stalk cell with intercellular junctions surround whole surface of a cell body (green arrows) that is part of a multicellular tube, prior to mitosis. (B) Stalk cell during metaphase, showing that the intercellular junctions (green arrows) and the extracellular lumen are not affected by the mitotic rounding. (C) Following anaphase, the furrowing of the actomyosin ring (wedges) symmetrically deforms the adjacent intercellular junctions (green arrows). (D) Late stage cytokinesis, with a narrow intercellular bridge in the plane of division (wedges). The angle between the deformed intercellular junctions has become more acute. (E) Formation of a new junction between the daughter cells (pink arrowheads), through the modification of the existing intercellular junctions. (A′-E′) Still pictures correspond to those from panels A-E, showing only the green channel (grayscale). (F) Partially rounded stalk cell that is a part of multicellular tube, prior to mitosis and the extracellular lumen are not affected by the mitotic rounding. (G) Stalk cell during anaphase, showing the separation of the daughter chromosomes (asterisks). (H) The beginning of membrane furrowing with actin accumulation (wedges). (I) Late stage cytokinesis, with a narrow connection bridge in the plane of division (red arrowheads). (J) Thickening of connection bridge between the daughter cells and connection formed between the two daughters cells (red arrowhead). (F′-J′) Still pictures corresponding to those from panels F-J, showing only the green channel (grayscale). (A″-E″) Schematic representation corresponding to the five stages from panels A-E and F-J. (In the schematic: red, actin; green, junctions; orange, nucleus; blue, cell body; black arrows, position of junctions.)

2013) together with the Tg(*kdrl:H2B-GFP*) (Kochhan et al., 2013) marker, which label cell membranes and chromatin, respectively. The mitotic rounding of the dividing cell did not deform the lumen inflated between the two cells (Fig. 7A-A″). According to our observations, the membrane furrowing that is presumably driven by the contraction of the actomyosin ring begins on the basolateral (outer) side of the vessel and proceeds towards its middle, where the cell connects to another EC, thereby supporting the lumen (Fig. 7C-C″; supplementary material Movie S6). During the late stages of cytokinesis, when the two sides of the membrane have been juxtaposed (Fig. 7D-D″), the new junction zips together (Fig. 7E-E″; supplementary material Movie S6).

Using the same membrane marker, we followed the lumen dynamics during cytokinesis in a cell that possesses a transcellular

Biology Open (2015) 4, 1259-1269 doi:10.1242/bio.012740

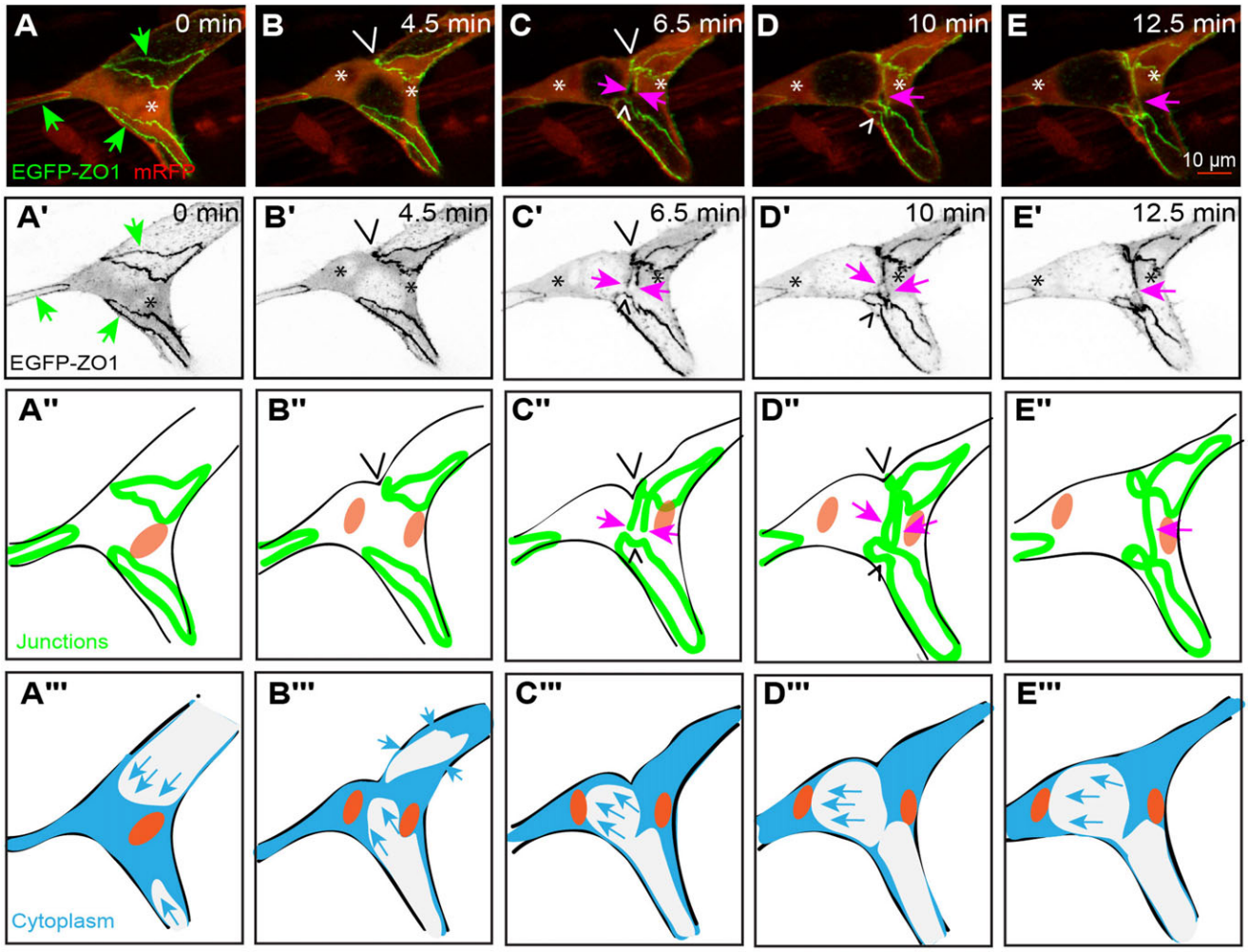

Fig. 6. Mitosis in a cell within the DLAV with a partial transcellular lumen. (A-E) Still pictures from time-lapse supplementary material Movie S5, with highlighted intercellular junctions (EGFP-ZO1) and cytoplasm (RFP). The location of the lumen is apparent as an empty zone bounded by red cytoplasm, and the approximate position of the nuclei is indicated by asterisks. (A) T-shaped cell within the DLAV with intercellular junctions (green arrows), during the metaphase. (B) Lumenal push, from the bottom, positions the nucleus close to the top ring and following anaphase furrowing is observed in the upper region of the cell (wedge). (C) The top ring (wedges) deforms during the anaphase, generating a pair of cellular processes that extend towards the opposite side of the cell (pink arrows). The lumen is partially constricted in the plane of division. (D) During late stage cytokinesis, the bottom ring is deformed as well (wedge) prior to the closure of the new junction (pink arrow). The lumen continues to shrink within the plane of division, without completely collapsing. (E) A complete, ring-like junction is established between the daughter cells (pink arrow), through the modification of the existing intercellular junctions. (A′-E′) Still pictures corresponding to those from panels A-E, showing only the green channel (grayscale). (A″-E″) Schematic representation corresponding to the five stages from panels A-E, depicting the nuclei and the junctions. (A‴-E‴) Schematic representation corresponding to the five stages from panels A-E, depicting the nuclei and the cytoplasm/lumen. (In the schematic; green: junctions, orange: nucleus, blue: cell body, blue arrows: ending and growth direction of lumen.)

lumen, in addition to a dead-end multicellular lumen that is supported together with a neighboring cell (Fig. 7F). As previously described in the article, the apical side that faces the lumen is visible as a nested membrane within the tube, while the basolateral membrane is seen on the outside of the blood vessel. The two lumens were initially in close proximity. However, at the onset of mitotic rounding of the transcellular lumen compartment collapsed, while the proximal multicellular luminal compartment appeared unchanged, apart from a degree of narrowing (Fig. 7G,G′). We observed that membrane furrowing was asymmetrical, on account of the position of the lower neighboring cell, relative to the plane of division (Fig. 7I,I′; supplementary material Movie S7). Following the establishment of a *de novo* junction and the completion of mitosis, both lumens began to expand, especially the upper transcellular lumen (Fig. 7J,J′; supplementary material Movie S7). Therefore, the transcellular lumen present within the unicellular tubes was found to be responsive to the changes in cell shape accompanying the mitotic process, and did not interfere with cytokinesis.

DISCUSSION

To date, the largest body of *in vivo* data on mitosis in a multicellular environment has been collected in *Drosophila* and describes the process in the embryonic epithelium (Guillot and Lecuit, 2013), the wing disc epithelium (Nakajima et al., 2013), the follicular epithelium (Morais-de-Sá and Sunkel, 2013), the dorsal thorax epithelium (Founounou et al., 2013; Herszterg et al., 2013) and the trachea (Denes et al., 2015; Kondo and Hayashi, 2013). With our analysis of cell division in the vasculature of the zebrafish embryo, we aimed to characterize those aspects of the mitotic process that are conserved between the tubular organs of vertebrates and those of insects. We have identified a sequence of cellular events that appears to be shared between the two cellular systems, which is not surprising given that all epithelial cells face a similar set

Biology Open (2015) 4, 1259-1269 doi:10.1242/bio.012740

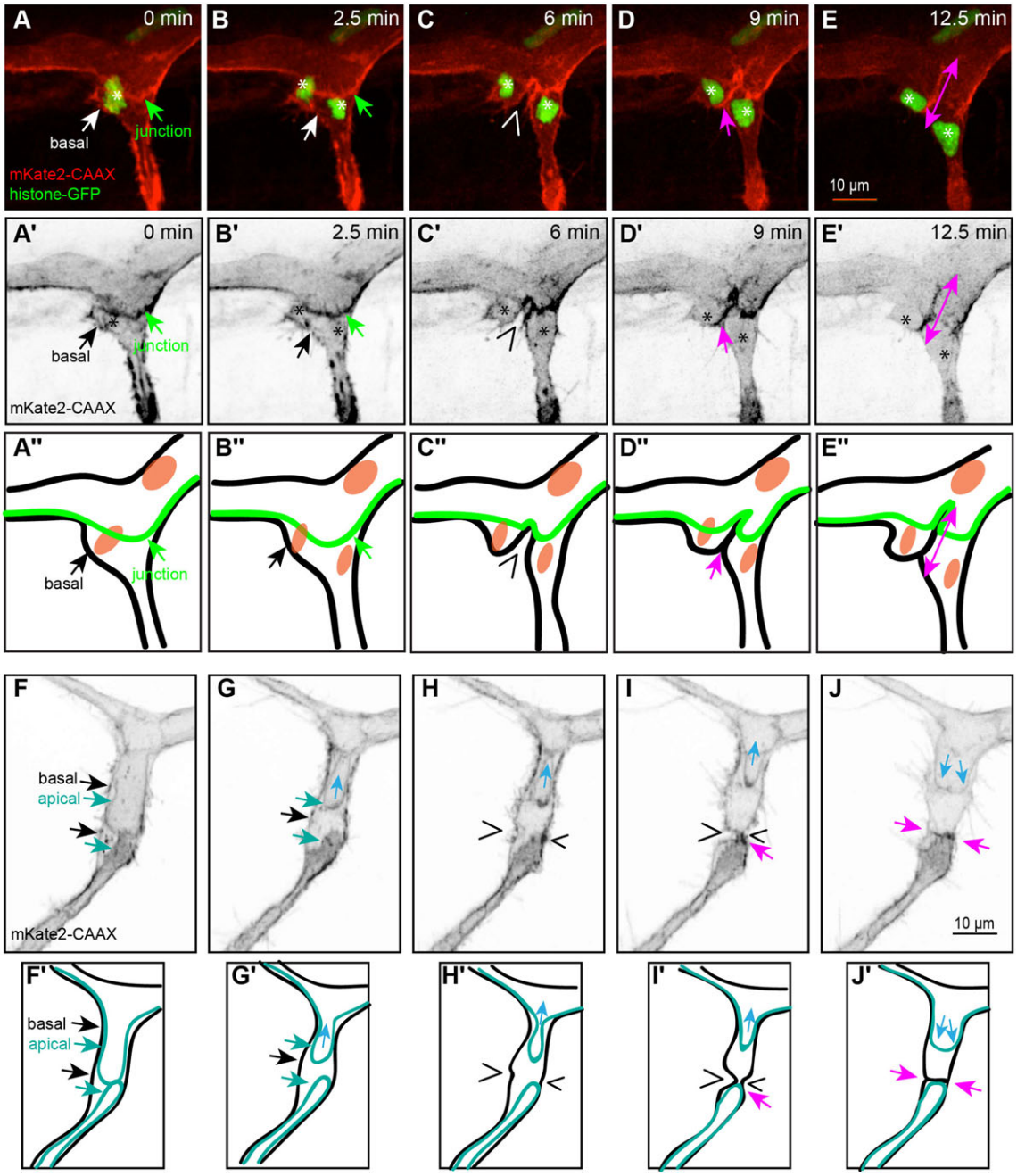

Fig. 7. Membrane furrowing and lumen dynamics in a dividing cell from the DLAV. (A-E) Still pictures from time-lapse supplementary material Movie S6, with highlighted membranes (mKate2-CAAX). The apical side (where the lumen is located) is apparent as a bright zone bounded by cell membranes, cell-cell contacts form a stripe of strong red signal (green arrow) and the position of the nuclei is shown by histone-GFP and asterisks. (A) Cell within the DLAV with a nucleus on the left (asterisk represents nuclei number.) connected to the ISV cells (intercellular junction, green arrow), prior to mitosis. (B) Cell after anaphase and before the start of cytokinesis. The daughter nuclei have separated but the membranes have not furrowed. (C) The membrane starts furrowing (wedge) asymmetrically during cytokinesis, generating a deep furrow that extends towards the middle of the vessel. (D) During late stage cytokinesis, the two sides of the membrane are juxtaposed (pink arrow). (E) The new junction between the two daughter cells forms through the zipping of the juxtaposed membrane, starting from the apical side (pink double arrow). (A′-E′) Still pictures corresponding to those from panels A-E, showing only the red channel (grayscale). (A″-E″) Schematic representation corresponding to the five stages from panels A-E, depicting cell-cell contacts (green line and arrow), the basal membrane (black) and the nuclei (orange). (F-J) Still pictures from time-lapse supplementary material Movie S7, with highlighted membranes (mKate2-CAAX). The apical side (where the lumen is located) is apparent as an intracellular membrane (turquoise arrows). (F) Cell within the DLAV, showing the position of the apical (turquoise arrows) and basal (black arrows) membranes, prior to mitosis. The region contains an upper trans-cellular lumen and a lower multicellular lumen. (G) The cell undergoes mitotic rounding and the upper transcellular lumen is pushed away from the future plane of mitosis (light blue arrow), while the lower multicellular lumen constricts but is not excluded from the region. (H) The cell after anaphase and before the start of cytokinesis. The upper lumen continues to shrink (light blue arrow) while the multicellular lumen remains unaffected. (I) The membrane starts furrowing (black wedges) asymmetrically deforms the basal membrane, with a deeper furrow on the left side of the cell, which is more distant from the multicellular junction on the right side. (J) Formation of a *de novo* junction between the two daughters cells (pink arrows). Following the end of mitosis, the upper lumen recovers and begins to push again into the vessel. (F′-J′) Schematic representation corresponding to the five stages from panels F-J, depicting the apical membrane (turquoise lines and arrows), the basal membrane (black/white arrows represent basal membrane).

Biology Open (2015) 4, 1259-1269 doi:10.1242/bio.012740

of constraints, such as retaining their apico-basal polarity and their barrier function throughout mitosis. In our study, we have examined the specific interactions between the lumen, the junctions and the actin distribution, within the different cellular architectures that are encountered in the embryonic zebrafish trunk vasculature (Fig. 1).

The sprouting of the tip cells from the dorsal aorta is the first step towards the formation of the SAs and the DLAV. Branch elongation takes place through a combination of tip cell migration and actin-mediated shape changes within the stalk cells (Sauteur et al., 2014). In most cases, the nascent sprout is not lumenized at this early stage (n=25). At this stage, ECs may undergo mitosis with little interference from the neighboring cells, as their intercellular junctions are located toward the proximal and distal tips of the cells, and therefore away from the future mitotic plane (Fig. 2A and Fig. 3A). These dividing cells were observed to go through the 'classic' stages, namely mitotic rounding during metaphase (Cadart et al., 2014), symmetrical membrane furrowing during cytokinesis (Green et al., 2012), and expansion of cell-cell contacts as the first step of *de novo* junction formation (Yamada and Nelson, 2007).

Whereas the formation of multicellular tubes depends on stalk cell elongation, which allows extensive 'cell pairing', in the absence of this pairing a unicellular tube can be formed via transcellular lumen formation. The mechanism of transcellular lumen formation depends by and large on directed membrane invagination along the blood vessel axis. Because of the small diameter of ECs, endothelial nuclei may impede this invagination process (Fig. 4A-A″). Despite the plasticity of these ECs, the lumen cannot easily penetrate through the region containing the nucleus, and under certain conditions, the nucleus may also be shifted back and forth within the cell, similar to a piston in a cylinder (Fig. 4A-B). During metaphase, the lumen is eventually excluded from the plane of division. However, the lumen is capable of re-perfusing the two daughter cells immediately after mitosis is complete (Fig. 4E). These dynamic changes of luminal compartments are consistent with our previous reports. Lumen forms and collapses repeatedly in blood vessels with erratic blood flow, during the early steps of vessel fusion (Lenard et al., 2013) or during vessel regression (Lenard et al., 2015). Cell division causes changes in the organization of the cytoskeleton, which may account for the instability of the generally fragile transcellular lumen.

The simplest multicellular tubes are composed of a pair of cells that envelop a lumen and are held together by continuous intercellular junctions along the vessel axis. Unlike the partial transcellular lumens, the extracellular lumen of multicellular tubes is more robust and does not collapse during mitotic rounding. We have also observed that the plane of division was always orthogonal to the axis of the lumen, thereby positioning the actomyosin ring close to the intercellular junctions. Within planar epithelial sheets, the neighboring cells that are flanking the mitotic plane and the associated actomyosin ring exert a strong influence on the progression of cytokinesis. The actin cytoskeleton of the neighboring cells is coupled to the plasma membrane through cadherin proteins, which are in turn the core components of adherens junctions (Harris and Tepass, 2010). In order for cytokinesis to take place, the ingression of the actomyosin ring must overcome the tensile forces generated by the neighboring cells (Bourdages and Maddox, 2013). However, it has also been shown that the juxtaposition of the furrowed membrane is actively supported by the neighboring cells, through actin polymerization at the base of the furrow (Founounou et al., 2013; Herszterg et al., 2013). Our analysis of cytokinesis in multicellular tubes reveals that membrane ingression takes place symmetrically on both sides of the contracting actomyosin ring (Fig. 5C-C″). The membrane of the counterpart cell undergoes a complementary deformation, ensuring that adhesion and barrier function are maintained for the duration of mitosis. We were able to investigate the localization of actin filaments and junctions in different cells. The sharp shoulders of the furrowed membrane (Fig. 5D′) are very similar to those described in planar epithelial sheets (Herszterg et al., 2014), which suggest that cytokinesis in tubular epithelia is probably a multicellular process as well.

Cells within the DLAV have a more balanced aspect ratio compared to stalk cells, with a central body and 3 sets of ring-shaped intercellular junctions at the tips of a T shape. Lumen perfusion can occur from either direction and on account of their three-fold symmetry, the prophase nucleus may be positioned close to only one of the rings (Fig. 6A,B). In such an orientation, the actin accumulates preferentially at an asymmetric position and the actomyosin ring preferentially deforms the intercellular junction that was adjacent or closest to the plane of division, resulting in an asymmetric cytokinesis event (Fig. 6C). Tubular cells from the trachea of *Drosophila* larvae have recently been shown to undergo such asymmetric cytokinesis (Denes et al., 2015). In both instances, the ingression of the actomyosin ring caused a local deformation of the junction, followed by the formation of a membrane protrusion that grew until it contacted another junction, where they finally connected (Fig. 6D). However, it is important to note that the rigid lumen found in the trachea forces the emerging junction to curve around it (Denes et al., 2015), whereas in the DLAV, the lumen slowly yields to the tension generated by cytokinesis (Fig. 6E,E‴).

Mitotic cells from polarized epithelia have also been shown to undergo asymmetric cytokinesis along the apico-basal axis. Because the cytokinetic furrow contracts faster from the basal side, the midbody eventually comes to rest at the apical side of the dividing cell (Founounou et al., 2013; Guillot and Lecuit, 2013). Our analysis shows that membrane ingression in cells within the DLAV takes place asymmetrically (Fig. 7C) and that the zipping of the two juxtaposed membranes begins at the apical side, where the lumen is located (Fig. 7D,E).

Conclusion

We found that in the absence of a lumen, endothelial cells in the segmental arteries divide symmetrically and form intercellular junctions *de novo*. The mechanisms of cell division in multicellular tubes closely resemble those seen in planar epithelial sheets: following actomyosin ring ingression and membrane furrowing, new junctions between the daughter cells are formed through the modification of pre-existing ones. However, we also observed asymmetric cytokinesis in T-shaped cells within the DLAV, in which the prophase nuclei were positioned closer to some intercellular junctions than to others.

MATERIALS AND METHODS

Zebrafish maintenance and strains

Zebrafish (*Danio rerio*) were maintained at standard conditions (Westerfield, 2007) and embryos were staged at 28.5°C, as previously described (Kimmel et al., 1995). The following transgenic lines were used in this study: Tg(fli1ep:gal4ff)^{ubs3} Tg(UAS:EGFP-ZO1-cmlc:EGFP)^{UBS5} (Herwig et al., 2011), Tg(5×UAS:mRFP) (Asakawa et al., 2008), Tg(BAC:*kdrl*:mKate2-CAAX)^{UBS16} and Tg(UAS:VE-cadherinΔC-EGFP)^{ubs12} (Lenard et al., 2013), Tg(*kdrl:H2B-GFP*)^{mu122} (Kochhan et al., 2013), Tg(UAS:EGFP-UCHD)^{ubs18} (Sauteur et al., 2014).

In vivo time-lapse analysis

Staged embryos that exhibited fluorescence were anaesthetized with tricaine solution (0.08%) and subsequently mounted in a 35-mm glass bottomed

petri dish (0.17 mm, MatTek), containing 0.7% low-melting agarose (Sigma), 0.08% tricaine and 0.003% PTU (Sigma). Long duration movies were recorded with a Leica TCS SP5 confocal microscope, using a 40× (NA=1.1) water immersion objective. Z-stacks with a 0.7- to 1-µm step size were acquired every 8 or 10 min.

High-resolution movies were acquired with a spinning disk confocal microscope (Perkin Elmer Ultraview), using a 63× (NA=1.2) water immersion objective. Z-stacks with a 0.2-µm step size were recorded every 30 s. For improved resolution, datasets were deconvolved using the Huygens Remote Manager software (Ponti et al., 2007).

Imaris (Bitplane), Volocity (PerkinElmer) and ImageJ (http://imagej.nih.gov/ij/) were used for additional data processing and analysis. All images are maximum intensity projections.

Acknowledgements
Confocal and Spinning disk microscopies were applied and image analysis was performed at the Imaging Core Facility of the Biozentrum (University of Basel). We thank the imaging facility staff for their generous support, Kumuthini Kulendra for fish care and other lab members for the scientific support and discussions.

Competing interests
The authors declare no competing or financial interests.

Author contributions
V.A. planned and performed experiments, prepared all the figures and contributed to the writing. A.L. contributed by supervising V.A. and critical discussions, A.S.D. wrote the manuscript. L.S. provided a movie and all authors edited the paper.

Funding
V.A. was supported by Fellowships For Excellence. This work has been supported by the Kantons Basel-Stadt and Basel-Land; and by a grant from the Swiss National Science Foundation (to M.A.).

Supplementary material
Supplementary material available online at
http://bio.biologists.org/lookup/suppl/doi:10.1242/bio.012740/-/DC1

References
Adams, R. H. and Alitalo, K. (2007). Molecular regulation of angiogenesis and lymphangiogenesis. *Nat. Rev. Mol. Cell Biol.* **8**, 464-478.
Asakawa, K., Suster, M. L., Mizusawa, K., Nagayoshi, S., Kotani, T., Urasaki, A., Kishimoto, Y., Hibi, M. and Kawakami, K. (2008). Genetic dissection of neural circuits by Tol2 transposon-mediated Gal4 gene and enhancer trapping in zebrafish. *Proc. Natl. Acad. Sci. USA* **105**, 1255-1260.
Bergert, M., Chandradoss, S. D., Desai, R. A. and Paluch, E. (2012). Cell mechanics control rapid transitions between blebs and lamellipodia during migration. *Proc. Natl. Acad. Sci. USA* **109**, 14434-14439.
Blum, Y., Belting, H.-G., Ellertsdottir, E., Herwig, L., Lüders, F. and Affolter, M. (2008). Complex cell rearrangements during intersegmental vessel sprouting and vessel fusion in the zebrafish embryo. *Dev. Biol.* **316**, 312-322.
Bourdages, K. G. and Maddox, A. S. (2013). Dividing in epithelia: cells let loose during cytokinesis. *Dev. Cell* **24**, 336-338.
Cadart, C., Zlotek-Zlotkiewicz, E., Le Berre, M., Piel, M. and Matthews, H. K. (2014). Exploring the function of cell shape and size during mitosis. *Dev. Cell* **29**, 159-169.
Childs, S., Chen, J.-N., Garrity, D. M. and Fishman, M. C. (2002). Patterning of angiogenesis in the zebrafish embryo. *Development* **129**, 973-982.
Denes, A. S., Kanca, O. and Affolter, M. (2015). A cellular process that includes asymmetric cytokinesis remodels the dorsal tracheal branches in Drosophila larvae. *Development* **142**, 1794-1805.
Ellertsdottir, E., Lenard, A., Blum, Y., Krudewig, A., Herwig, L., Affolter, M. and Belting, H.-G. (2010). Vascular morphogenesis in the zebrafish embryo. *Dev. Biol.* **341**, 56-65.
Fededa, J. P. and Gerlich, D. W. (2012). Molecular control of animal cell cytokinesis. *Nat. Cell Biol.* **14**, 440-447.
Founounou, N., Loyer, N. and Le Borgne, R. (2013). Septins regulate the contractility of the actomyosin ring to enable adherens junction remodeling during cytokinesis of epithelial cells. *Dev. Cell* **24**, 242-255.
Gerhardt, H. and Betsholtz, C. (2003). Endothelial-pericyte interactions in angiogenesis. *Cell Tissue Res.* **314**, 15-23.
Green, R. A., Paluch, E. and Oegema, K. (2012). Cytokinesis in animal cells. *Annu. Rev. Cell Dev. Biol.* **28**, 29-58.
Guillot, C. and Lecuit, T. (2013). Adhesion disengagement uncouples intrinsic and extrinsic forces to drive cytokinesis in epithelial tissues. *Dev. Cell* **24**, 227-241.
Harris, T. J. C. and Tepass, U. (2010). Adherens junctions: from molecules to morphogenesis. *Nat Rev. Mol. Cell Biol.* **11**, 502-514.
Herszterg, S., Leibfried, A., Bosveld, F., Martin, C. and Bellaiche, Y. (2013). Interplay between the dividing cell and its neighbors regulates adherens junction formation during cytokinesis in epithelial tissue. *Dev. Cell* **24**, 256-270.
Herszterg, S., Pinheiro, D. and Bellaiche, Y. (2014). A multicellular view of cytokinesis in epithelial tissue. *Trends Cell Biol.* **24**, 285-293.
Herwig, L., Blum, Y., Krudewig, A., Ellertsdottir, E., Lenard, A., Belting, H.-G. and Affolter, M. (2011). Distinct cellular mechanisms of blood vessel fusion in the zebrafish embryo. *Curr. Biol.* **21**, 1942-1948.
Isogai, S., Horiguchi, M. and Weinstein, B. M. (2001). The vascular anatomy of the developing zebrafish: an atlas of embryonic and early larval development. *Dev. Biol.* **230**, 278-301.
Kimmel, C. B., Ballard, W. W., Kimmel, S. R., Ullmann, B. and Schilling, T. F. (1995). Stages of embryonic development of the zebrafish. *Dev. Dyn.* **203**, 253-310.
Kochhan, E., Lenard, A., Ellertsdottir, E., Herwig, L., Affolter, M., Belting, H.-G. and Siekmann, A. F. (2013). Blood flow changes coincide with cellular rearrangements during blood vessel pruning in zebrafish embryos. *PLoS ONE* **8**, e75060.
Kondo, T. and Hayashi, S. (2013). Mitotic cell rounding accelerates epithelial invagination. *Nature* **494**, 125-129.
Kunda, P., Pelling, A. E., Liu, T. and Baum, B. (2008). Moesin controls cortical rigidity, cell rounding, and spindle morphogenesis during mitosis. *Curr. Biol.* **18**, 91-101.
Lancaster, O. M., Le Berre, M., Dimitracopoulos, A., Bonazzi, D., Zlotek-Zlotkiewicz, E., Picone, R., Duke, T., Piel, M. and Baum, B. (2013). Mitotic rounding alters cell geometry to ensure efficient bipolar spindle formation. *Dev. Cell* **25**, 270-283.
Lawson, N. D. and Weinstein, B. M. (2002). In vivo imaging of embryonic vascular development using transgenic zebrafish. *Dev. Biol.* **248**, 307-318.
Lenard, A., Ellertsdottir, E., Herwig, L., Krudewig, A., Sauteur, L., Belting, H.-G. and Affolter, M. (2013). In vivo analysis reveals a highly stereotypic morphogenetic pathway of vascular anastomosis. *Dev. Cell* **25**, 492-506.
Lenard, A., Daetwyler, S., Betz, C., Ellertsdottir, E., Belting, H.-G., Huisken, J. and Affolter, M. (2015). Endothelial cell self-fusion during vascular pruning. *PLoS Biol.* **13**, e1002126.
Levayer, R. and Lecuit, T. (2012). Biomechanical regulation of contractility: spatial control and dynamics. *Trends Cell Biol.* **22**, 61-81.
Morais-de-Sá, E. and Sunkel, C. (2013). Adherens junctions determine the apical position of the midbody during follicular epithelial cell division. *EMBO Rep.* **14**, 696-703.
Nakajima, Y.-I., Meyer, E. J., Kroesen, A., McKinney, S. A. and Gibson, M. C. (2013). Epithelial junctions maintain tissue architecture by directing planar spindle orientation. *Nature* **500**, 359-362.
Phng, L.-K., Gebala, V., Bentley, K., Philippides, A., Wacker, A., Mathivet, T., Sauteur, L., Stanchi, F., Belting, H.-G., Affolter, M. et al. (2015). Formin-mediated actin polymerization at endothelial junctions is required for vessel lumen formation and stabilization. *Dev. Cell* **32**, 123-132.
Ponti, A., Schwarb, P., Gulati, A. and Bäcker, V. (2007). Huygens remote manager. *Imaging Microsc.* **9**, 57-58.
Rosenblatt, J., Cramer, L. P., Baum, B. and McGee, K. M. (2004). Myosin II-dependent cortical movement is required for centrosome separation and positioning during mitotic spindle assembly. *Cell* **117**, 361-372.
Sauteur, L., Krudewig, A., Herwig, L., Ehrenfeuchter, N., Lenard, A., Affolter, M. and Belting, H.-G. (2014). Cdh5/VE-cadherin promotes endothelial cell interface elongation via cortical actin polymerization during angiogenic sprouting. *Cell Rep.* **9**, 504-513.
Siekmann, A. F. and Lawson, N. D. (2007). Notch signalling limits angiogenic cell behaviour in developing zebrafish arteries. *Nature* **445**, 781-784.
Wacker, A. and Gerhardt, H. (2011). Endothelial development taking shape. *Curr. Opin. Cell Biol.* **23**, 676-685.
Westerfield, M. (2007). The Zebrafish Book. A Guide for the Laboratory Use of Zebrafish (Danio rerio), 5th Edition. University of Oregon Press, Eugene.
Yamada, S. and Nelson, W. J. (2007). Localized zones of Rho and Rac activities drive initiation and expansion of epithelial cell cell adhesion. *J. Cell Biol.* **178**, 517-527.
Zeng, G., Taylor, S. M., McColm, J. R., Kappas, N. C., Kearney, J. B., Williams, L. H., Hartnett, M. E. and Bautch, V. L. (2007). Orientation of endothelial cell division is regulated by VEGF signaling during blood vessel formation. *Blood* **109**, 1345-1352.

Part II: Characterizing the vascular lumen invagination process: vesicle/membrane trafficking & subcellular events in sprouting angiogenesis

5 Introduction

5.1 Morphological changes during lumen formation in the zebrafish vasculature

Another key step during sprouting angiogenesis in addition to anastomosis is the development of interconnected luminal space, which allows blood flow circulation. However, it has not been demonstrated yet what is the origin of the vascular lumen during angiogenic sprouts.

Two different lumen formation models in the vasculature have been proposed: cell hollowing and cord hollowing (Figure 8 A, B). The cell hollowing model was suggested as a major mechanism in vascular lumen formation (Davis and Camarillo, 1996; Kamei et al., 2006). According to the cell-hollowing model (Figure 8 (B)), endothelial cells form large intracellular vacuoles, which fuse with one another, giving raise to a seamless vascular lumen. Later, it was shown by *in vitro* studies that the pinocytosis pathway is involved in this formation (Davis and Camarillo, 1996). Similar large luminal spaces have been reported *in vitro* in HUVEC culture (Childs et al., 2002). Furthermore, a recent study (Yu et al., 2015) shows that during sprouting angiogenesis, small membrane vesicles coalescence into larger membrane structures, which could be representative

of vacuoles. Nonetheless, the study lacks the demonstration of whether large membrane structures contribute to the lumen expansion process.

However, other studies have indicated that cord hollowing (Figure 8 (A)) is the major mechanism of vascular lumen formation (Blum et al., 2008b; Herbert et al., 2009; Jin et al., 2005; Parker et al., 2004; Strilić et al., 2009). In the cord hollowing model, when two cells make a contact, they initiate junction formation at the contact site and eventually deposit the apical membrane components via vesicles, which contribute to expanding the membrane surface for lumen formation. In addition to these models, a new model has been proposed: The "plasma membrane invagination model" (Herwig et al., 2011). A single endothelial cell can generate an internal lumen when an apical membrane invaginates and extends towards the interior of the cell. In the plasma membrane invaginating model, blood pressure pushes through an already-existing lumen into another cell and extends the continuity of the lumen. Lumen formation in sprouting angiogenesis was investigated with different tools including membrane, cytoskeleton and junctional markers (Blum et al., 2008b; Herwig et al., 2011; Lenard et al., 2013) and they reported lumen formation through cord hollowing and apical membrane (lumen) invagination processes (Figure 8 (C)) *in vivo*. Additionally, a recent study also supports the lumen invagination process *in vivo*, demonstrating lumen expansion during sprouting angiogenesis by using a membrane tagged marker expressed in vasculature (Gebala et al., 2016).

Membrane invagination requires new materials to feed the apical lumen extension process. However, it is not known yet how the lumen extends

during the lumen invagination process. It is important to dissect potential mechanisms such as endosome trafficking that might deliver the needed material to the apical compartment.

Together, current understanding *in vivo* suggests that the cord hollowing mechanism creates a *de novo* lumen at the two cell contact side. Eventually, the *de novo* formed lumen connects with the rest of the vasculature either by plasma membrane invagination in the presence of blood pressure or by junctional rearrangements in the absence of blood pressure (Herwig et al., 2011; Lenard et al., 2013). However, a recent study suggests, similar to endothelial cell culture experiments, that *de novo* lumen appears through the mechanism of vacuoles fusion *in vivo* (Yu et al., 2015).

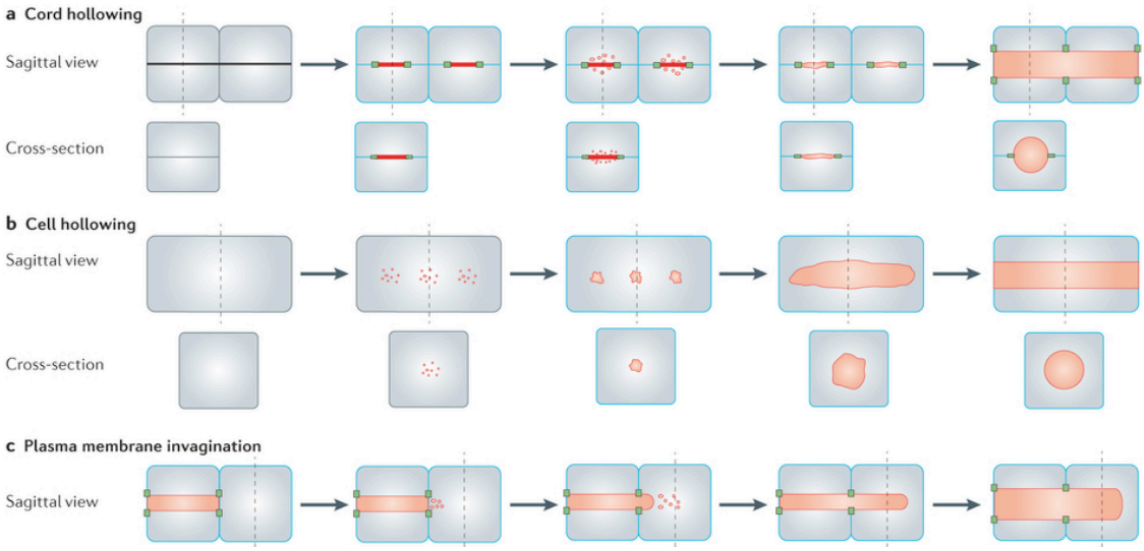

Figure 8: Morphological mechanisms of lumen formation
(**A**) In cord hollowing, the lumen forms at the contact surface between cells. Vesicles, delivered by exocytosis, fuse to the apical membrane at the cell-cell contact side and increase the membrane surface area by delivering fluids and other materials that are required for lumen expansion. Eventually

adjacent lumens connect and form a continuous lumen. (**B**) In cell hollowing, vesicles fuse to vacuoles and vacuoles fuse with one another to form a continuous lumen. The difference from cord hollowing is that these vesicles are not delivered to the plasma membrane but rather they fuse within the cytoplasm. (**C**) In plasma membrane invagination, an already-existing apical membrane extends by adding membrane material to invaginating lumen with vesicle delivery (Sigurbjornsdottir et al., 2014).

5.1.1 Lumen formation steps

The lumen formation process can be categorized into 4 different steps: positioning, growth, maintenance or structuring and maturation of the lumen.

The first step consists of positioning the site, where the new space will appear by adding new membrane material through the plasma membrane. For example, when two endothelial cells contact each other, apical cell polarity is established at the cellular intersection and eventually, a lumen starts forming. The site at which the lumen will be formed is determined through direct cell-cell interactions *in vivo* (e.g. zebrafish) or interactions with ECM *in vitro* (e.g. Madin–Darby canine kidney (MDCK) cells). For example, β1-integrin in MDCK cells is necessary to initiate polarization, and a lack of β1-integrin results in an absence of lumen (O'Brien et al., 2001; Yu et al., 2008). In vitro studies show that cells require the integrin to bind the ECM, which then induces the initiation of intracellular vacuole formation downstream of ECM-integrin interactions, resulting in the activation of cytoskeletal regulators (e.g. ARP2/3). In addition, when the apical membrane initiation site (AMIS) is determined at the patch of contact surface, apical membrane material or apical polarity proteins are delivered to form the platform of apical polarity determinants such as podocalyxin

(reviewed in Apodaca et al., 2012; Martin-Belmonte and Mostov, 2008). Small GTPases (e.g. RAB11A), which might regulate vesicle/membrane trafficking, are associated with apical polarity proteins such as PAR3, CDC42 and CRB (Bryant et al., 2010).

In summary, transmembrane proteins (e.g. E-cadherin or integrin) become activated through interaction with the microenvironment via either direct cell-cell contact or cell ECM contact. This results in intracellular signaling cascade activation that then leads to cytoskeletal rearrangements, which are necessary to deliver apical determinants to the lumen initiation site (reviewed in Sigurbjörnsdóttir et al., 2014).

The second step is the growth initiation, in which polarized trafficking plays a role to deliver needed materials towards the apical membrane in order to generate and expand a new luminal space. The secretory pathway is involved in supplying CRB or podocalyxin to the AMIS. However, in the lumen growth stage, vesicular transport of large amount of membrane materials is needed. For this, the vesicle transport machinery together with the cytoskeleton guide the delivery of vesicles, and thus play a crucial role to managing the lumen expansion process properly (Gervais and Casanova, 2010).

Lumen growth occurs very rapidly in angiogenic sprouts. This raises a concern: cells cannot provide all needed material via the secretory pathway since the lumen invagination might be very rapid due to the blood pressure. However, a role of vesicle/ membrane trafficking has not been investigated in detail, for example, and it is not known whether it provides a source of

needed materials to the invaginating lumen. This will be a scope of my second project.

Since lumen growth is dynamic, it needs correct shape formation. The third step is the structuring of the lumen into the correct shape with the help of cytoskeleton and other regulators. For example, blood pressure speeds up lumen invagination dramatically. To create a lumen, bringing apical membrane material per se is not sufficient. Extensive apical membrane growth has to be organized and structured in a spatial and temporal manner. Otherwise, new membrane will not form a lumen properly. Studies in *Drosophila* suggest that cytoskeletal tracks not only facilitate vesicle trafficking by acting as a guide for lumen formation, but also might give physical support and to structure extensively in the growing lumen (Lee and Kolodziej, 2002). However, the role of the cytoskeleton constructing the luminal plasma membrane is still unclear.

The fourth step is the maturation of lumen growth in a spatial and temporal regulated manner to attain physiological function. Maturation covers lumen expansion to generate the proper diameter, stabilizing the structure and equilibrate the system to fulfill the requirements of physiological purpose. Two mechanisms are known to have a role in lumen inflation: one is depositing anti-adhesive molecules and the second is creating a turgor pressure. For example, the deposition of podocalyxin at the apical membrane creates negative charges, which then force luminal membranes to go apart (Meder et al., 2005). In addition, inducing the turgor by activation of apical channels and pumps is another way of enlarging the luminal space (Bagnat

et al., 2007; Bryant and Mostov, 2008). The secretory machinery also can induce expansion of the initial lumen by bringing various molecules and remove the fluid from the luminal space in *Drosophila* trachea (Tsarouhas et al., 2007).

Recent studies have shown that the apical membrane invagination mechanism most likely contributes to lumen formation during sprouting angiogenesis in zebrafish; however, it needs further investigation to understand the processes driven by intrinsic and extrinsic factors. From the vesicle/ membrane trafficking point of view, it has not been well understood yet how plasma membrane invagination is regulated at the cellular and molecular level during sprouting angiogenesis *in vivo*. Here, we focus to investigate the relationship between vesicle/membrane trafficking dynamics and apical membrane invagination or lumen expansion processes in sprouting angiogenesis.

5.2 Dissecting the cellular and subcellular events in blood vessel lumen formation and expansion

5.2.1 Vesicle/membrane trafficking

Vesicles are small structures, consisting of fluid enclosed by a lipid bilayer inside the cell. They naturally form during the process of secretion (e.g. exocytosis), uptake (e.g. phagocytosis and endocytosis), and transport of materials within the cytoplasm. Vacuoles, lysosomes, transport vesicles, secretory vesicles and extracellular vesicles represent some vesicle examples. Rab GTPases regulate many steps in membrane traffic such as vesicle formation, vesicle movement along cytoskeleton and membrane

fusion. The Rab family of GTPases is a member of the Ras superfamily and acts as molecular switches, based on oscillations between GTP- and GDP-bound forms, regulating membrane and protein trafficking. GDP/GTP exchange factors (GEF) activate the Rabs by inducing an exchange from GDP-bound to GTP-bound forms (Figure 9). Rabs are peripheral membrane proteins and bound to the cytosolic part of a specific intracellular membrane via prenyl groups on two cysteines in the C-terminus, which facilitate communication between membrane structures by interactions between specific Rabs and their effector proteins that help formation, motility and tethering of vesicles in and between membrane-bound organelles.

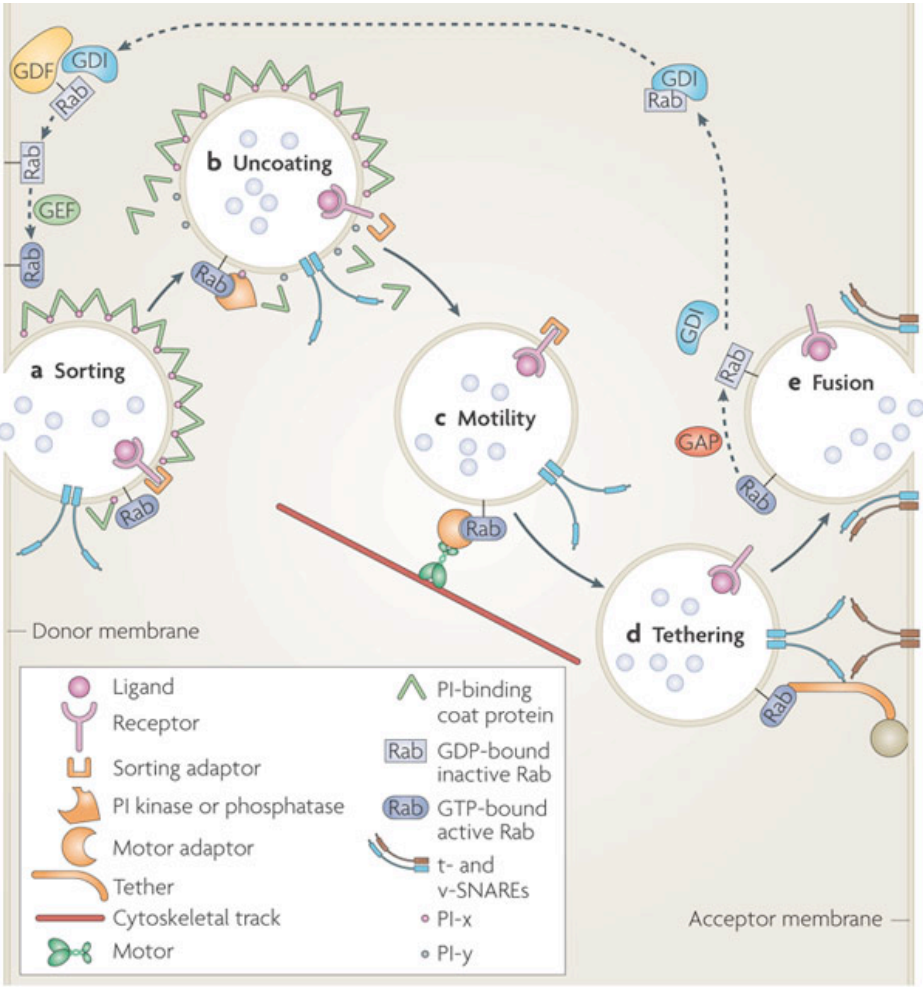

Figure 9: Membrane trafficking steps
Membrane trafficking is a multi step process and controlled by a Rab GTPase and its effector proteins (orange color). (**a**) A sorting adaptor can be activated by an active GTP-bound Rab to sort a receptor into a budding vesicle from plasma membrane. (**b**) Phosphoinositide (PI) kinases or phosphatases are recruited to vesicle membrane and the PI composition of a transport vesicle might be changed (conversion of PI-x into PI-y), which cause uncoating through the dissociation of PI-binding coat proteins. (**c**) Rab GTPases can mediate vesicle transport along cytoskeleton (e.g. actin filaments or microtubules) by recruiting motor adaptors or by binding directly to motor proteins. (**d**) Rab GTPases can mediate vesicle tethering by recruiting tethering factors, which interact with molecules in the acceptor membrane. For example, tethering factors might interact with SNAREs and their regulators to activate SNARE complex formation that helps in membrane fusion. (**e**) After membrane fusion and exocytosis, the Rab GTPase is converted to its inactive GDP-bound form through hydrolysis of GTP, which is stimulated by a GTPase-activating protein (GAP) (Stenmark et al., 2009).

More than 65 *rab* genes have been identified with distinct functions and localizations patterns in vertebrates (Zhang et al., 2007). There is a high degree of functional conservation for specific Rab proteins from yeast to humans.

Due to their established localization and functions as well as the conservation across evolution, Rab5c (early), Rab7 (late), and Rab11a (recycling) representing well characterized markers for their respective vesicles were chosen to study the vesicle/membrane trafficking during lumen invagination in sprouting angiogenesis. In this thesis, I focus on a transient overexpression of Rab5c (early endosome), Rab7 (late endosome),

and Rab11a (recycling endosome trafficking) during lumen invagination process in sprouting angiogenesis at zebrafish embryos.

RAB5 was first identified in neuroendocrine tumor cells, in a screen to analyze homologous genes to yeast *sec4*. Initially, RAB5 localization was associated with membrane and vesicle structures. From electron microscopy, it was demonstrated that RAB5 was localized on early endosomes, on the cytoplasmic side of the plasma membrane (Chavrier et al., 1990; Gorvel et al.,1990). Multiple studies indicated that RAB5 functions in vesicle transport and regulates a variety of receptor-mediated signaling pathways. For example, studies in zebrafish have indicated that Rab5c is involved in the regulation of both the FGF and Wnt signaling pathway and interferes with E-cadherin endocytosis via a Wnt11-dependent pathway (Nowak et al., 2011; Tay et al., 2010; Ulrich et al., 2005). Most vertebrates have 3 paralogs of Rab5, however in zebrafish there are additional *rab5* genes. In total, Rab5a, Rab5aa, Rab5b are ubiquitously expressed in zebrafish. As Rab5c expression is enriched in the vasculature (Clark et al., 2011; Thisse et al., 2004), we chose Rab5c as a candidate to study early endosome trafficking during sprouting angiogenesis

RAB7 was first identified in Buffalo rat liver cells, in a screen to analyze homologous genes to *ras* and *ras*-related genes (Bucci et al., 1988). Later, RAB7 was identified as a member of the Rab family. Immuno-electron microscopy and marker colocalization observations have shown that RAB7 localizes to vesicle structures, which have been identified as late endosomes (Chavrier et al., 1990). Other functional studies have demonstrated that RAB7-tagged vesicles are involved in degradation and biogenesis of

lysosomes (Feng et al., 1995). Additionally, RAB7 functional studies are associated with severe disease outputs in such cancer, neuropathy and lipid metabolism syndromes (Zhang et al., 2009). *Rab7* is the only homolog in zerbrafish and this gene was chosen as a late endosomal marker, with distinct pattern and function. There are some hypothetical proteins that share significant homology with Rab7, suggesting that zebrafish might have other Rab7 paralogs (Clark et al., 2011; Thisse et al., 2004). Previous research in zebrafish showed that notochord vacuoles formation (biogenesis and maintenance) requires late endosomal trafficking and Rab7 is the classical regulator of the late endosomes (Ellis et al., 2013). For this reason, we have chosen Rab7 as a candidate to study late endosomal trafficking during the lumen invagination process in sprouting angiogenesis.

RAB11 was first identified in MDCK cells in a screen to analyze transcripts homologous to yeast YPT1/SEC4 (Chavrier et al., 1990). RAB11 localization was observed in recycling compartments/endosomes from immunofluorescent images. For example, over-expressing RAB11 showed co-localization with transferrin receptor at the membrane surface (Ullrich et al., 1996). Previous research has suggested that Rab11a is needed for lumen formation and apical trafficking in MDCK cells and *Drosophila* embryos, showing that apical trafficking of Rab11a-positive endosomes needs microtubules (MTs) for the movement *in vitro*. Similarly, it was demonstrated that the MT cytoskeleton serve as railroads for vesicle trafficking. For example, Rab11a-tagged vesicles move along MTs and are required for lumen formation during neural rod development in zebrafish (Buckley et al., 2012). Furthermore, RAB11 was implicated maintaining apical adherens junctions and in regulating a variety of signaling pathways.

Although many vertebrates only have a single *rab11* gene, zebrafish has four paralogs; *rab11a, rab11a-like, rab11ba*, and *rab11bb* (Clark et al., 2011; Thisse et al., 2004). Rab11a is expressed ubiquitously and a well-studied paralog of *Drosophila* RAB11. Since we previously generated Rab11bb construct to study the localization and dynamics in vasculature (unpublished data), we have chosen Rab11a as another representative of recycling endosomes.

In *Drosophila*, N-terminally tagged fluorescent Rab proteins were generated for nearly all Rabs to investigate their function *in vivo*. Recently, all 27 Rabs have been endogenously tagged with fluorescent proteins to exclude overexpression-generated artifacts, which resolved the precise localization of Rabs (Dunst et al., 2015). In vertebrates, however, Rab-based endosome biology is, to a large extend, still limited to cell culture.

Strikingly, our observations from the CAAX-mCherry transgenic zebrafish line showed that some vesicle-like structures appear, move in the cytoplasm and some dissolve on the invaginating lumen, suggesting that these structures might be exocytotic vesicles. Based on this observation, our curiosity in endosome biology increased. To study lumen dynamics, we used a CAAX-mCherry transgenic zebrafish line. The CAAX motif (C: cysteine, A: aliphatic amino acid and X: any amino acid) is attached to Ras protein (H-Ras, in this case) and X is defining the prenylation of C (cysteine residue) with farnesylation (15C) or geranylgeranylation (20C). Prenylation domain is integrating into lipid bilayers and H-Ras protein that linked to membrane with prenylation stays in the cytoplasm visualized by a tagged fluorescent protein. The CAAX represents a post-translational modification

motif that undergoes three consecutive enzymatic reactions: polyisoprene lipid chain addition to the cysteine residue, the cleavage of the AAX domain and methyl group addition at the C-terminus of the protein. This modifications lead to a hydrophobic domain formation, which provide affinity for lipid bilayers (Wright and Philips, 2006). Therefore, CAAX carries and anchors any fused protein of interest to the peripheral membrane by prenylation, allowing visualization of the apical and basal membrane, which was also applied in previous studies (Gebala et al., 2016; Lenard et al., 2013).

From the literature, we found that in 2011, ubiquitously expressed N-terminal EGFP fused Rab5c, Rab7 and Rab11a transgenic zebrafish lines were created and validated to investigate localization and dynamics of endosome biology during development in neural retina and hind brain (Clark et al., 2011).

Taking a step further, we have ordered the same constructs and re-cloned them under the vascular specific promoter *fli1ep* to investigate cellular and sub-cellular vascular events. More specifically, we wanted to observe the localization and dynamics of endosomal trafficking during the lumen invagination process to see whether their localization and dynamics might correlate with the lumen expansion process. For this, we applied high spatio-temporal resolution microscopy in order to resolve the Rabs' localization and dynamics. Recently, it was shown in *Drosophila* that Rab11, Rab39 and large lysosomal vesicles were involved in anastomotic tube fusion events in tracheal development (Caviglia et al., 2016). We were encouraged from the *Drosophila* tracheal tube research, indicating the importance of endosomal

trafficking at the fusion process, which raises the question whether similar endosomal pathways play a role during lumen formation in sprouting angiogenesis (Figure 10). Similarly, we want to find out what Rabs with distinct function and distribution pattern might regulate the lumen invagination process in sprouting angiogenesis (Figure 11).

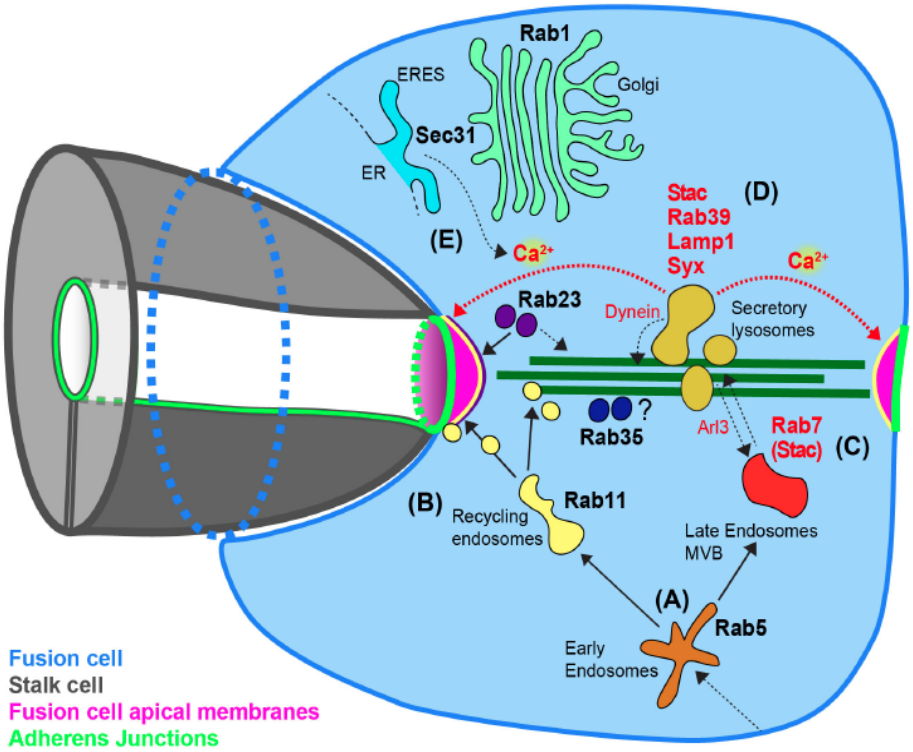

Figure 10: Tracheal tube formation
A tracheal tip cell (gray: cell body, white: tube) contacted with another tip cell (blue). Apical membrane compartments (magenta color) at the contact interface represent the growing part of the tube. Microtubules are positioned in between the apical membrane compartments (green) facilitating trafficking. Endosomal vesicle trafficking contributes tube extension (e.g. Rab11, Rab23 and Staccato) (Caviglia et al., 2014).

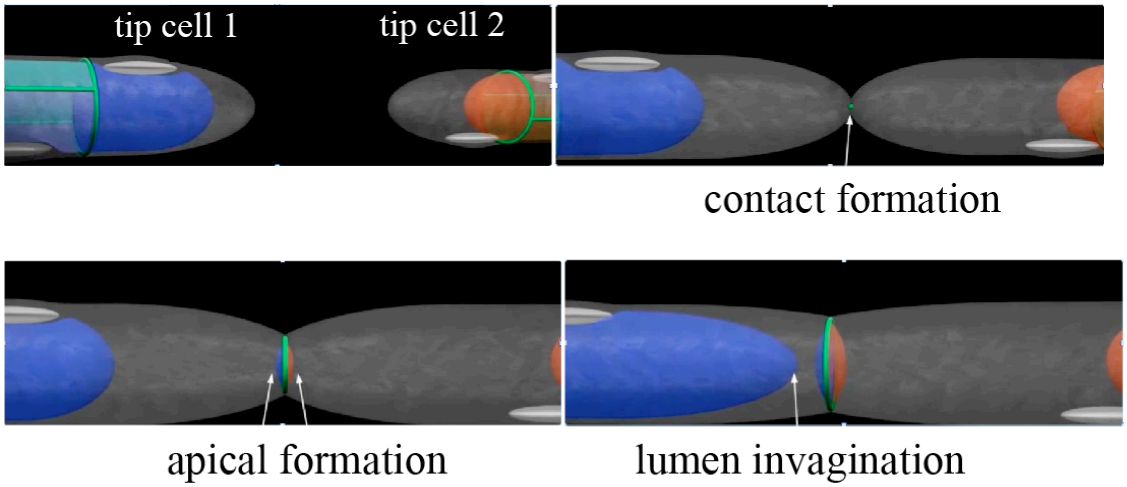

Figure 11: Anastomosis and lumen invagination process.
Two tip cells come in close contact (gray color), lumens inside (blue and orange color) and junctions (green color). Tip cells contact one another and junctions were deposited at the connection site. Polarization is taken place (orange and blue) and junctions are in ring shape (green). Lumen invaginates (blue) from left to right.

5.3 Aim of the lumen invagination project

Here, we aim to visualize the localization and dynamics of vesicle/membrane trafficking during apical lumen compartment invagination, a process of lumen expansion during sprouting angiogenesis. For this purpose we designed EGFP-fused Rabs, tagging early, late and recycling endosomes to visualize dynamics of subcellular vesicular trafficking. We transiently characterized and used distinct Rabs with different function and localization patterns. This approach will allow, for the first time, the visualization of specific sub-fractions of vesicle/membrane trafficking during vascular lumen growth and investigate their function.

In summary, the visualization of vesicle/membrane trafficking during lumen invagination will allow us to:

(1) Investigate the subcellular distribution of EGFP:Rabs; Rab5c-early endosome, Rab7-late endosome and Rab11a-recycling endosome during lumen invagination

(2) Assess the contribution of early, late or recycling endosomal pathways to the lumen invagination process.

Moreover, the characterized and differentially localized Rabs will provide a novel tool-set to gear up the studies in order to understand the lumen expansion process in a novel way.

6 Materials and Methods

6.1 Cloning of plasmids

Initially, plasmids were cloned downstream of a 4 times non-repetitive (4xnr) UAS (upstream activation sequence), which is driven by the Gal4 transcription factor (Akitake et al., 2011). Since there is a risk of silencing transgenic DNA due to the repetitive sequences, less non-repetitive sequence such as 4xnr compared to 15xnr reduces the silencing over generations.
To increase target efficacy of mRNAs to ribosomes, Kozak sequence, ACC, was introduced in the upstream of the translation the constructs before ATG site. Further to design a plasmid, it is critical to contain a SV40 (Simian virus 40) terminator sequence at the end of the coding sequence because SV40 sequences terminates transcription and poly-adenlylates mRNA by adding polyA tail. Lastly, to promote trangenesis, all plasmids were flanked by Tol2 transposable element site, which is needed for Tol2 transposase-dependent genome integration (Asakawa et al., 2008; Kawakami et al., 2000).

6.2 Transgenesis

DNA plasmids were designed including promoter region (e.g. *fli1ep*), coding fluorescent protein (e.g. EGFP, mcherry etc.) and coding DNA sequence (e.g. *rab5c*) and regulatory elements if needed. The plasmids were cloned with using the Multisite Gateway system (Life Technologies) into destination vectors (e.g. pDestTol2CG2) from the Tol2Kit (Kwan et al.,

2007). The plasmids were injected together with Tol2 transposase RNA to improve transgenesis (increasing genome insertion) into one cell stage eggs of Tg(*kdrl*:mCherry:CAAX) (Lenard et al., 2013). In the following day, at 1dpf the embryos were manually dechorionated by forceps and screened under the fluorescent binocular for a transient expression. Embryos that expressed the plasmids, visualized by a transgenesis marker (e.g. cmlc-eGFP, a heart marker) were raised to adulthood. After 3 months, grown fish were crossed out to wild-type fish to screen for germline transmission. The F1 offspring was then screened for positive expression again and the ones with the strongest expression were selected under fluorescent binocular and raised to adulthood for transgenic expression.

6.3 Cloned Plasmids

The *fli1ep* promoter (ordered from ADDGENE) was used to drive endothelial expression. *rab5c, rab7* and *rab11a* 3`entry clones were ordered from ADDGENE (Clark et al., 2011). Tg(*Fli1ep*:eGFP-*rab5c*), Tg(*Fli1ep*:eGFP-*rab7*), and Tg(*Fli1ep*:eGFP-*rab11a*) constructs were generated with the Gateway cloning system (Life technologies). For transient expression, 30-100 nM plasmid injections were performed at the single cell stage and survived embryos were picked. Positive embryos were selected at 2 dpf (days post-fertilization) for high expression under fluorescent binoculars. Selected embryos were further imaged either by confocal or spinning disk microscopies.

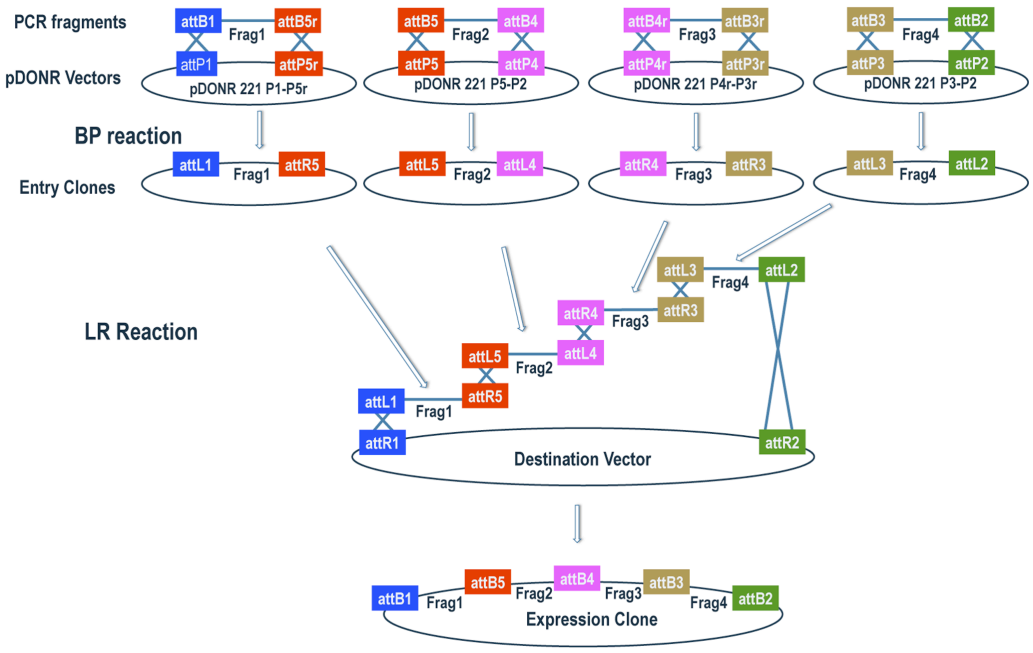

Figure 12: Three-fragment Gateway cloning.
Multiple fragments were amplified with PCR using primers that incorporate flanking sites (e.g. attB1, attB5r). In the BP reaction these fragments were combined with donor vectors. In the LR reaction these three entry clones were combined with a destination vector to produce an expression clone containing all three fragments in a specific orientation (the figure was taken from (Petersen and Stowers, 2011). For example, fragment 1 represents 4xUAS or *fli1ep* (promoters), fragment 2 represents non-stop EGFP and fragment 3 represents rabs (*rab5c*, *rab7* and *rab11a*).

6.3.1 Cloning of the EGFP-*rab5c* construct

To generate pT2_4xUAS:EGFP:*rab5c* plasmid, isolated pDEST-destination vector, p-5`entry clone (4xUAS), p-middle entry clone (EGFP) and p-3`entry clone (*rab5c*) were put together with LR clonase at 25°C for 16 hours (Figure 13). Later, the mix pladmids were electroporated. Injected plasmid expression was too high, which was all over the cytoplasm.

To reduce the expression, the 4xUAS promoter was changed to a *fli1ep* promoter. For this, the same strategy was applied to generate *fli1ep*:EGFP-

rab11a plasmid. Finally, the plasmid was sequenced in both cases to ensure correct sequence. Map of the expression clone is provided below.

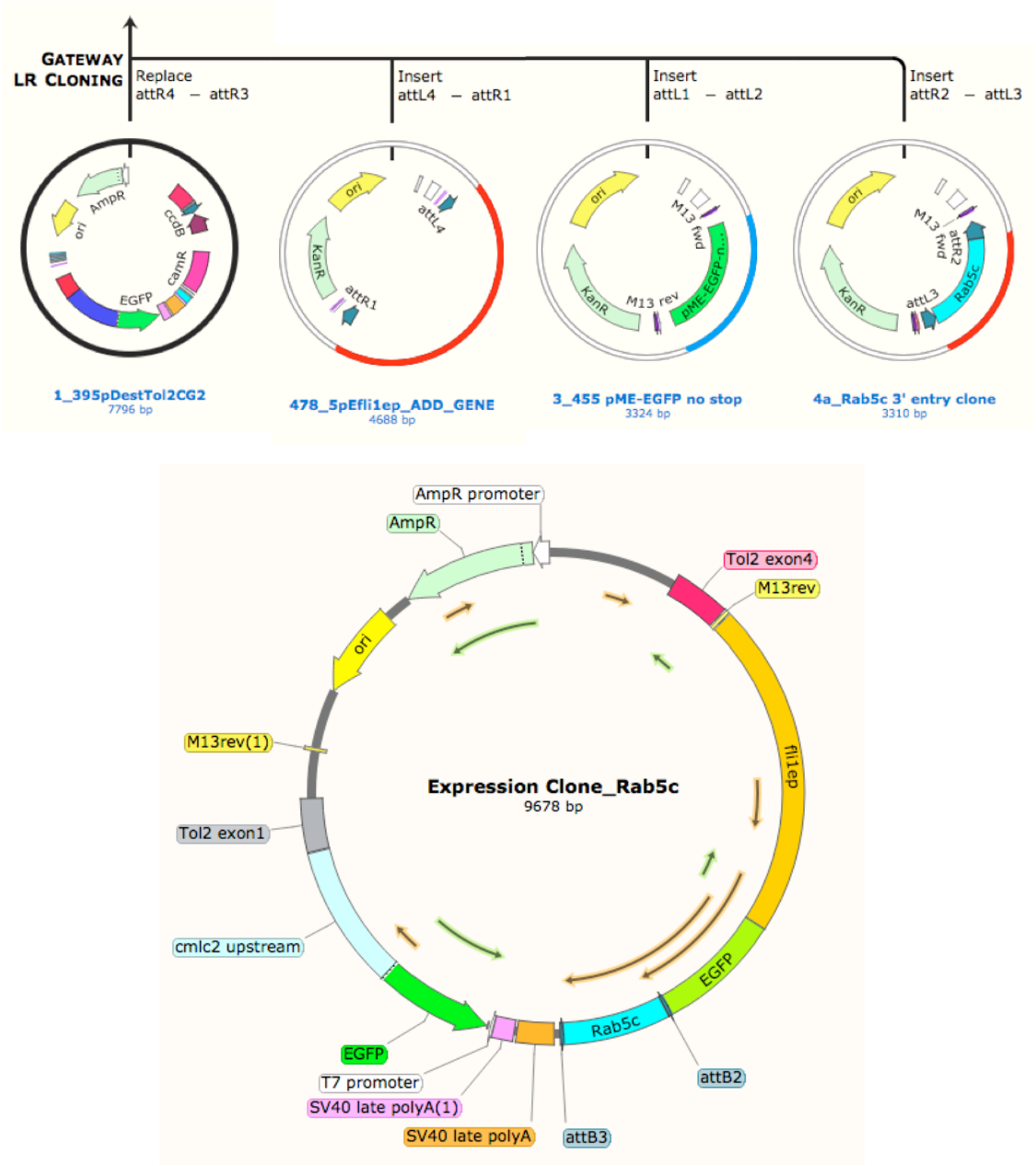

Figure 13: Schematic Gateway cloning steps and *fli1ep*:EGFP:*rab7*
Four modules are represented from snapgene software. (1) Destination vector. (2) Fli promoter. (3) non-stop EGFP and (4) *rab5c* entry clones. With LR clonase, four modules are combined and full construct represented as Expression Clone_Rab5c (*fli1ep*:EGFP:*rab5c*).

6.3.2 Cloning of the EGFP-*rab7* construct

To generate pT2_4xUAS:EGFP:*rab7* plasmid, isolated pDEST-destination vector, p-5`entry clone (4xUAS), p-middle entry clone (EGFP) and p-3`entry clone (*rab7*) were put together with LR clonase at 25°C for 16 hours. Later, the mix pladmids were electroporated. Injected plasmid expression was too high, which was all over the cytoplasm.

To reduce the expression, the 4xUAS promoter was changed to a *fli1ep* promoter. For this, the same strategy were applied to generate *fli1ep*:EGFP:*rab11a* plasmid (Figure 14). Finally, the plasmid was sequenced in both cases to ensure correct sequence.

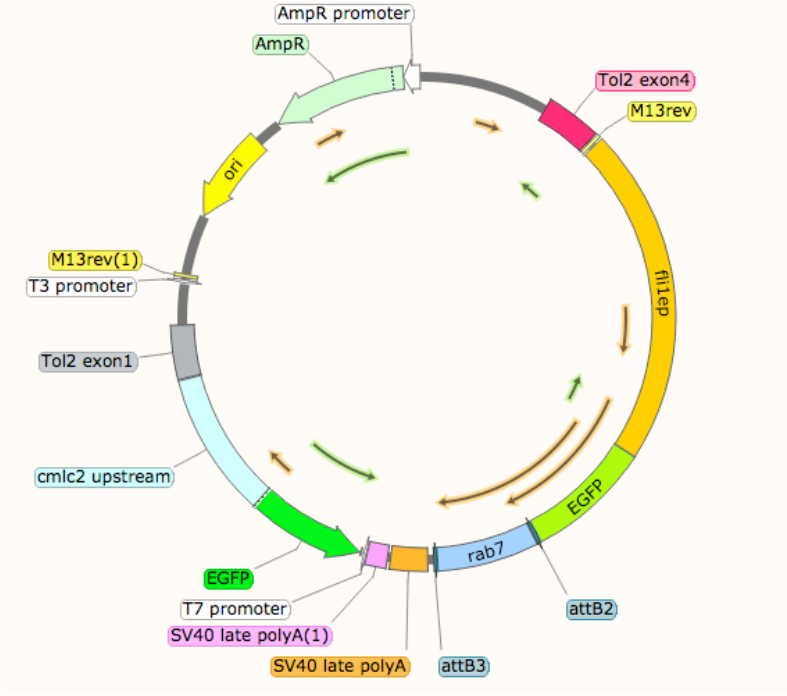

Figure 14: Full construct represented as *fli1ep*:EGFP:*rab7*.

6.3.3 Cloning of the EGFP-*rab11a* construct

To generate pT2_4xUAS:EGFP:*rab11a* plasmid, isolated pDEST-destination vector, p-5`entry clone (4xUAS), p-middle entry clone (EGFP) and p-3`entry clone (*rab*11a) were put together with LR clonase at 25°C for 16 hours. Later, the mix pladmids were electroporated and selected by mini and midi preps. Ready plasmids were injected into a single cell stage of egg. Injected plasmid expression in vasculature was too high, which was all over the cytoplasm.

To reduce the expression, the 4xUAS promoter was changed to a *fli1ep* promoter. Therefore, the same strategy were applied to generate *fli1ep*:EGFP:*rab11a* plasmid (Figure 15). Finally, the plasmid was sequenced in both cases to ensure correct sequence.

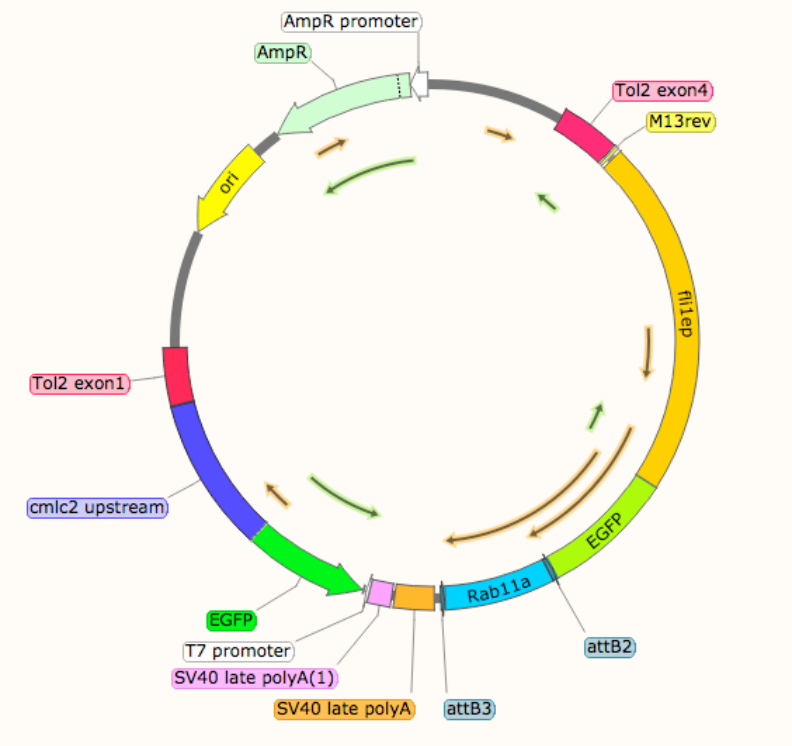

Figure 15: Full construct represented as *fli1ep*:EGFP:Rab11a.

6.3.4 Cloning of the EGFP-*rab35* plasmid

To generate pT2_4xUAS:EGFP:*rab35* plasmid, the two plasmids 3`E p_Rab35-NT and pT2_4xUAS:eGFP:*rab11bb* were digested with BsRGI (NEB) and Xhol (NEB), cutting out Rab11bb sequence out and generating sticky sequence for both p_Rab35-NT and pT2_4xUAS:eGFP plasmids that form pT2_4xUAS:eGFP:*rab35* plasmid via homologous recombination. Individual fragments were dephosphorylated and run on the gel electrophoresis. Later, extracted DNA fragments were ligated. Finally, the plasmid was sequenced to ensure correct sequence.

6.4 List of other transgenic fish lines

-Tg(*fli1ep*:GAL4FF)^{UBS3}, (UAS:RFP), (UAS:EGFP-ZO-1)^{UBS5}
-Tg(*fli1ep*:GAL4FF)$^{UBS2-4}$, (UAS:mRFP), (UAS:VE-cadherinΔC-EGFP)^{ubs12}
-Tg(fli1ep:GAL4FF)^{ubs3}; (UAS:mRFP); Tg(UAS:EGFP-UCHD)^{ubs18}
-*kdrl*:mKate2- CAAX
-*kdrl*:mCherry-CAAX^{ubs916}
-*kdrl*:H2B-GFP
-*kdrl*:EGFP:EB3
- *fli1ep*:GolT-mCerry

7 RESULTS

7.1 Visualization of lumen invagination and junctions

We imaged lumen invagination with cytoplasmic markers combined with ZO1 or Ve-cadherin junctional markers (Figure 16, 17). This allows us to visualize different cellular architectures including unicellular and multicellular tubes. We observed that lumen invagination occurs in unicellular tubes at the early stage of sprouting angiogenesis. For example, when two cells contacted each other, junctional material was deposited at the contact site (Figure 16 (A)). Lumen invagination started from a cell towards the neighboring cell (Figure 16 (B)). While the lumen growth reached the cell-cell contact site, junctional ring formed (Figure 16 (C-E)). Further, lumen pushed through neighboring cell and the nucleus was pushed on the site (Figure 16 (D)). Further, lumen invagination can also happen from both sides towards each other (Figure 17 (C)). Depending on the blood flow pressure, one invaginates always faster than another.

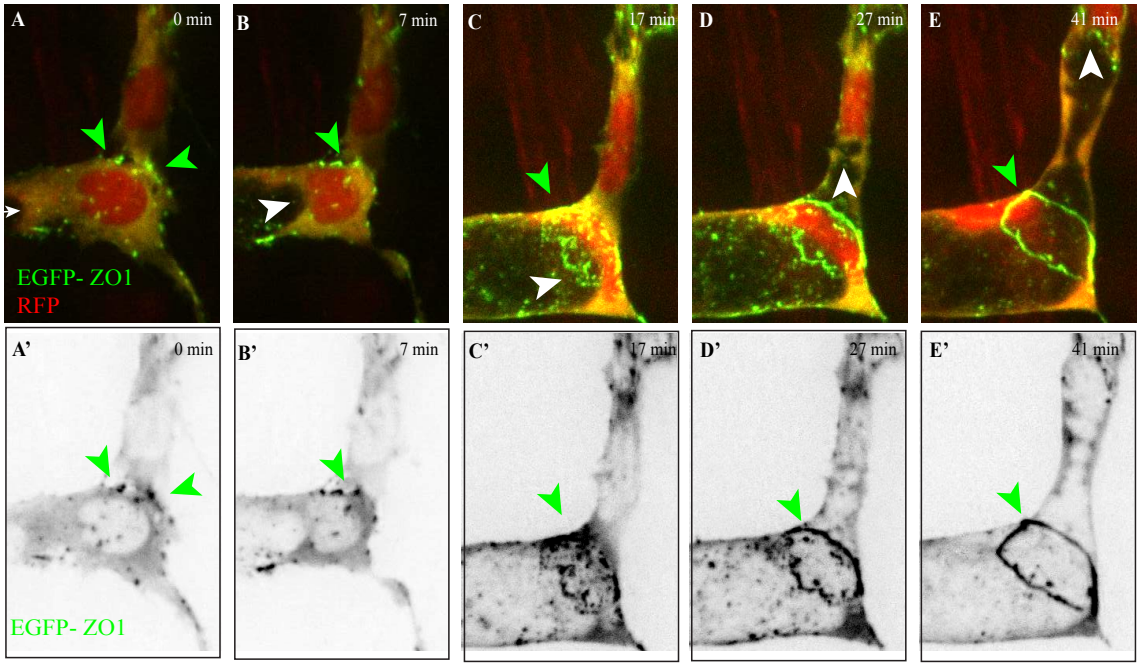

Figure 16: Lumen invagination process in newly contacted cells
(A-E) Still pictures from time-lapse movie S1, with highlighted ZO1 (EGFP-ZO1) and cytoplasm (RFP). The location of the lumen is apparent as a black zone bounded by cytoplasm, white arrowhead indicates the direction of lumen invagination, green arrowheads indicate the position of junctions. **(A)** Newly contacted two endothelial cells, junctions are deposited at the contact interface (green arrowheads). **(B)** Lumen invaginates from SA to DLAV (white arrowhead). **(C)** Junctions start forming ring shape (green arrowhead) and lumen invagination pushes nucleus. **(D)** Lumen invaginates into next cell (white arrowhead) and junctional ring becomes more structured. **(E)** Lumen invagination continuous in the neighboring cell (white arrowhead) and nucleus is pushed on the side. **(A'-E')** Still pictures correspond to those from panels A-E, showing only the green channel (grayscale). (In the schematic; green: ZO1, red: cytoplasm).

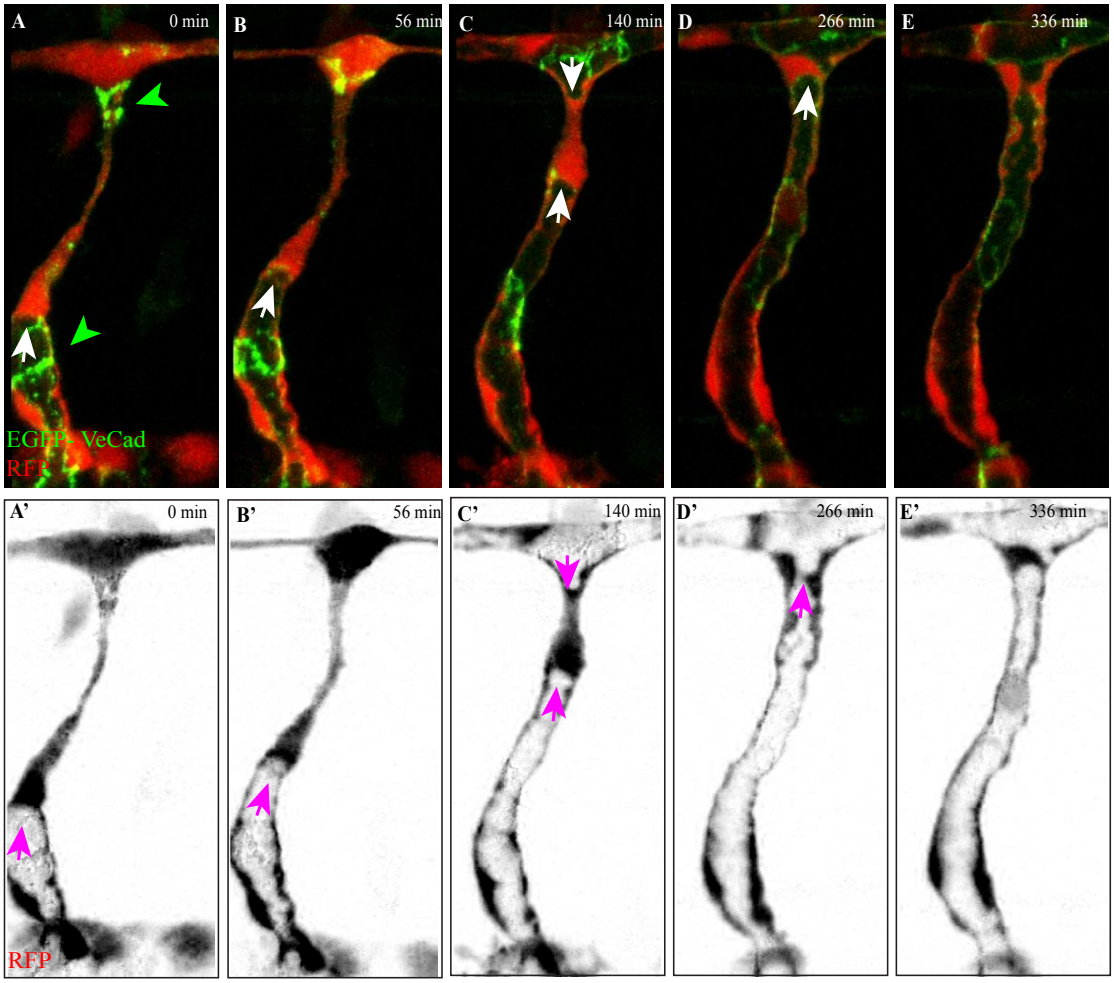

Figure 17: Lumen invagination process in unicellular tube
(A-E) Still pictures from time-lapse movie S2, with highlighted VeCadherin (EGFP-VeCad) and cytoplasm (RFP). The location of the lumen is apparent as a black zone bounded by cytoplasm, white arrows indicate the direction of lumen invagination, green arrowheads indicate the position of junctions. **(A)** Lumen invaginates from SA to DLAV to form unicellular tube (white arrows). **(B-E)** Lumen invagination continues from both sites (SA to DLAV and vice versa) (white arrows). **(A'-E')** Still pictures correspond to those from panels A-E, showing only the green channel (grayscale). (In the schematic; green: VeCad, red: cytoplasm).

7.2 Visualization of apical membrane compartment

In this study, we established high spatial and temporal resolution imaging in a CAAX-mCherry transgenic zebrafish line. In particular, this setup let us visualize both the endothelial cell membrane (basal) and the apical membrane compartment (lumen) within the endothelial cells in order to distinguish dynamic lumen growth from different cellular arrangements.

In comparison with the apical membrane fusion process in the *Drosophila* tracheal system (Caviglia et al., 2016), the apical membrane compartment of vascular endothelial cells is extremely dynamic due to the blood pressure changes (Gebala et al., 2016). By imaging the CAAX-mCherry transgenic zebrafish line, we observed that the lumen at the leading edge does not always grow continuously. It is rather that the apical compartments (lumen) in endothelial cells can break and fuse repeatedly during vascular sprouting depending on the pressure fluctuation (Figure 18).

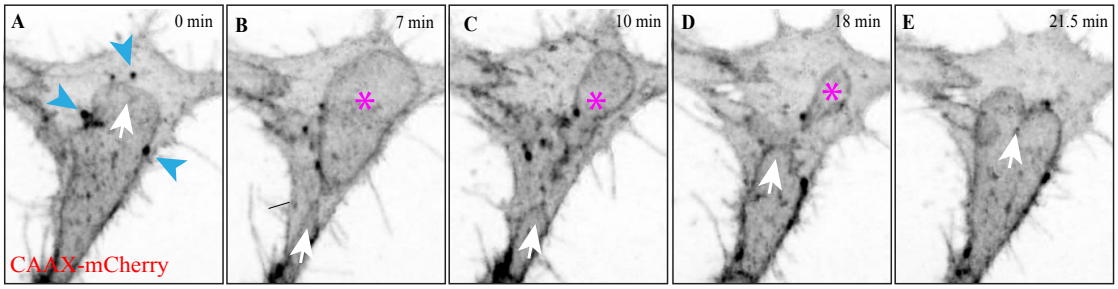

Figure 18: Lumen invagination dynamics
(A-E) Still pictures from time-lapse movie S3, with highlighted membrane (CAAX-mCherry). The location of the lumen is apparent as a gray zone bounded by cytoplasm, white arrows indicate the direction of lumen invagination, magenta asterisks indicate the collapsing of lumen and blue arrowheads indicate the approximate position of vesicle-like structures. **(A)** Lumen invagination into an endothelial cell from SA to DLAV (white

arrow), vesicle-like structures (blue arrowheads). **(B-E)** Invaginating lumen started to disintegrate into two parts and the upper part is collapsed in a while (asterisk). Eventually lumen starts invaginating from down again. (white arrow). (In the schematic; red: membrane).

7.3 Vesicle-like structures fuse with invaginating lumen

In addition, we showed that some vesicle-like structures ranging between 200-500 nm, labeled with CAAX-mCherry, form and move in the cytoplasm and eventually some dissolve into the growing apical membrane. We do not know from where these vesicle-like structures originate and to which destination they travel. However, we observed that sometimes, they dissolve (n=5; where n represents the number of the examined vessels) on the invaginating membrane (apical lumen compartment) (Figure 19). Based on these observations, we hypothesized that these vesicle-like structures are real vesicles.

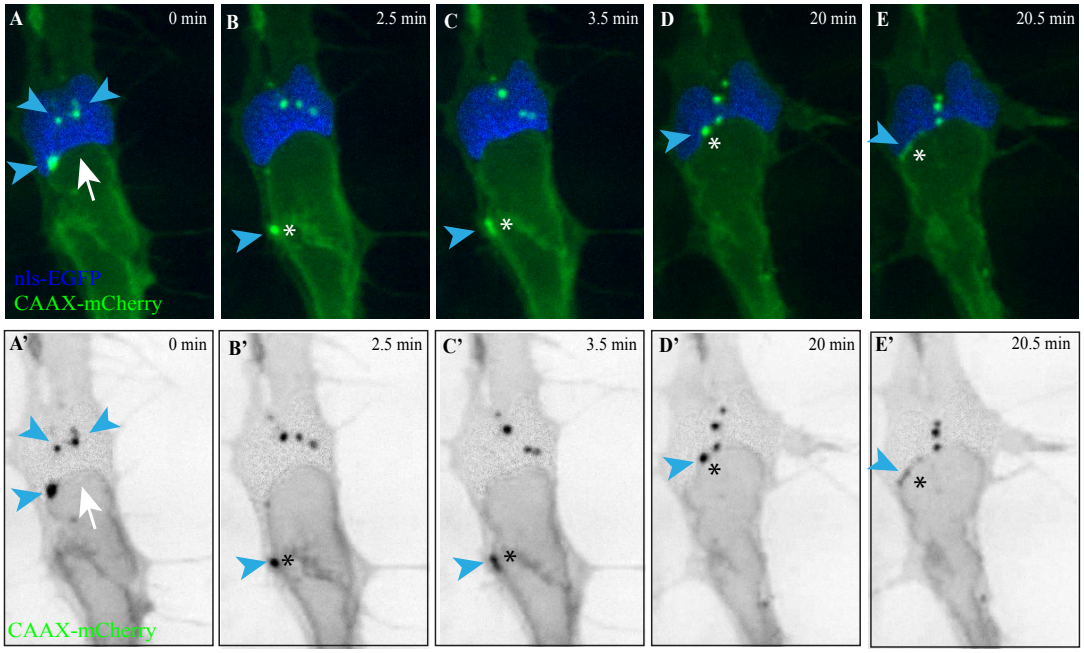

Figure 19: Vesicle-like structures and lumen invagination
(A-E) Still pictures from time-lapse movie S4, with highlighted nucleus (nls-GFP, blue color) and membrane (CAAX-mCherry, green). The location of the lumen is apparent as a gray zone bounded by cytoplasm, white arrows indicate the direction of lumen invagination, and blue arrowheads indicate the approximate position of vesicle-like structures originated from CAAX-mCherry line. **(A-C)** Lumen invagination into an endothelial cell at DLAV (white arrow), vesicle-like structures (blue arrow heads) appears and dissolve on the growing lumen lateral site (white astricks) . **(D-E)** Lumen invagination continues and vesicle-like structures dissolve at the front part of invaginating lumen (white astricks). **(A'-E')** Still pictures correspond to those from panels A-E, showing only the green channel (grayscale). (In the schematic; green: membrane, blue: nucleus).

7.4 Visualizing the localization and dynamics of early, late and recycling endosomes during the lumen invagination process

As a next level, we addressed the question whether vesicle/membrane trafficking correlates with the lumen invagination process. In the long term, we aim to identify the role of vesicle/membrane trafficking on building the apical membrane compartment during sprouting angiogenesis.

To address how vesicle/membrane trafficking promotes fusion and coalescence of apical membrane compartments during sprouting angiogenesis, we applied live imaging of vesicle trafficking to screen candidate assigned Rab proteins, for those, which have a distinct distribution pattern and function. To analyse the subcellular distribution of Rab proteins, we generated N-terminally EGFP-tagged constructs, which were expressed transiently in zebrafish embryos. Initially, we focused on *rab5c*, *rab7* and *rab11a* constructs, which were characterized and validated previously in zebrafish (Clark et al., 2011). Therefore, we sub-cloned the same *rab* constructs under a vascular-specific promoter (*fli1ep*) and injected the constructs into single cell stage *kdrl*: CAAX-mCherry fish eggs to observe transient expression. Then, we imaged the localization and dynamics of Rabs within endothelial cells during lumen invagination in sprouting angiogenesis.

At first, we analysed Rab5c transient expression pattern within the CAAX-mCherry transgenic line. We demonstrated that Rab5c was generally distributed over the cell when there was no lumen formation yet (not shown). However, strikingly, we observed during lumen invagination that Rab5c accumulated at the leading edge of the invaginating lumen (n=5)

(Figure 20). This observation might indicate that Rab5c retrieves the membrane material at the leading edge of invaginating lumen.

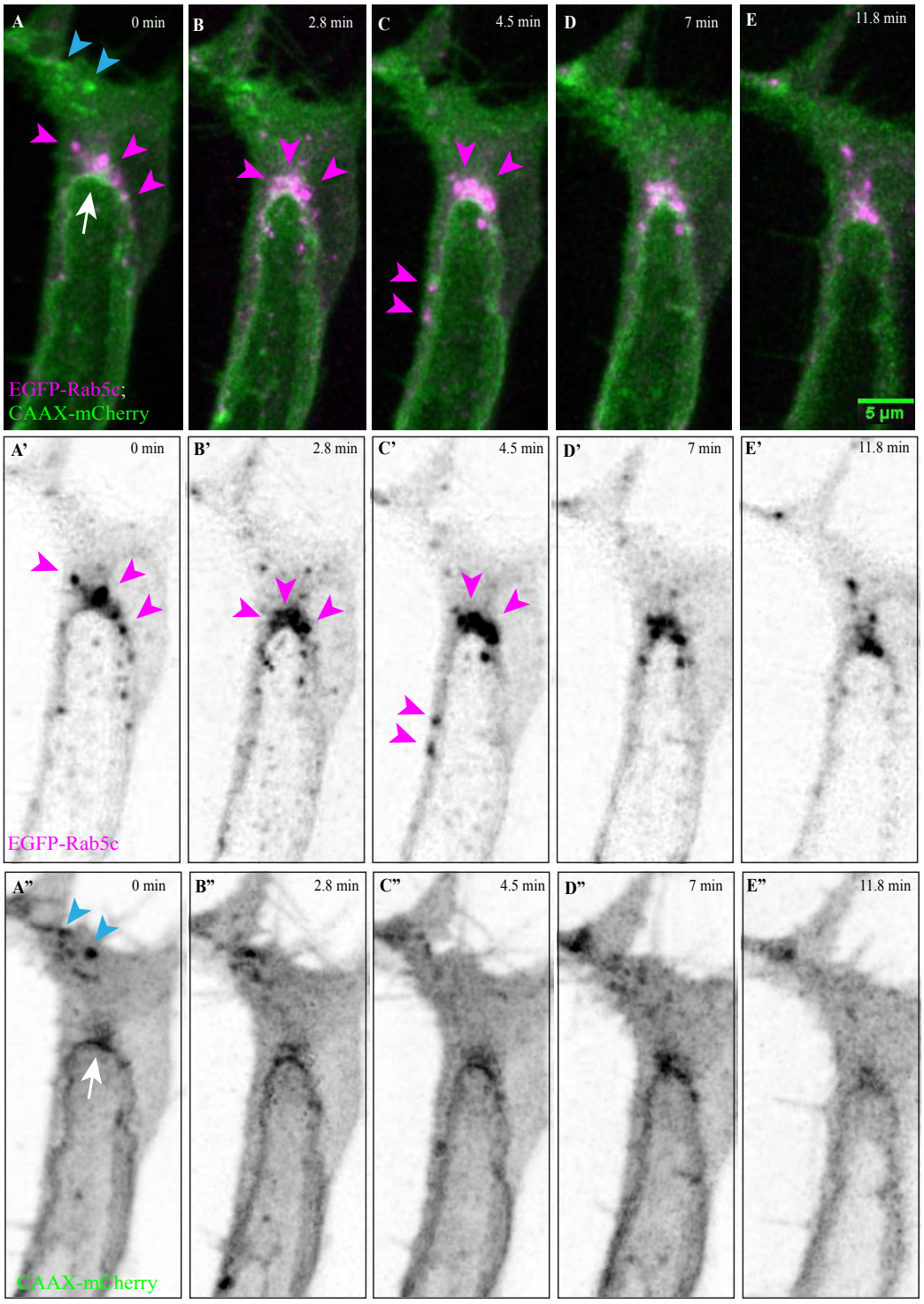

Figure 20: Lumen invagination and Rab5c-early endosome trafficking
(A-E) Still pictures from time-lapse movie S5, with highlighted Rab5c (EGFP-Rab5c) and membrane (CAAX-mCherry). The location of the lumen is apparent as a gray zone bounded by cytoplasm, white arrows indicate the direction of lumen invagination, magenta arrowheads indicate the approximate position of Rab5c location and blue arrowheads indicate the approximate position of vesicle-like structures. **(A)** Lumen invagination into an endothelial cell at DLAV (white arrow). Vesicle-like structures (blue arrowheads) and Rab5c vesicles (magenta arrowheads) are not co-localized. However, Rab5c tagged vesicles are confined at the tip of the invaginating lumen **(B-E)** Lumen invagination seems slow and Rab5c tagged vesicles are kept their position at the tip of invaginating lumen (magenta arrowheads). **(A'-E')** Still pictures correspond to those from panels A-E, showing only the green channel (grayscale). **(A''-E'')** Still pictures corresponding to those from panels A-E, showing only the red channel (grayscale). (In the schematic; green: Rab5c, red: membrane).

As a next experiment, we analysed transient Rab7 expression in the CAAX-mCherry transgenic line. We showed that Rab7 expression, similar to that of Rab5c, was all over the cell when there was no lumen formation yet (not shown). However, during lumen invagination, we observed that Rab7 vesicles seem to form a donut-shaped structure in tip cell and distributed randomly rather than in a specific pattern. Strikingly, we demonstrated that CAAX-mCherry vesicles-like structures were positioned within the donut shapes formed by EGFP-Rab7 and co-localized with the later (n=5) (Figure 21). However, we need to do further experiments and analyses to find out whether Rab7 stays intact in cytoplasm, when some CAAX-mCherry vesicles-like structures dissolve on the invaginating lumen.

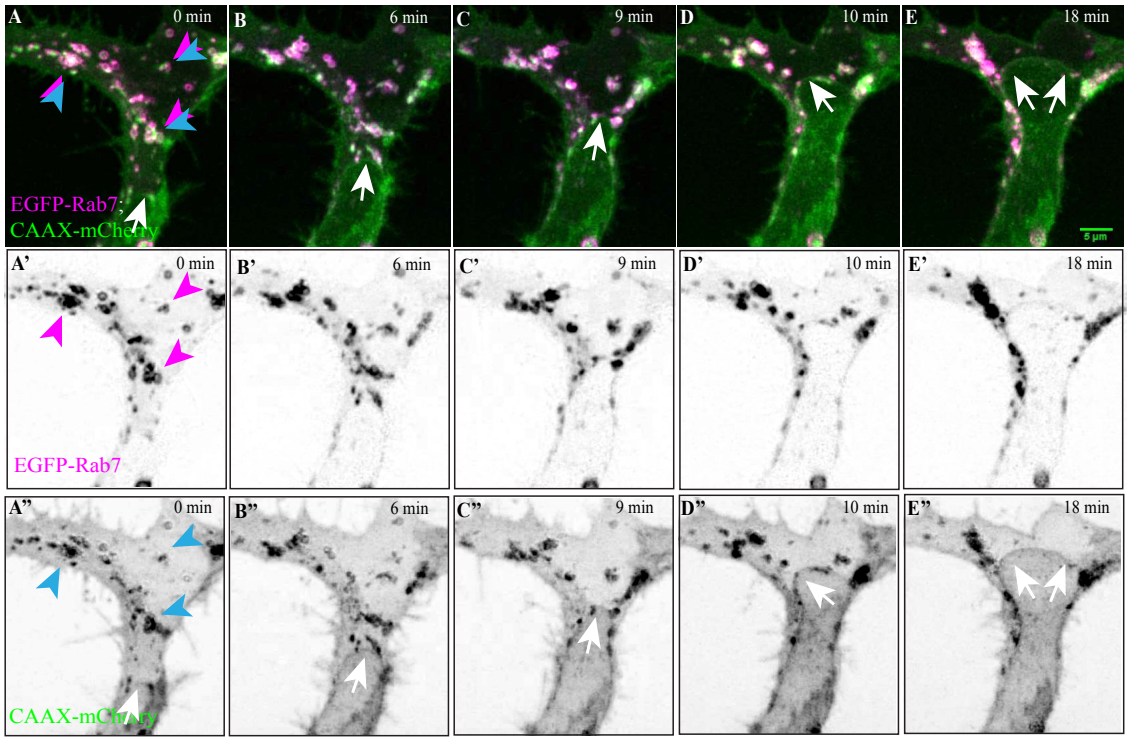

Figure 21: Lumen invagination and Rab7-late endosome trafficking
(A-E) Still pictures from time-lapse movie S6, with highlighted Rab7 (EGFP-Rab7) and membrane (CAAX-mCherry). The location of the lumen is apparent as a gray zone bounded by cytoplasm, white arrows indicate the direction of lumen invagination, magenta arrowheads indicate the approximate position of Rab7 location and blue arrowheads indicate the approximate position of vesicle-like structures. **(A)** Lumen invagination into an endothelial cell from SA to DLAV (white arrow). Vesicle-like structures (blue arrowheads) and Rab7 vesicles (magenta arrowheads) are co-localized. **(B-E)** Lumen invagination continues and Rab7 tagged vesicles are co-localized with vesicle-like structures. **(A'-E')** Still pictures correspond to those from panels A-E, showing only the green channel (grayscale). **(A''-E'')** Still pictures corresponding to those from panels A-E, showing only the red channel (grayscale). (In the schematic; green: Rab7, red: membrane).

Last, we analysed transient Rab11a expression within the CAAX-mCherry transgenic line. We demonstrated that Rab11a expression was distributed all over the cell in the absence of lumen formation. However, in the presence of

lumen invagination, Rab11a was also distributed all over the cell (n=4), more close to the invaginating lumen (Figure 22). This observation suggests that Rab11a vesicles might recycle membrane compartments to the growing lumen, which might contribute to the extension of the lumen.

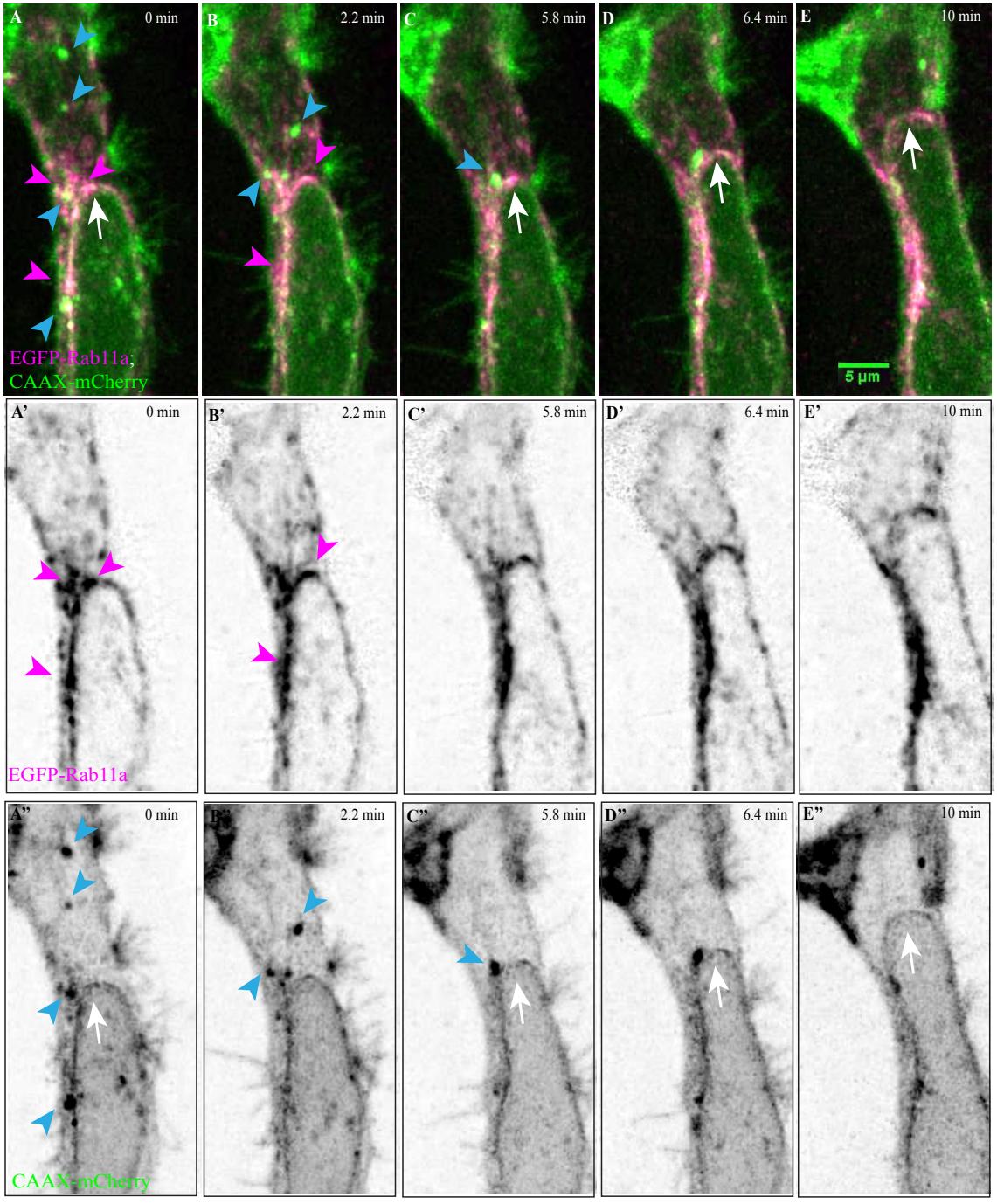

Figure 22: Lumen invagination and Rab11a-recycling endosome trafficking
(A-E) Still pictures from time-lapse movie S7, with highlighted Rab11a (EGFP-Rab11a) and membrane (CAAX-mCherry). The location of the lumen is apparent as a gray zone bounded by cytoplasm, white arrows indicate the direction of lumen invagination, magenta arrowheads indicate the approximate position of Rab11a location and blue arrowheads indicate the approximate position of vesicle-like structures. **(A)** Lumen invagination into an endothelial cell at DLAV (white arrow). Vesicle-like structures (blue arrowheads) and Rab11a vesicles (magenta arrowheads) are not co-localized. **(B-E)** Lumen invagination continues and Rab11a tagged vesicles are localized close to invaginating lumen. **(A'-E')** Still pictures correspond to those from panels A-E, showing only the green channel (grayscale). **(A''-E'')** Still pictures corresponding to those from panels A-E, showing only the red channel (grayscale). (In the schematic; green: Rab11a, red: membrane).

Taken together, we showed that Rab5c-positive early endosomes were enriched at the leading edge of the apical lumen compartment, whereas Rab7 and Rab11a, which mark late and recycling endosomes, respectively, were distributed throughout the cytoplasm of endothelial cells (Figure 22). We did not observe any co-localization of Rab5c and Rab11a with vesicle-like structures originated from CAAX-mCherry. Interestingly, EGFP-tagged Rab7 vesicles were co-localized with vesicle-like structures labeled by CAAX-mCherry.

7.5 Visualizing microtubule dynamics and localization during lumen invagination process

From the previous research, it has been shown that some of the Rab vesicles move along the MTs (microtubules) and contribute to lumen formation (Blasky et al., 2015). To get familiar with MTs dynamics and localization during lumen invagination, we imaged angiogenesis in an embryo expressing both EB3-EGFP (end binding protein 3) (Stefan Schulte-Merkers lab) and CAAX-mCherry. We observed a positional correlation between vesicle-like structures movement originated from CAAX-mCherry transgenice line and microtubule-based cytoskeletal tracks, indicating that vesicles might move on microtubule tracks. However, further studies are needed to prove the correlation. Furthermore, we wanted to investigate the cytoskeletal dynamics during lumen invagination. Interestingly, we observed that the microtubule cytoskeleton, which might serve as a transport route, always seemed to connect the invaginating lumens (Figure 23). When the two apical lumen compartments get close to within a certain distance to each other before the fusing process, the microtubule-organizing center always moves to the side (n=3) (Figure 23 (E)). This observation suggests that microtubules might also guide the direction of the lumen growth process in addition to serving as a cytoskeletal track.

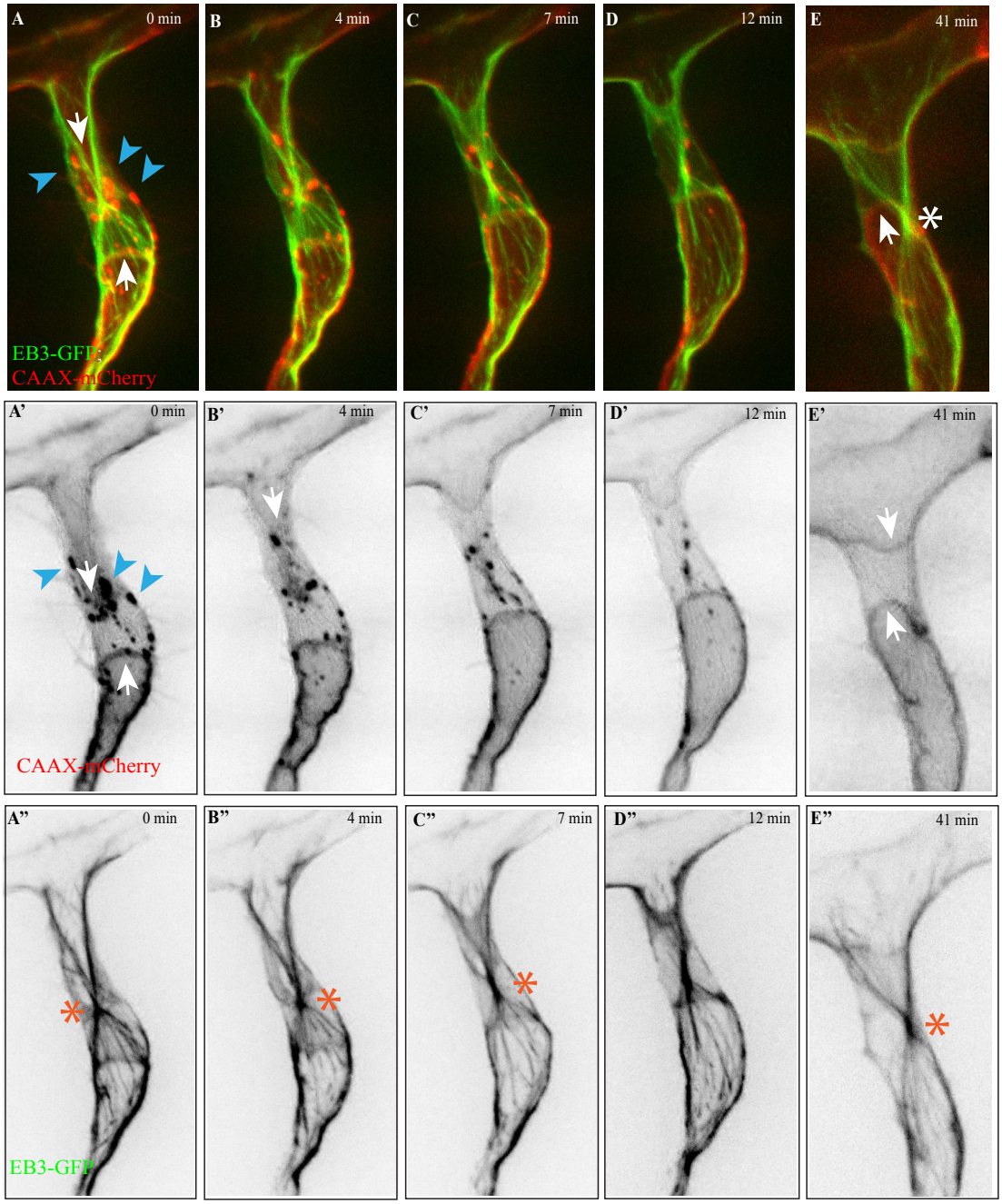

Figure 23: Lumen invagination and microtubules

(A-E) Still pictures from time-lapse movie S8, with highlighted microtubules (EB3-EGFP) and membrane (CAAX-mCherry). The location of the lumen is apparent as a red zone bounded by cytoplasm, white arrows indicate the direction of lumen invagination and blue arrowheads indicate the approximate position of vesicle-like structures and orange asterisk indicate the position on microtubule organization center. **(A)** Two lumen invaginates towards each other (white arrows) and vesicle-like structures

(blue arrowheads) formed from the upper invaginating lumen. **(B-D)** Lumen invagination from the upper part seems to form big vesicle-like structures (blue arrow heads), indicating lumen continuity is broken (white arrows). **(E)** The lumen invagination from SA to DLAV comes close to another invaginating lumen from DLAV to SA (white arrows) and microtubule organization center is pushed on the site (asterisk). **(A'-E')** Still pictures correspond to those from panels A-E, showing only the red channel (grayscale). **(A''-E'')** Still pictures corresponding to those from panels A-E, showing only the green channel (grayscale). (In the schematic; green: microtubules, red: membrane).

7.6 Visualizing actin distribution during lumen invagination process

Previous research has shown that when the lumen invaginates, there are some spherical deformations happening at the leading edge. Because of the blood pressure fluctuations, endothelial cells react towards deformations by recruiting actomyosin clusters, visualized by life-actin. The actomyosin forces, generated in the cytoplasm, put these spherical deformations back on the growing lumen. This process was described as reverse blebbing, and was claimed as a mechanism contributing to lumen expansion (Gebala et al., 2016). To analyze the distribution of the actin cytoskeleton during the lumen invagination process, we used a UCHD-GFP transgenic line (Sauteur et al., 2014), which labels filamentous actin. Similar to previous research, we observed the recruitment of actin at the leading edge of the expanding lumen. However, recruitment of actin was far less specific than previously reported and positioned not only at the leading edge of the lumen but also on the side of the lumen (Figure 24). The results indicate that during lumen invagination, the actin cytoskeleton might keep the lumen intact. To better

understand the role of the actin cytoskeleton at the lumen invagination process, further functional studies are needed.

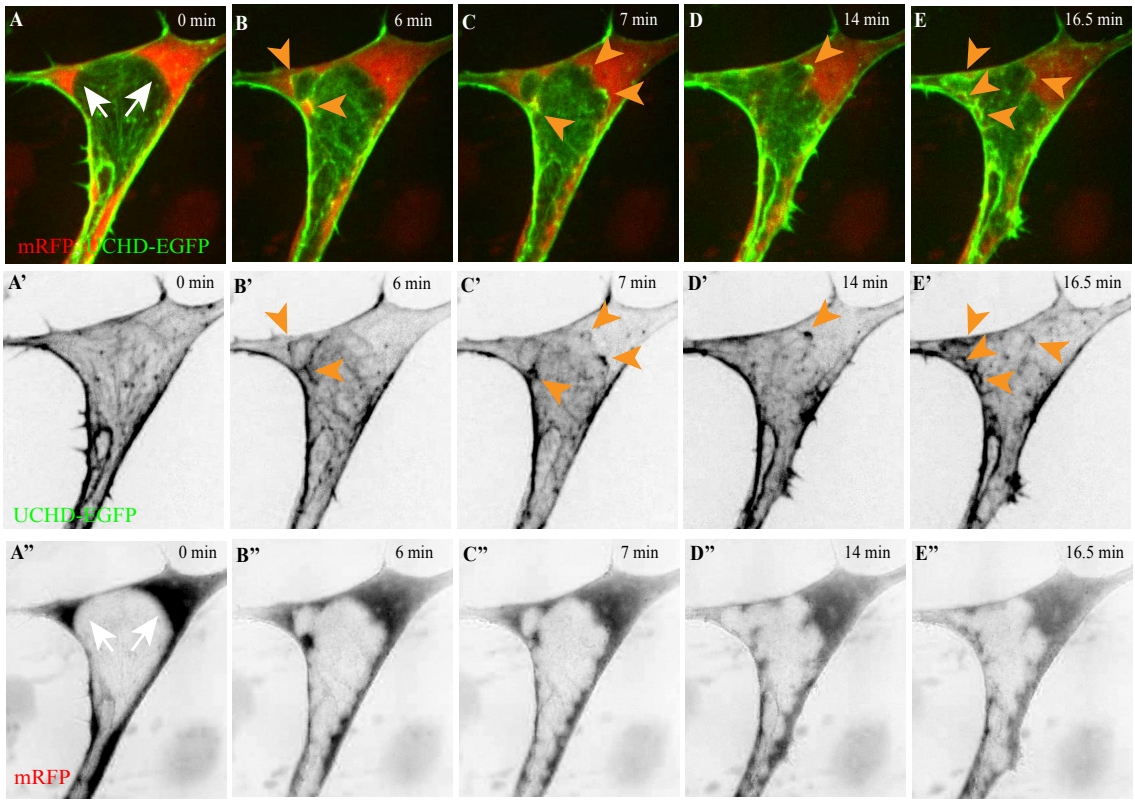

Figure 24: Lumen invagination and actin cytoskeleton
(A-E) Still pictures from time-lapse movie S9, with highlighted actin cytoskeleton (EGFP-UCHD) and cytoplasm (RFP). The location of the lumen is apparent as an empty zone bounded by red cytoplasm, white arrows indicate the direction of lumen invagination and orange arrowheads indicate the approximate position of actomyosin accumulations. **(A)** Lumen invagination into an endothelial cell from SA to DLAV (white arrows). **(B-E)** The lumen structure is not smooth on the edge and form blebs towards cytoplasm from apical and vice versa (orange arrowheads). **(A'-E')** Still pictures correspond to those from panels A-E, showing only the green channel (grayscale). **(A''-E'')** Still pictures corresponding to those from panels A-E, showing only the red channel (grayscale). (In the schematic; green: actin, red: cytoplasm).

7.7 Visualizing Golgi apparatus during lumen invagination

One of the major platform for retrograde trafficking is endosome-to-trans Golgi network (TGN) pathway. This path diverts proteins and lipids away from lysosomal degradation by transporting cargoes from the early endosome/recycling endosome or the late endosome pathways to TGN (reviewed in Lu and Hong, 2014). This data demonstrates the close relation between Golgi and endosomal trafficking pathways.

Previous research has shown that the Golgi apparatus changes its position relative to the nucleus depending on blood flow in zebrafish (Kwon et al., 2016). To identify a possible correlation between Golgi apparatus and apical membrane invagination, we used a transgenic zebrafish line in which the Golgi apparatus is labeled with a fluorescent protein. During sprouting angiogenesis, in which blood flow is not established yet and cells migrate towards the dorsal side, we observed that the Golgi apparatus is always positioned at the front end of the nucleus, agreeing with previous observations (Kwon et al., 2016). During lumen growth, the Golgi apparatus was positioned at the apical side of the cell. While the lumen was expanding and pushing the nucleus to the side, the Golgi apparatus also is positioned on the lumen side (Figure 25). This finding suggests that the building blocks of apical membrane compartments might emerge from the Golgi as well. Since endosomal proteins are shuttled from ER to Golgi and some of the proteins are transported from endosomal pathways to TGN (Lu and Hong, 2014), observing the Golgi behavior might give additional insight into the lumen invagination process.

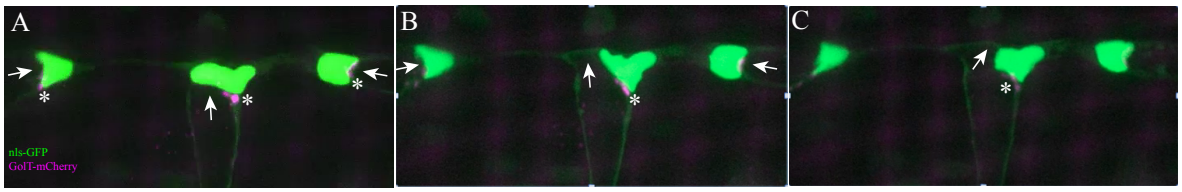

Figure 25: Lumen invagination and Golgi apparatus
(A-C) Still pictures from time-lapse movie S10, with highlighted Golgi apparatus (GolT-mCerry) and nucleus (nls-GFP). The location of condensed Golgi aparatus is apparent as a zone of magenta signal (white asterisks). **(A)** Lumen invagination process (white arrows), with the approximate position of the Golgi indicated by the white asterisks, which is the tip of invaginating lumens. **(B-C)** Lumen invagination pushes the nucleus to the right site from down to open the space (white arrows) and Golgi does not move with invaginating lumen, but rather Golgi stays behind of nucleus when lumen invaginates further.

7.8 Conclusion

In summary, we have developed novel tools that allow the *in vivo* visualization of Rab5c- early endosome, Rab7- late endosome, and Rab11a- recycling endosome within endothelial cells. We have imaged the endosomal trafficking with cutting edge spatio-temporal resolution within the endothelial cells during the lumen invagination process in sprouting angiogenesis. Interestingly, Rab5c expression is confined to the leading edge of the invaginating lumen. CAAX-mCherry originated vesicle-like structures co-localize with EGFP-tagged Rab7 late endosomal vesicles, demonstrating a correlation of their dynamics and localization. Overall, we analyzed the distinct localization and dynamic pattern of vesicle/membrane trafficking during lumen invagination. To map endothelial cell behavior during lumen invagination, we also observed dynamic rearrangements of sub-cellular

structures, which are involved in cell architecture changes. For example, microtubules (MTs) are enriched in-between the invaginating lumens and move to the side when two invaginating lumens come in close contact. MTs may provide a highway for transporting vesicles towards the growing lumen, since similar process was described in tube formation in the *Drosophila* trachea (Caviglia and Luschnig, 2014; Caviglia et al., 2016). One more key player, actomyosin contraction, is activated in different positions when the lumen starts invaginating into an endothelial cell. Because of pressure fluctuations, the invaginating apical membrane can break in it's continuity, and eventually fuses back. During lumen expansion, it has also been observed that many blebs can form (Gebala et al., 2016). During this process, actin accumulation occurs on the blebbing sites and may regulate lumen maintenance, recovering lumen continuity by pushing these bubbles back to the apical membrane. Another key player, the Golgi apparatus, is used for planar cell polarity indication and positioned at the tip of the invaginating lumen, indicating the Golgi might shuttle building blocks of apical membrane compartments. Establishing and analysing the distribution pattern of endosomal trafficking, cytoskeleton (MTs, actin) and Golgi apparatus during lumen invagination, we are able to describe the lumen invagination process and observe endothelial cell behavior in detail at cellular and subcellular level *in vivo*.

8 Discussions and Outlook

8.1 Lumen invagination and vesicle/membrane trafficking in sprouting angiogenesis

8.1.1 Visualization of apical membrane compartment: CAAX-positive, vesicle-like structures fuse to invaginating lumen during sprouting angiogenesis.

The mechanism of how a lumen expands during sprouting angiogenesis is not understood yet. One of the studies in the field proposed a vacuole fusion model, in which vacuoles in the cell emerge via pinocytic pathways and form large intracellular, luminal spaces. These vacuoles eventually come together and fuse with one another to form interconnected lumen, during sprouting angiogenesis independent of blood flow (Kamei et al., 2006). Similar large luminal spaces have been reported *in vitro* in HUVEC culture (Childs et al., 2002 and Kamei et al., 2006). Furthermore, a recent study (Yu et al., 2015) shows that during sprouting angiogenesis, small membrane vesicles coalesce into larger membrane structures, which could be representative of vacuoles. In these studies, both prenylated Cdc42 and cytoplasmic GFP tools were applied to visualize luminal membrane structures. Nonetheless, the study lacks the demonstration of whether these large membrane structures contribute to the lumen expansion process. In a number of other studies, using membrane and junctional markers, it was reported that the lumen is formed in zebrafish by a combination of lumen invagination and cord hollowing process, rather than by vacuole fusion (Blum et al., 2008a; Fededa and Gerlich, 2012; Gebala et al., 2016; Green et

al., 2012; Herwig et al., 2011; Lenard et al., 2013; Levayer and Lecuit, 2012).

To visualize the lumen expansion process, we also used a CAAX-mCherry transgenic zebrafish line, which allows to visualize apical and basal compartments. However, to the earlier claim, we did not observe large vacuolar structures when the lumen forms. However, this does not exclude that vacuoles are involved in the lumen formation process. Interestingly, our results show that some vesicle-like structures, labeled with CAAX-mCherry, form and move in the cytoplasm and eventually fuse to the growing membrane. These observations indicate that vesicle trafficking might contribute to lumen expansion during the invagination process (Figure 19).

Recently, it was shown in the *Drosophila* tracheal system, that vesicle/membrane trafficking plays a critical role in tube formation. For example, Rab11, Rab39 and lysosomal vesicles regulate the lumen fusion process, a last step of lumen expansion, in tracheal tip cells (Caviglia et al., 2016; reviewed in Caviglia and Luschnig, 2014). This data from *Drosophila* suggest that similar events might occur in vertebrates. Along those lines, integration of vesicle-like structures, originated from CAAX-mCherry transgenic zebrafish line, into the growing lumen, is a potential indication for vesicle/membrane trafficking during lumen invagination process. Although the two systems, tracheal tube formation and vascular network formation, are from different organisms, we might benefit from *Drosophila* research. These are many differences between lumen formation in tracheal tube and in the vasculature. Tubes in *Drosophila* are solid, carry air and cells are very small. However, endothelial cells are larger and allow better resolve

the subcellular events by imaging and there is blood instead of air, and lumen growth is dynamic and fragile. Most importantly, we are able to record the dynamics of cellular and subcellular events *in vivo*.

In light of our findings, it is crucial that we can visualize apical and basal compartments in endothelial cells with the CAAX-mCherry transgenic line. Additionally, we identified vesicle-like structure formation and fusion to the invaginating lumen. These findings open important questions in whether these vesicle-like structures are real vesicles and might contribute to lumen growth.

8.1.2 Dynamics and localization of early, late and recycling endosomes during lumen invagination process in sprouting angiogenesis

Very often, we observe that the vascular lumen forms rapidly via lumen invagination processes and cells might provide a reservoir of membrane materials (lipids, proteins as building blocks) via vesicle/membrane trafficking in order to expand the lumen as an addition to *de novo* production of the building blocks (e.g. exocytosis).

Imaging the membrane marker, CAAX-mCherry, we observed that vesicle-like structures dissolve on growing lumen. This observation encouraged us to hypothesize that vesicle/membrane trafficking contributes to extend rapidly invaginating lumen by providing building blocks.

To address whether these vesicle-like structures are endosomes, we generated tagged version of different Rab proteins driven by an endothelial

specific promoter –*fli1ep*:EGFP-*rab*5c, *fli1ep*: EGFP-*rab*7, and *fli1ep*: EGFP-*rab*11a. To observe the dynamics and localization of endocytotic pathways during the lumen invagination process, we analysed the expression of distinct Rabs upon transient expression. During tube expansion in *Drosophila* trachea, Rab5 is required to remove luminal material to generate an open space, indicating the importance of early endocytotic pathways (Tsarouhas et al., 2007).

Rab5c is an early endosomal marker and when it is expressed under the *fli* promoter in zebrafish, the expression is mostly confined at the leading edge of the invaginating lumen (Figure 20). Therefore, Rab5c accumulation at the leading edge might indicate to retrieve apical membrane from the invaginating lumen. We observed that when two lumens fuse with one another, one invaginates faster and another invaginates slower probably due to a blood pressure change. Interestingly, Rab5c accumulate at the slow invaginating lumen (n=3), but does not accumulate at the fast invaginating lumen, which is at the opposite side. The reason why Rab5c expression is not seen in both invaginating lumen might be due to mosaic expression. The lumen in which Rab5c accumulate grows very slow, which might be explained by apical membrane removal from the leading edge. Removing of apical membrane material from invaginating lumen via early endosomal pathway might be the reason for the slow growth. More research is needed to elucidate the role of early endosome on lumen invagination process during sprouting angiogenesis. It might be interesting to follow up whether Rab5c always accumulates on one side of an invaginating lumen. Also, it will be interesting to know what will be the next Rabs, which take over vesicles from Rab5c in the cell to see what happens on these Rab5c-tagged

vesicles. For this, we need to visualize multiple Rabs simultaneously during the lumen invagination process with different fluorescent proteins. This will allow us to address some issues such as whether Rab5c-tagged vesicles are recycled, or moved to late endosomes and so on to observe the next stages of vesicle trafficking.

Previous research (Ellis et al., 2013) in zebrafish showed that notochord vacuoles biogenesis and maintenance requires late endosomal trafficking regulated by Rab32a and H^+-ATPase–dependent acidification. However dominant negative (DN) expression of Rab7 (the classical regulator of late endosomes) gave no phenotype. We can argue that DN experimental setup is not ideal for functional studies: since the time of expression is not controlled and there might be compensation due to possibly existing isoforms of Rab7.
In the vascular system, we aimed to observe the localization and dynamics of Rab7 during the lumen invagination process. Similar to Rab5c, Rab7 expression was randomly distributed in the absence of lumen. Strikingly, however, Rab7 vesicles were co-localized with CAAX-tagged vesicle-like structures and moved together in the cytoplasm of ECs during the lumen invagination process (Figure 21). More analyses are needed to identify whether CAAX-tagged vesicle-like structures still fuse to the growing lumen. Since Rab7 regulates late endosome formation, Rab7-tagged vesicles should remain in the cytoplasm when CAAX-tagged vesicle-like structures fuse with growing lumen. Another interesting observation was that Rab7-tagged vesicles are smaller in size at DLAV (n=2). However, they form big donut shape vesicles at the tip cells (n=2). They also seem to have an influence on the size of vesicle-like structures originating from CAAX-

mCherry in tip cells. Co-localization of CAAX-mCherry vesicle-like structures and Rab7-labeled late endosomes show that we have already strong evidence for late endosomes might be involved in the lumen growth. Further research is needed to elucidate what these late endosomes contains and how they might contribute to lumen invagination process.

Rab11a regulates recycling endosomes and the expression is all over the cell both in the absence and presence of lumen (Figure 22). It is difficult to interpret the recycling endosomes' expression during the lumen invagination process. One suggestion is that when the lumen invaginates rapidly, there is a high demand of building blocks to supply membrane to growing lumen. Therefore, recycling endosomes might be involved in supplying building blocks to extend lumen rapidly by bringing material from cytoplasm to apical. However, these preliminary results might give some indications about the events and show some correlations. More research is needed to elucidate the role of recycling endosomes during the lumen growth. Endothelial cells in vascular network have confined space, and need to be lumenized for functioning. Rab5c vesicles might retrieve the membrane material through the leading edge of apical membrane, which does not grow fast and Rab11a vesicles might bring the membrane material towards the fast growing apical membrane compartment. The system should be in an equilibrium within the confined space. However, we need more research to validate the statement. For example, simultaneously tagging Rab5c and Rab11a with different fluorescent markers and observe them during the lumen invagination process could help to understand whether there is an exchange between the two endocytotic pathways.

In addition, we dissected the subcellular rearrangements during the lumen invagination process with different tools, such as the Golgi apparatus tagged with mCherry. Particularly, the Golgi apparatus migh help us to visualize the interaction between Golgi and endocytotic pathways. We observed that vesicle-like structures, originated by GolT-mCherry appear and move in the cytoplasm (n=1, not shown). Our preliminary finding suggests that building blocks of apical membrane compartments might emerge from the Golgi as well, indicating both biosynthesis of trafficking via exocytosis and endocytotic trafficking via endocytosis. However, to what extend endocytosis and exocytosis contribute to lumen growth is a complex and challenging issue to understand.

For the functional studies, we develop some novel approaches to manipulate the localization or degradation of our protein of interest. First, we want to identify which Rabs are potentially promising candidates to study further based on the localization and dynamic point of view during lumen invagination. Additionally, we also investigate the correlation of Rabs with other tools (CAAX-mCherry and podocalyxin) from the dynamic localization aspects. For the moment, Rab7 is a strong candidate to investigate further since it co-localize with vesicle-like structures, originate from CAAX-mCherry. Rab7 overexpression might have an influence on the size of vesicle-like structures originated from CAAX-mCherry. To find out, we analyze Rab7 and CAAX-mCherry expression alone and together.

Overexpression analysis might give us some indications to follow up. However, to determine the role of specific proteins such as Rabs, we need to manipulate the function of a protein of interest specifically. There is a couple of ways to study the function of proteins (e.g. Rab7) For example, generating endogenously tagged (e.g. HA or Suntag) Rab7 or other Rabs, which are potentially involved in the lumen growth process. Endogenous tagging in zebrafish is still not easy, but hopefully better approaches will be developed in near future. Once we have an endogenously tagged protein of interest, we can manipulate it's cellular localization and change the dynamics of the protein of interest by applying nanobody-trap methods, darpins or chromobodies. For example, overexpressed Rab5c-tagged GFP was mis-localized by the expression of a CAAX tagged Darpin binding GFP (Brauchle et al., 2014 and reviewed in Bieli et al., 2016). With these new methods, we can possibly dissect the events more specifically and analyze the consequences of subcellular disturbances and observe cell behaviors during lumen invagination process in order to map the functional activities. It is difficult to predict how these methods can solve the functional problems. For example, one has to make sure that the Rabs were mislocalized but what if there is no effect on vesicle formation because vesicles themselves were not catched by the trapping system but only the Rab of interest. Nonetheless, one needs to create, test and optimize novel tools in zebrafish. As soon as we have better tools, we can fine-tune the tools and find out the best way to address questions of interest more specifically.

8.2 Guidance of the invaginating lumen; visualizing microtubule dynamics and localization during lumen invagination process

Another interesting question is that how a growing lumen can be guided correctly in one particular direction or keep the proper polarity within a cell. It is known that the cytoskeleton plays an important role in cell polarity (reviewed in Blasky et al., 2015). In addition, microtubules (MTs) represent railroads for vesicle trafficking between growing apical membranes during *Drosophila* tube formation (Caviglia et al., 2016; reviewed in Caviglia and Luschnig, 2014). However, there is not much information about the dynamics of MTs during lumen growth *in vivo*. To study MTs dynamics and look at a possible role of the cytoskeleton in guiding lumen growth, we used an EB3-GFP transgenic line and visualized during lumen invagination process.

MTs might guide lumen growth, regulate polarity and also facilitate vesicle/membrane trafficking during the lumen invagination process in sprouting angiogenesis. For example, we observe that microtubules (MTs) are enriched between the invaginating lumens and move to the side when two invaginating lumens come in close contact. In addition, vesicle-like structures, originated from CAAX-mCherry, seem to move on MTs during lumen growth. MTs might provide a highway for transporting vesicles towards the growing lumen in sprouting angiogenesis (Figure 23). For further analysis, we need to manipulate MTs with drugs or laser ablation to better dissect their role during lumen invagination process *in vivo*.

8.3 The maintenance of the invaginating lumen; visualizing actin distribution during lumen invagination process

How a lumen adapts to the dynamic blood flow changes and maintains its structure during lumen expansion is not well understood yet. The cytoskeleton has a wide range of roles in maintaining cell shape, organizing trafficking, and regulating cell division and more. A recent study (Gebala et al., 2016) shows that because of the blood flow, spherical deformational changes take place at the tip of an expanding lumen. In order to contribute to the expansion of the lumen, local and transient recruitment and contraction of the actin cytoskeleton might be necessary. However, it is not clear, local recruitment and contraction of actomyosin is needed for lumen expansion in vascular sprouts rather than keeping the lumen stability. We used a UCHD-GFP transgenic line (Sauteur et al., 2014), which labels filamentous actin, to analyze the distribution of the actin cytoskeleton during lumen growth. Our preliminary observations using the UCHD-GFP line shows that due to the pressure changes, there is intensive accumulation of actin pulses at the growing end/or tip of a lumen. Based on our observations, we assume that during lumen invagination, the actin cytoskeleton has a role in keeping the lumen intact due to fluctuating blood flow changes. As a role of actin in the stability of lumen is also supported by observations in which actomyosin contraction is activated in different positions such as at tip or lateral side of a lumen when the lumen starts invaginating into an endothelial cell. Because of the pressure fluctuation, the invaginating apical membrane can break in continuity and create many blebs (Gebala et al., 2016). During this process, actin accumulation occurs on the blebbing sides and may regulate lumen

maintenance by recovering lumen continuity by pushing these bubbles back to the apical membrane (Figure 24). Therefore, it is possible that actin polymerization or actomyosin contraction is required to avoid that these structures detach from a growing lumen. These results indicate that the actin cytoskeleton keeps lumen maintenance rather than contributes to lumen growth during lumen invagination. To better understand the function of the actin cytoskeleton, we need to manipulate its structure and/or function during the lumen invagination process with precise tools and in specific cells rather than applying drugs, which have effects on whole body tissues.

As a summary, we showed that Rab7-labeled late endosomal vesicles co-localize with CAAX-mCherry vesicle like structures, which is a strong candidate for lumen invagination process to follow up. In addition, we need to screen other Rabs, which are involved in distinct endosomal pathway regulations and identify the potential ones based on their expression (dynamics and localization), correlation with lumen growth and co-localization with other markers such as membrane marker or podocalyxin. We also need to image other markers such as photo-convertible membrane marker (Dendra transgenic line from Herwig Baier lab). We can photo-convert a part of cytoplasm or growing lumen and image the color changes in time, which can give us additional information about the lumen invagination process. Further, we should also generate and screen new tools not only directed to proteins but also to lipids, which are highly present in membranes (e.g. BoDIPY), to visualize lumen invagination. Since we are

advanced in imaging technology to visualize the dynamics of events by different tools (e.g. Rabs, lipid markers), we might have preliminary indications (e.g. correlation with other markers, CAAX-mCherry, podocalyxin) that can be used as a base for follow-up experiments. Next, we need to develop novel tools to more functional studies in zebrafish using CRISPR/Cas9 that undertake and allows us to edit (e.g. delete or add) a gene of interest at the DNA level. At the protein level, we would like to establish and use tools to degrade or to mislocalize a protein of interest with applying nanobodies or darpins, which was initiated in our lab in *Drosophila*. Similarly, we need to establish a similar system in the zebrafish vasculature to manipulate proteins of interest (e.g. endosomal pathway regulators: Rab7-late, Rab5-early endosomes) and further to visualize the dynamics of cellular behavior during vascular development with a high spatio-temporal resolution. Further, as a long term goal we aim to visualize these endosomal vesicles with applying correlative light and electron microscopy (CLEM) technique during lumen invagination process. Revealing cellular ultrastructure will allow to improve our understanding about lumen invagination process in depth. To map endothelial cell behaviors in each step during blood vessel network formation, we need to dissect subcellular events with high-resolution images and functional studies and new tools will help us to come there soon.

9 Appendix

9.1 Further Publications

regulating macrophage responses to cancer that could motivate the development of new anti-tumour approaches. From a pharmacological standpoint, the real challenge lies in developing treatments that would target the miRNA machinery in tumours in a macrophage-specific fashion. Intratumoral delivery of miRNA mimics or Dicer antagonists to target tumour-associated myeloid cells by nanoparticles or similar carriers may provide such a strategy[15]. However, the outcome of this type of therapy may be limited by the rapid TAM turnover in the tumours and the complexity of the immune cell composition and dynamics in distinct tumour types. Future studies taking this into consideration will be necessary to devise effective therapeutic strategies.

COMPETING FINANCIAL INTERESTS.
The authors declare no competing financial interests.

1. Noy, R. & Pollard, J. W. *Immunity* **41,** 49–61 (2014).
2. Baer, C. *et al. Nat. Cell Biol.* **18,** 790–802 (2016).
3. Biswas, S. K. & Mantovani, A. *Nat. Immunol.* **11,** 889–896 (2010).
4. Helm, O. *et al. Int. J. Cancer* **135,** 843–861 (2014).
5. Movahedi, K. *et al. Cancer Res.* **70,** 5728–5739 (2010).
6. Lindsay, M. A. *Trends Immunol.* **29,** 343–351 (2008).
7. Koralov, S. B. *et al. Cell* **132,** 860–874 (2008).
8. Cobb, B. S. *et al. J. Exp. Med.* **203,** 2519–2527 (2006).
9. Squadrito, M. L. *et al. Cell Rep.* **1,** 141–154 (2012).
10. Wang, Z. *et al. Sci. Rep.* **6,** 25602 (2016).
11. Wang, Y. *et al. PLoS ONE* **7,** e44399 (2012).
12. De Palma, M. *et al. Cancer Cell* **8,** 211–226 (2005).
13. Ginhoux, F. *et al. Nat. Immunol.* **17,** 34–40 (2016).
14. Luheshi, N. M. *et al. Oncotarget* **7,** 18508–18520 (2016).
15. Cubillos-Ruiz, J. R. *et al. Cancer Res.* **72,** 1683–1693 (2012).

Mapping the molecular steps of secretory-lysosome-driven tracheal tube fusion

Vahap Aydogan, Heinz-Georg Belting and Markus Affolter

During development, tubular networks form through the joining of lumenized branches. Further insights into tracheal tube fusion in *Drosophila melanogaster* now reveal the molecular steps that promote the connection of two apical membrane compartments within a single cell through secretory lysosomes.

Biological tubes exist in many forms in organisms from plants to animals, and the architecture of such tubular systems has fascinated biologists for centuries. Tubular networks can be established through different morphogenetic mechanisms[1]. In many cases, they are formed by individual branches that interconnect and fuse in order to establish a continuous lumen. At the cellular level, luminal connectivity can be achieved by cell rearrangements or by a cell-hollowing mechanism that involves invagination of luminal and apical cell membranes and their intracellular fusion. Until now, the exact cellular mechanisms that underlie cell hollowing have been unclear. Stefan Luschnig and colleagues[2] have now identified a molecular pathway that mediates the intracellular fusion of separate luminal compartments *in vivo*, demonstrating that individual steps in generating continuous luminal networks are controlled by distinct molecular mechanisms. Surprisingly, this work revealed that molecules best known for their role in calcium-triggered exocytosis in vertebrates are involved in this membrane fusion event in the fly embryo. These studies open up the possibility of investigating whether similar processes also occur in other tubular networks, such as in the developing vasculature in vertebrates.

Studies on tubular fusion events have been pioneered in the *Drosophila* tracheal system[3,4]. Subsequent work has uncovered a sequence of morphogenetic cell behaviours that underlie tube fusion[5]. Following cell fate determination and migration, specialized tip cells (so-called fusion cells) of adjacent tracheal branches recognize each other and form ring-shaped adherens junctions at the contact site. These junctional rings encompass an apical membrane domain and each fusion cell therefore possesses an apical pole on either end. The apical domains are then connected by a microtubule-based cytoskeletal track, which serves as a transport route for Rab11-positive recycling endosomes. These in turn contribute to apical membrane growth and invagination. However, the precise molecular cascade that leads to the completion of this process through the connection and fusion of the two apical membrane domains to generate a continuous lumen has remained unknown.

Luschnig and colleagues shed light into this process by isolating a *Drosophila* mutant in which the very last step, the connection of the separate apical compartments generated in the fusion cells, was defective, despite all other steps involved in the formation of an interconnected tracheal network proceeding in a normal manner. This defect resulted in a failure to connect the individual tracheal metameres, causing segmental interruptions in the main tracheal tube — a phenotype that led to naming this mutant *staccato* (*stac*). It emerged that the gene defective in the *stac* mutant fly encoded a calcium-binding-motif-containing protein similar to mammalian Munc13-4, a vesicle priming factor best known for its function during the maturation and exocytosis of lysosome-related organelles (LROs), including Weibel–Palade bodies, granules in platelets and neutrophils, and lytic granules in lymphocytes. Mutations in *Munc13-4* are also associated with a genetic disorder known as familial haemophagocytic lymphohistiocytosis type 3, a hyperinflammatory syndrome resulting from a lack of lytic granule release by cytotoxic cells[6].

To address how Stac/Munc13-4 promotes the fusion and coalescence of apical membrane compartments in the developing tracheal system, the authors used a large and diverse toolbox that included fosmid-based rescue with GFP-tagged wild-type and mutant Stac, live imaging of vesicle trafficking in wild-type and

Vahap Aydogan, Heinz-Georg Belting and Markus Affolter are in the Biozentrum of the University of Basel, Klingelbergstrasse 50/70, CH-4056 Basel, Switzerland.
e-mail: markus.affolter@unibas.ch

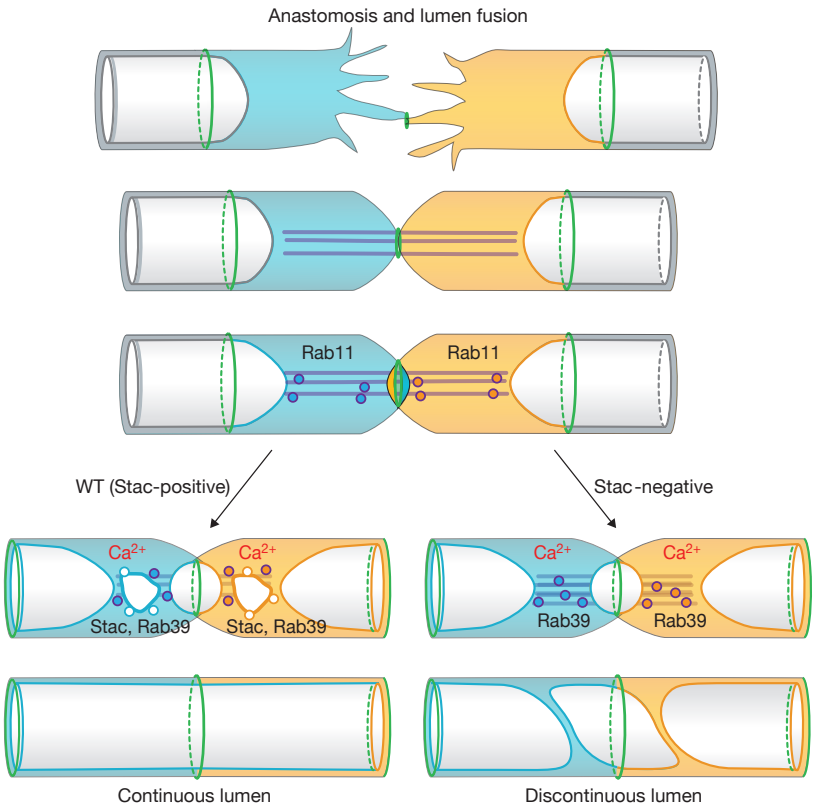

Figure 1 Lumen formation in the tracheal system of wild-type and *staccato* mutant *Drosophila* embryos. Top: Fusion cells migrate towards each other, establish contact and form adherens junctions (green) at the contact sites. Microtubules and actin bundles guide membrane trafficking, which contributes to apical membrane insertion and lumen extension at both ends of the bipolar fusion cells. Bottom: Membrane trafficking in fusion cells of the *Drosophila* tracheal system in the presence (left) and absence (right) of Stac. Stac vesicles derived from late endosomes (larger vesicles) are required to fuse the two individual apical membrane compartments in fusion cells. In the absence of Stac, the apical membrane compartments grow normally but do not connect, leading to a discontinuous lumen and a non-functional tubular network.

mutant embryos, screening of a complete library of endogenously tagged Rab proteins, and calcium measurements. They discovered that, in line with its proposed function, Stac protein localized to large vesicles that formed only in fusion cells. Stac-positive vesicles moved within the cytoskeletal track region of tip cells, which connect the growing apical membranes, and were found to accumulate at the site of lumen fusion (Fig. 1).

Given that organized vesicle trafficking is tightly linked to Rab GTPases, the Luschnig group joined forces with the group of Suzanne Eaton, who had previously established a collection of fly strains, in which 27 *Drosophila rab* genes were tagged at the endogenous locus with YFP–Myc[7]. Using this resource to compare the dynamic localization of Stac with respect to the complete set of Rab proteins revealed that Stac vesicles represent a late-endosomal compartment marked by Rab7 and Rab39. Expression of dominant-negative versions of different Rab proteins and epistasis analyses further confirmed that Stac vesicles were derived from the maturation of late endosomes into LROs, a process that requires Rab39. Labelling with lysosomal markers indicated that Stac vesicles represented a subset of Lamp1-positive lysosomes with mildly acidic content, and that these vesicles associated with the central track and moved in a dynein/dynactin-motor-dependent manner.

However, as all tracheal cells express Stac, the question remains why such large Stac vesicles, as those required for apical membrane fusion, do not form in all tracheal cells. The authors showed that the fusion-cell-specific small GTPase Arf-like 3 (Arl3)[8,9] was both necessary and sufficient for Stac vesicle formation, and acted upstream of Rab39 and Stac in tracheal tube fusion. To further unravel the molecular function of Stac and find an explanation as to why Stac vesicles promote the connection of adjacent apical compartments, the authors mined the literature based on the homology of Stac to mammalian Munc13-4. Interaction of Munc13-4 with the t-SNARE Syntaxin has been previously reported, either on the plasma membrane or on granules, thereby facilitating membrane fusion[10,11]. In line with this, Luschnig and colleagues demonstrated that Stac vesicles carry SNARE machinery components and contribute to membrane formation of the transcellular lumen. The observation that Stac contains two calcium-binding C2 domains raises the interesting question of whether calcium might be required for Stac function and where this calcium might originate. Using calcium sensors, the authors showed that subcellular calcium spikes around ER exit sites in fusion cells correlated with tracheal lumen formation, suggesting that polarization of the ER around the fusion cell apical domains leads to localized calcium release. These events create a microdomain of elevated calcium levels near the membranes, and might trigger the fusion of Stac vesicles and the two independently growing apical compartments. This last series of experiments closed the loop from the identification of Stac to local calcium spikes and membrane fusion processes that are dependent on organelles resembling secretory lysosomes.

Several intriguing questions remain. As LROs are found as single vesicles or multivesicular bodies[10], it would be interesting to follow the Stac-containing vesicles during the fusion process using time-resolved electron microscopy or correlative light electron microscopy analyses. In a recent study using transmission electron microscopy, a multimembrane compartment was visualized in tracheal terminal cells, which generated a highly ramified intracellular lumen[12]. It might be insightful to examine whether a reservoir of multimembrane vesicles also contributes to tube fusion in the *Drosophila* trachea or in other branched networks. An additional question is what we can learn about the development of other tubular organs from this work in the fly embryo. Apical membranes reportedly also have to connect in a topologically similar manner during the anastomosis of blood vessels in zebrafish embryos[13]. Whether a similar molecular mechanism is involved in the intracellular connection of luminal compartments of blood vessels can now be tested using approaches such as those presented here, namely genetic analyses combined with subcellular localization studies. In comparison with the apical membrane fusion process described in the *Drosophila* tracheal system, the apical membrane compartment of vascular endothelial cells

seems to be extremely dynamic. During sprout lumenization, the apical compartment can break and fuse repeatedly[14], and the same phenomenon has been observed during vascular pruning[15]. It will be interesting to explore whether LROs are involved in these dynamic processes.

Luschnig and colleagues demonstrate in an impressive manner that studies elucidating the formation of tubular networks in invertebrates continue to provide fruitful ground for similar work in vertebrates. The refined toolbox available to undertake such studies in *Drosophila* will continue the cross-fertilization between different model systems. Subsequent findings might in turn propose the contribution of additional or different mechanisms that ensure that tube formation is correctly executed to meet the needs of the organism.

COMPETING FINANCIAL INTERESTS
The authors declare no competing financial interests.

1. Varner, V. D. & Nelson, C. M. *Development* **141,** 2750–2759 (2014).
2. Caviglia, S., Brankatschk, M., Fischer, E. J., Eaton, S. & Luschnig, S. *Nat. Cell Biol.* **18,** 727–739 (2016).
3. Samakovlis, C. *et al. Development* **122,** 1395–1407 (1996).
4. Tanaka-Matakatsu, M., Uemura, T., Oda, H., Takeichi, M. & Hayashi, S. *Development* **122,** 3697–3705 (1996).
5. Caviglia, S. & Luschnig, S. *Semin. Cell Dev. Biol.* **31,** 82–90 (2014).
6. Feldmann, J. *et al. Cell* **115,** 461–473 (2003).
7. Dunst, S. *et al. Dev. Cell* **33,** 351–365 (2015).
8. Kakihara, K., Shinmyozu, K., Kato, K., Wada, H. & Hayashi, S. *Mech. Dev.* **125,** 325–336 (2007).
9. Jiang, L., Rogers, S. L. & Crews, S. T. *Dev. Biol.* **311,** 487–499 (2007).
10. Marks, M. S., Heijnen, H. F. G. & Raposo, G. *Curr. Opin. Cell Biol.* **25,** 495–505 (2013).
11. Ma, C., Li, W., Xu, Y. & Rizo, J. *Nat. Struct. Mol. Biol.* **18,** 542–549 (2011).
12. Nikolova, L. S. & Metzstein, M. M. *Development* **142,** 3964–3973 (2015).
13. Lenard, A. *et al. Dev. Cell* **25,** 492–506 (2013).
14. Gebala, V., Collins, R., Geudens, I., Phng, L.-K. & Gerhardt, H. *Nat. Cell Biol.* **18,** 443–450 (2016).
15. Lenard, A. *et al. PLoS Biol.* **13,** e1002126 (2015).

p21 shapes cancer evolution

Vasily S. Romanov and K. Lenhard Rudolph

Although known to induce cellular senescence, an important tumour suppressor mechanism, mutation of *CDKN1A* — the gene encoding p21 (also known as WAF1 or CIP1) — is rare in human cancers. Now, a study reports a previously unappreciated oncogenic effect of p21 overexpression that shapes cancer genome evolution through induction of replication stress.

Since its discovery more than 20 years ago, our view on p21 has changed. Rather than simply being a cell cycle inhibitor, senescence inducer and tumor suppressor, it is now appreciated as a much more complex and broader regulator of additional cellular programs such as apoptosis, DNA repair, actin cytoskeleton remodelling, and cell migration[1]. Besides the original binding partners of p21 — cyclin E/A–CDK2 complexes and the DNA polymerase δ cofactor PCNA — additional interaction partners were identified, including transcription factors (E2F1, STAT3 and c-Myc), transcription coactivators (p300 and CBP), cyclin D–CDK4/6 complexes, ASK1 and JNK stress kinases, procaspase-3, poly(ADP-ribose) polymerase 1 (PARP1) and a regulator of the actomyosin cytoskeleton, the kinase ROCK1 (Fig. 1)[2]. All these protein interactions may mediate the diverse functions of p21 in cell physiology. In addition, other as yet unknown mechanisms are likely to contribute to the regulation of cellular processes by p21.

p21-dependent suppression of cell proliferation by inhibition of cyclin–kinase complexes, PCNA, transcription factors and coactivators are regarded as mechanisms that impair the formation of tumours in response to p53 activation. However, p21 deletion does not abrogate tumour suppression mediated by p53-dependent regulation of metabolism and antioxidant function[3]. Instead, p21 contributes to leukaemia cancer growth by slowing the accumulation of DNA damage in leukaemia stem cells and thus maintaining their capacity to self-renew[4]. Moreover, p21-dependent activation of cyclin D–CDK4/6 complexes, inhibition of apoptosis and induction of cell motility contribute to p21-dependent promotion of tumorigenesis, which has been observed in several mouse models[5]. Interestingly, the tumour-suppressive activities of p21 are associated with its nuclear localization, whereas its localization in the cytoplasm associates with oncogenic effects (Fig. 1)[2]. Intriguingly, mutations or deletions of the *CDKN1A* gene are very rare in human tumours. Instead, the inactivation of p21-dependent tumour-suppressive functions and activation of its oncogenic features commonly occur by its relocation from the nucleus to the cytoplasm; overexpression or cytoplasmic localization of p21 correlates with poor prognosis in a broad range of tumours[6]. But a completely different oncogenic mechanism of nuclear p21 is now presented by Galanos *et al.*[7] in this issue of *Nature Cell Biology*. The authors demonstrate that a subset of p53-deficient cancer cells and tumours exhibit chronic overexpression of nuclear p21, which in turn leads to deregulation of replication licensing, replication stress and genomic instability.

The authors initially observed that p21 expression correlates with the proliferation marker Ki67 in a subset of atypical cancer cells and in pre-neoplastic lesions with p53 aberrations. This led them to set up two cell-culture-based systems of inducible p21 expression in a p53-negative background. Although p21 induction results in senescence of most cells, the authors noticed the emergence of p21-positive cells that escaped senescence and re-entered the cell cycle. Proteomic and gene expression analyses of p21-positive senescence 'escapers' identified transcription-independent upregulation of replication licensing factors (RLFs) — CDT1, CDC6 and ORC2. Shutting down p21 expression conversely led to a ubiquitylation-dependent decrease in Cdt1. p21, CDT1 and CDC6 share the same E3 ubiquitin ligase, CRL4–CDT2, and, based on the fact that p21 has the strongest affinity for PCNA binding among all other PCNA-interacting proteins[8], Galanos *et al.* tested the hypothesis

Vasily S. Romanov and K. Lenhard Rudolph are at the Leibniz Institute on Aging, Fritz Lipmann Institute (FLI), Beutenbergstr. 11, 07745 Jena, Germany.
e-mail: Lenhard.Rudolph@Leibniz-FLI.de

9.2 List of abbreviations

4xnr 4x non-repetitive

4xUAS 4 times non-repetitive UAS

aa amino acid

AJ adherens junction

AMIS apical membrane initiation sites

CRISPR clustered regularly interspaced short palindromic repeats

DA dorsal aorta

ddH2O double deionized water (Quarz-Water)

DLAV dorsal longitudinal anastomotic vessel

Dll4 Delta-like-4

DNA deoxyribonucleic acid

dpf days post-fertilization

e.g. example given

EC endothelial cell

ECM extracellular matrix

GEF guanine-nucleotide-exchange factor

EGFP enhanced green fluorescent protein

hpf hours post-fertilization

HyD hybrid detector

Hz hertz

ISV intersegmental vessel

kb kilobase

Kdrl Kinase insert domain receptor-like

MDCK Madin-Darby canine kidney (cells)

min minute

mRNA messenger RNA

NA Numerical aperture

o/n overnight

OD 0.6/0.8 Optical density at 600/800nm wavelength

PCR Polymerase Chain Reaction

PCV posterior cardinal vein

PFA paraformaldehyde

PTU 1-Phenyl-2-thiourea

RNA Ribonucleic acid

rpm rounds per minute

RT room temperature

SA segmental artery

sec second

SIV subintestinal vessels

SV segmental vein

SV40 Simian virus 40

sVEGFR1 soluble Vascular endothelial growth factor receptor 1

Temp. temperature

TJ tight junction

UAS upstream activation sequence

UCHD Utrophin calponin homology domain

VE-cad Vascular endothelial cadherin (Cdh5)

VEGFA Vascular endothelial growth factor A

VEGFR Vascular endothelial growth factor receptor tyrosine kinase

wt wild-type

Zo-1 Zonula occludens 1

9.3 Movie Legends

Movie caption S1a and S1b

Time-lapse movie showing the lumen invagination process from the SA to DLAV of a 30-50 hpf Tg(*fliep*:GFF)^{ubs3},(UAS:RFP), (UAS:EGFP-ZO-1)^{ubs5} transgenic embryos, imaged at 30 seconds intervals by spinning disk confocal microscopy. The cell is undergoing apical membrane invagination; lumen invaginates from one cell to the neighboring cell and junctional ring form at the interface, followed by the invagination of the lumen into the neighboring cell.

(S1a movie= EGFP-ZO1 + RFP; S1b movie= EGFP-ZO1, gray).

Movie caption S2

Time-lapse movie showing the lumen invagination process from the SA of a 30-50 hpf Tg(*fliep*:GFF)^{ubs3}, (UAS:mRFP), (UAS:VE-cadherinΔC-EGFP)^{ubs12}, imaged at 8 minutes intervals by confocal microscopy. The cell is undergoing lumen invagination; lumen invaginates in a single cell from down to up. Later, upper lumen starts invaginating towards down from neighboring cell. Because of the blood flow pressure, lumen invagination from down to up is faster. Eventually, lumen is opening in whole vessel.

Movie caption S3

Time-lapse movie showing the lumen invagination process from the SA of a 30-50 hpf Tg(BAC:*kdrl*:CAAX-mCherry) transgenic embryos, imaged at 30 seconds intervals by spinning disk confocal microscopy. Vesicle-like structures appear and come close to invaginating lumen. The invaginating

lumen is broken into two pieces because of the blood flow fluctuations. Lumen, which disintegrated from the down part of lumen collapses and eventually the lumen from down, starts invaginating again.

Movie caption S4a and S4b

Time-lapse movie showing the lumen invagination process from the SA of a 30-50 hpf Tg(BAC:*kdrl*:CAAX-mCherry) and Tg(*kdrl:H2B-GFP*)^{mu122} transgenic embryos, imaged at 30 seconds intervals by spinning disk confocal microscopy. Vesicle-like structures appear and move in the cytoplasm and eventually some dissolve on the invaginating lumen on the lateral and front part of the apical membrane.
(S4a movie= CAAX-mCherry + H2B-GFP; S4b= CAAX-mCherry, gray).

Movie caption S5

Time-lapse movie showing the lumen invagination process from DLAV of a 30-50 hpf Tg(*fli1ep*:EGFP:*rab*5c) injected construct in Tg(BAC:*kdrl*:CAAX-mCherry) transgenic embryos, transient expression imaged at 10 seconds intervals by spinning disk confocal microscopy. The lumen invaginates and Rab5c-early endosome vesicles are confined at the tip of the lumen.

Movie caption S6

Time-lapse movie showing the lumen invagination process from SA of a 30-50 hpf Tg(*fli1ep*:EGFP:*rab*7) injected construct in Tg(BAC:*kdrl*:CAAX-mCherry) transgenic embryos, transient expression imaged at 10 seconds intervals by spinning disk confocal microscopy. The lumen invaginates and

Rab7-late endosome vesicles are co-localized with vesicle-like structures, originated from CAAX-mCherry.

Movie caption S7

Time-lapse movie showing the lumen invagination process from DLAV of a 30-50 hpf Tg(*fli1ep*:GAL4FF)UBS3; (UAS:mRFP); Tg(UAS:EGFP-UCHD)UBS18 transgenic embryos, transient expression imaged at 10 seconds intervals by spinning disk confocal microscopy. The lumen invaginates and Rab11a-late endosome vesicles are localized randomly within the cell, mostly close to invaginating lumen.

Movie caption S8a and S8b

Time-lapse movie showing the lumen invagination process from SA of a 30-50 hpf Tg(*fli1ep*:EGFP:EB3) and Tg(BAC:*kdrl*:CAAX-mCherry) transgenic embryos, imaged at 30 seconds intervals. Microtubules are positioned in between the growing lumens. The lumen is collapsed at the upper part and generates many vesicle-like structures, which seems to move along the microtubules. When lumen invagination continuous towards DLAV, microtubules move to the side.

(Movie S8b is the continuation of movie S8a with the same markers).

Movie caption S9

Time-lapse movie showing the lumen invagination process from SA of a 30-50 hpf Tg(*fli1ep*:GAL4FF)^{UBS3}; (UAS:mRFP); Tg(UAS:EGFP-UCHD)^{UBS18} transgenic embryos, imaged at 30 seconds intervals by spinning disk confocal microscopy. Because of blood pressure fluctuation, the lumen structure is not smooth on the edge and form blebs from apical to cytoplasm and vice versa.

Movie caption S10

Time-lapse movie showing the lumen invagination process from SA of a 30-50 hpf (*kdrl*:GolT-mCerry) and nucleus (*kdrl*:nls-GFP) transgenic embryos, imaged at 30 seconds intervals by spinning disk confocal microscopy. During the lumen invagination from SA to DLAV, Golgi apparatus is positioned at the tip of the invaginating lumen. Eventually, apical membrane invagination pushes the nucleus on the side and Golgi stays at the behind of nucleus.

10 Bibliography

Adams, R. H. and Alitalo, K. (2007). Molecular regulation of angiogenesis and lymphangiogenesis. *Nat Rev Mol Cell Biol* **8**, 464–478.

Aird, W. C. (2011). Discovery of the cardiovascular system: from Galen to William Harvey. *Journal of Thrombosis and Haemostasis* **9**, 118–129.

Akitake, C. M., Macurak, M., Halpern, M. E. and Goll, M. G. (2011). Transgenerational analysis of transcriptional silencing in zebrafish. *Developmental Biology* **352**, 191–201.

Alon, T., Hemo, I., Itin, A., Pe'er, J., Stone, J. and Keshet, E. (1995). Vascular endothelial growth factor acts as a survival factor for newly formed retinal vessels and has implications for retinopathy of prematurity. *Nat Med* **1**, 1024–1028.

Apodaca, G., Gallo, L. I. and Bryant, D. M. (2012). Role of membrane traffic in the generation of epithelial cell asymmetry. *Nat Cell Biol* **14**, 1235–1243.

Arima, S., Nishiyama, K., Ko, T., Arima, Y., Hakozaki, Y., Sugihara, K., Koseki, H., Uchijima, Y., Kurihara, Y. and Kurihara, H. (2011). Angiogenic morphogenesis driven by dynamic and heterogeneous collective endothelial cell movement. *Development* **138**, 4763–4776.

Asakawa, K. and Kawakami, K. (2010). A transgenic zebrafish for monitoring in vivo microtubule structures. *Dev. Dyn.* **239**, 2695–2699.

Asakawa, K., Suster, M. L., Mizusawa, K., Nagayoshi, S., Kotani, T., Urasaki, A., Kishimoto, Y., Hibi, M. and Kawakami, K. (2008). Genetic dissection of neural circuits by Tol2 transposon-mediated Gal4 gene and enhancer trapping in zebrafish. *Proc. Natl. Acad. Sci. U.S.A.* **105**, 1255–1260.

Aydogan, V., Belting, H.-G. and Affolter, M. (2016). Mapping the molecular steps of secretory-lysosome-driven tracheal tube fusion. *Nature Publishing Group* **18**, 720–722.

Aydogan, V., Lenard, A., Denes, A. S., Sauteur, L., Belting, H.-G. and

Affolter, M. (2015). Endothelial cell division in angiogenic sprouts of differing cellular architecture. *Biol Open* **4**, 1259–1269.

Bagnat, M., Cheung, I. D., Mostov, K. E. and Stainier, D. Y. R. (2007). Genetic control of single lumen formation in the zebrafish gut. *Nat Cell Biol* **9**, 954–960.

Betz, C., Lenard, A., Belting, H.-G. and Affolter, M. (2016). Cell behaviors and dynamics during angiogenesis. *Development* **143**, 2249–2260.

Bieli, D., Alborelli, I., Harmansa, S., Matsuda, S., Caussinus, E. and Affolter, M. (2016). Development and Application of Functionalized Protein Binders in Multicellular Organisms. *Int Rev Cell Mol Biol* **325**, 181–213.

Blasky, A. J., Mangan, A. and Prekeris, R. (2015). Polarized Protein Transport and Lumen Formation During Epithelial Tissue Morphogenesis. *Annu. Rev. Cell Dev. Biol.* **31**, 575–591.

Blum, Y., Belting, H.-G., Ellertsdottir, E., Herwig, L., Lüders, F. and Affolter, M. (2008a). Complex cell rearrangements during intersegmental vessel sprouting and vessel fusion in the zebrafish embryo. *Developmental Biology* **316**, 312–322.

Blum, Y., Belting, H.-G., Ellertsdottir, E., Herwig, L., Lüders, F. and Affolter, M. (2008b). Complex cell rearrangements during intersegmental vessel sprouting and vessel fusion in the zebrafish embryo. *Developmental Biology* **316**, 312–322.

Bourdages, K. G. and Maddox, A. S. (2013). Dividing in Epithelia: Cells Let Loose during Cytokinesis. *Dev. Cell* **24**, 336–338.

Brauchle, M., Hansen, S., Caussinus, E., Lenard, A., Ochoa-Espinosa, A., Scholz, O., Sprecher, S. G., Plückthun, A. and Affolter, M. (2014). Protein interference applications in cellular and developmental biology using DARPins that recognize GFP and mCherry. *Biol Open* **3**, 1252–1261.

Bryant, D. M. and Mostov, K. E. (2008). From cells to organs: building polarized tissue. *Nat Rev Mol Cell Biol* **9**, 887–901.

Bryant, D. M., Datta, A., Rodríguez-Fraticelli, A. E., Peränen, J., Martin-Belmonte, F. and Mostov, K. E. (2010). A molecular network for de novo generation of the apical surface and lumen. *Nature Publishing Group* **12**, 1035–1045.

Bucci, C., Frunzio, R., Chiariotti, L., Brown, A. L., Rechler, M. M. and Bruni, C. B. (1988). A new member of the ras gene superfamily identified in a rat liver cell line. *Nucleic Acids Res.* **16**, 9979–9993.

Buckley, C. E., Ren, X., Ward, L. C., Girdler, G. C., Araya, C., Green, M. J., Clark, B. S., Link, B. A. and Clarke, J. D. W. (2012). Mirror-symmetric microtubule assembly and cell interactions drive lumen formation in the zebrafish neural rod. *The EMBO Journal* **32**, 30–44.

Cadart, C., Zlotek-Zlotkiewicz, E., Le Berre, M., Piel, M. and Matthews, H. K. (2014). Exploring the Function of Cell Shape and Size during Mitosis. *Dev. Cell* **29**, 159–169.

Carmeliet, P. (2005). Angiogenesis in life, disease and medicine. *Nature* **438**, 932–936.

Caviglia, S. and Luschnig, S. (2014). Tube fusion: Making connections in branched tubular networks. *Seminars in Cell & Developmental Biology* **31**, 82–90.

Caviglia, S., Brankatschk, M., Fischer, E. J., Eaton, S. and Luschnig, S. (2016). Staccato/Unc-13-4 controls secretory lysosome-mediated lumen fusion during epithelial tube anastomosis. *Nature Publishing Group* **18**, 727–739.

Chavrier, P., Parton, R. G., Hauri, H. P., Simons, K. and Zerial, M. (1990). Localization of low molecular weight GTP binding proteins to exocytic and endocytic compartments. *Cell* **62**, 317–329.

Childs, S., Chen, J.-N., Garrity, D. M. and Fishman, M. C. (2002). Patterning of angiogenesis in the zebrafish embryo.

Clark, B. S., Winter, M., Cohen, A. R. and Link, B. A. (2011). Generation of Rab-based transgenic lines for in vivo studies of endosome biology in zebrafish. *Dev. Dyn.* **240**, 2452–2465.

Cong, L., Ran, F. A., Cox, D., Lin, S., Barretto, R., Habib, N., Hsu, P.

D., Wu, X., Jiang, W., Marraffini, L. A., et al. (2013). Multiplex genome engineering using CRISPR/Cas systems. *Science* **339**, 819–823.

Davis, G. E. and Camarillo, C. W. (1996). An alpha 2 beta 1 integrin-dependent pinocytic mechanism involving intracellular vacuole formation and coalescence regulates capillary lumen and tube formation in three-dimensional collagen matrix. *Exp Cell Res* **224**, 39–51.

Dejana, E. (2004). Endothelial cell-cell junctions: happy together. *Nat Rev Mol Cell Biol* **5**, 261–270.

Dejana, E., Corada, M. and Lampugnani, M. G. (1995). Endothelial cell-to-cell junctions. *FASEB J.* **9**, 910–918.

Denes, A. S., Kanca, O. and Affolter, M. (2015). A cellular process that includes asymmetric cytokinesis remodels the dorsal tracheal branches in Drosophila larvae. *Development* **142**, 1794–1805.

Dunst, S., Kazimiers, T., Zadow, von, F., Jambor, H., Sagner, A., Brankatschk, B., Mahmoud, A., Spannl, S., Tomancak, P., Eaton, S., et al. (2015). Endogenously tagged Rab proteins: a resource to study membrane trafficking in Drosophila. *Dev. Cell* **33**, 351–365.

Ellertsdottir, E., Lenard, A., Blum, Y., Krudewig, A., Herwig, L., Affolter, M. and Belting, H.-G. (2010). Vascular morphogenesis in the zebrafish embryo. *Developmental Biology* **341**, 56–65.

Ellis, K., Bagwell, J. and Bagnat, M. (2013). Notochord vacuoles are lysosome-related organelles that function in axis and spine morphogenesis. *The Journal of Cell Biology* **200**, 667–679.

Fededa, J. P. and Gerlich, D. W. (2012). Molecular control of animal cell cytokinesis. *Nature Publishing Group* **14**, 440–447.

Feng, Y., Press, B. and Wandinger-Ness, A. (1995). Rab 7: an important regulator of late endocytic membrane traffic. *J Cell Biol* **131**, 1435–1452.

Founounou, N., Loyer, N. and Le Borgne, R. (2013). Septins Regulate the Contractility of the Actomyosin Ring to Enable Adherens Junction Remodeling during Cytokinesis of Epithelial Cells. *Dev. Cell* **24**, 242–255.

Gebala, V., Collins, R., Geudens, I., Phng, L.-K. and Gerhardt, H. (2016). Blood flow drives lumen formation by inverse membrane blebbing during angiogenesis in vivo. *Nature Publishing Group* **18**, 443–450.

Gerhard, G. S., Kauffman, E. J., Wang, X., Stewart, R., Moore, J. L., Kasales, C. J., Demidenko, E. and Cheng, K. C. (2002). Life spans and senescent phenotypes in two strains of Zebrafish (Danio rerio). *Exp. Gerontol.* **37**, 1055–1068.

Gerhardt, H. (2003). VEGF guides angiogenic sprouting utilizing endothelial tip cell filopodia. *The Journal of Cell Biology* **161**, 1163–1177.

Gervais, L. and Casanova, J. (2010). In vivo coupling of cell elongation and lumen formation in a single cell. *Curr. Biol.* **20**, 359–366.

Green, R. A., Paluch, E. and Oegema, K. (2012). Cytokinesis in Animal Cells. *Annu. Rev. Cell Dev. Biol.* **28**, 29–58.

Guillot, C. and Lecuit, T. (2013). Adhesion Disengagement Uncouples Intrinsic and Extrinsic Forces to Drive Cytokinesis in Epithelial Tissues. *Dev. Cell* **24**, 227–241.

Harris, T. J. C. and Tepass, U. (2010). Adherens junctions: from molecules to morphogenesis. 1–13.

Hellström, M., Phng, L.-K., Hofmann, J. J., Wallgard, E., Coultas, L., Lindblom, P., Alva, J., Nilsson, A.-K., Karlsson, L., Gaiano, N., et al. (2007). Dll4 signalling through Notch1 regulates formation of tip cells during angiogenesis. *Nature* **445**, 776–780.

Herbert, S. P. and Stainier, D. Y. R. (2011). Molecular control of endothelial cell behaviour during blood vessel morphogenesis. *Nat Rev Mol Cell Biol* **12**, 551–564.

Herbert, S. P., Huisken, J., Kim, T. N., Feldman, M. E., Houseman, B. T., Wang, R. A., Shokat, K. M. and Stainier, D. Y. R. (2009). Arterial-venous segregation by selective cell sprouting: an alternative mode of blood vessel formation. *Science* **326**, 294–298.

Herszterg, S., Leibfried, A., Bosveld, F., Martin, C. and Bellaiche, Y.

(2013). Interplay between the dividing cell and its neighbors regulates adherens junction formation during cytokinesis in epithelial tissue. *Dev. Cell* **24**, 256–270.

Herszterg, S., Pinheiro, D. and Bellaiche, Y. (2014). A multicellular view of cytokinesis in epithelial tissue. *Trends in Cell Biology* **24**, 285–293.

Herwig, L., Blum, Y., Krudewig, A., Ellertsdottir, E., Lenard, A., Belting, H.-G. and Affolter, M. (2011). Distinct cellular mechanisms of blood vessel fusion in the zebrafish embryo. *Current Biology* **21**, 1942–1948.

Howe, K., Clark, M. D., Torroja, C. F., Torrance, J., Berthelot, C., Muffato, M., Collins, J. E., Humphray, S., McLaren, K., Matthews, L., et al. (2013). The zebrafish reference genome sequence and its relationship to the human genome. *Nature* **496**, 498–503.

Hwang, W. Y., Fu, Y., Reyon, D., Maeder, M. L., Tsai, S. Q., Sander, J. D., Peterson, R. T., Yeh, J.-R. J. and Joung, J. K. (2013). Efficient genome editing in zebrafish using a CRISPR-Cas system. *Nat. Biotechnol.* **31**, 227–229.

Isogai, S., Horiguchi, M. and Weinstein, B. M. (2001). The Vascular Anatomy of the Developing Zebrafish: An Atlas of Embryonic and Early Larval Development. *Developmental Biology* **230**, 278–301.

Jakobsson, L., Franco, C. A., Bentley, K., Collins, R. T., Ponsioen, B., Aspalter, I. M., Rosewell, I., Busse, M., Thurston, G., Medvinsky, A., et al. (2010). Endothelial cells dynamically compete for the tip cell position during angiogenic sprouting. *Nat Cell Biol* **12**, 943–953.

Jin, S.-W., Beis, D., Mitchell, T., Chen, J.-N. and Stainier, D. Y. R. (2005). Cellular and molecular analyses of vascular tube and lumen formation in zebrafish. *Development* **132**, 5199–5209.

Kamei, M., Saunders, W. B., Bayless, K. J., Dye, L., Davis, G. E. and Weinstein, B. M. (2006). Endothelial tubes assemble from intracellular vacuoles in vivo. *Nature* **442**, 453–456.

Kawakami, K., Shima, A. and Kawakami, N. (2000). Identification of a functional transposase of the Tol2 element, an Ac-like element from the Japanese medaka fish, and its transposition in the zebrafish germ lineage.

Proc. Natl. Acad. Sci. U.S.A. **97**, 11403–11408.

Kimmel, C. B., Ballard, W. W., Kimmel, S. R., Ullmann, B. and Schilling, T. F. (2005). Stages of embryonic development of the zebrafish. *Dev. Dyn.* **203**, 253–310.

Kondo, T. and Hayashi, S. (2013). Mitotic cell rounding accelerates epithelial invagination. *Nature* **494**, 125–129.

Kunda, P., Pelling, A. E., Liu, T. and Baum, B. (2008). Moesin Controls Cortical Rigidity, Cell Rounding, and Spindle Morphogenesis during Mitosis. *Current Biology* **18**, 91–101.

Kwan, K. M., Fujimoto, E., GRabher, C., Mangum, B. D., Hardy, M. E., Campbell, D. S., Parant, J. M., Yost, H. J., Kanki, J. P. and Chien, C.-B. (2007). The Tol2kit: a multisite gateway-based construction kit for Tol2 transposon transgenesis constructs. *Dev. Dyn.* **236**, 3088–3099.

Kwon, H.-B., Wang, S., Helker, C. S. M., Rasouli, S. J., Maischein, H.-M., Offermanns, S., Herzog, W. and Stainier, D. Y. R. (2016). In vivo modulation of endothelial polarization by Apelin receptor signalling. *Nat Comms* **7**, 11805.

Lancaster, O. M., Le Berre, M., Dimitracopoulos, A., Bonazzi, D., Zlotek-Zlotkiewicz, E., Picone, R., Duke, T., Piel, M. and Baum, B. (2013). Mitotic Rounding Alters Cell Geometry to Ensure Efficient Bipolar Spindle Formation. *Dev. Cell* **25**, 270–283.

Lawson, N. D. and Weinstein, B. M. (2002a). In Vivo Imaging of Embryonic Vascular Development Using Transgenic Zebrafish. *Developmental Biology* **248**, 307–318.

Lawson, N. D. and Weinstein, B. M. (2002b). Arteries and veins: making a difference with zebrafish. *Nat. Rev. Genet.* **3**, 674–682.

Lawson, N. D., Vogel, A. M. and Weinstein, B. M. (2002). sonic hedgehog and vascular endothelial growth factor act upstream of the Notch pathway during arterial endothelial fluctuation. *Dev. Cell* **3**, 127–136.

Lee, S. and Kolodziej, P. A. (2002). The plakin Short Stop and the RhoA GTPase are required for E-cadherin-dependent apical surface remodeling during tracheal tube fusion. *Development* **129**, 1509–1520.

Lenard, A., Ellertsdottir, E., Herwig, L., Krudewig, A., Sauteur, L., Belting, H.-G. and Affolter, M. (2013). In vivo analysis reveals a highly stereotypic morphogenetic pathway of vascular anastomosis. *Dev. Cell* **25**, 492–506.

Levayer, R. and Lecuit, T. (2012). Biomechanical regulation of contractility: spatial control and dynamics. *Trends in Cell Biology* **22**, 61–81.

Lu, L. and Hong, W. (2014). From endosomes to the trans-Golgi network. *Seminars in Cell & Developmental Biology* **31**, 30–39.

Martin-Belmonte, F. and Mostov, K. (2008). Regulation of cell polarity during epithelial morphogenesis. *Current Opinion in Cell Biology* **20**, 227–234.

Meder, D., Shevchenko, A., Simons, K. and Füllekrug, J. (2005). Gp135/podocalyxin and NHERF-2 participate in the formation of a preapical domain during polarization of MDCK cells. *J Cell Biol* **168**, 303–313.

Meeker, N. D., Hutchinson, S. A., Ho, L. and Trede, N. S. (2007). Method for isolation of PCR-ready genomic DNA from zebrafish tissues. *BioTechniques* **43**, 610–612– 614.

Monahan-Earley, R., Dvorak, A. M. and Aird, W. C. (2013). Evolutionary origins of the blood vascular system and endothelium. *J. Thromb. Haemost.* **11 Suppl 1**, 46–66.

Muñoz-Chápuli, R., Carmona, R., Guadix, J. A., Macías, D. and Pérez-Pomares, J. M. (2005). The origin of the endothelial cells: an evo-devo approach for the invertebrate/vertebrate transition of the circulatory system. *Evol. Dev.* **7**, 351–358.

Nakajima, Y.-I., Meyer, E. J., Kroesen, A., McKinney, S. A. and Gibson, M. C. (2013). Epithelial junctions maintain tissue architecture by directing planar spindle orientation. *Nature* **500**, 359–362.

Nowak, M., Machate, A., Yu, S. R., Gupta, M. and Brand, M. (2011). Interpretation of the FGF8 morphogen gradient is regulated by endocytic trafficking. *Nature Publishing Group* **13**, 153–158.

O'Brien, L. E., Jou, T. S., Pollack, A. L., Zhang, Q., Hansen, S. H., Yurchenco, P. and Mostov, K. E. (2001). Rac1 orientates epithelial apical polarity through effects on basolateral laminin assembly. *Nat Cell Biol* **3**, 831–838.

Parker, L. H., Schmidt, M., Jin, S.-W., Gray, A. M., Beis, D., Pham, T., Frantz, G., Palmieri, S., Hillan, K., Stainier, D. Y. R., et al. (2004). The endothelial-cell-derived secreted factor Egfl7 regulates vascular tube formation. *Nature* **428**, 754–758.

Parng, C., Seng, W. L., Semino, C. and McGrath, P. (2002). Zebrafish: a preclinical model for drug screening. *Assay Drug Dev Technol* **1**, 41–48.

Petersen, L. K. and Stowers, R. S. (2011). A Gateway MultiSite recombination cloning toolkit. *PLoS ONE* **6**, e24531.

Poole, T. J. and Coffin, J. D. (1989). Vasculogenesis and angiogenesis: two distinct morphogenetic mechanisms establish embryonic vascular pattern. *J. Exp. Zool.* **251**, 224–231.

Potente, M., Gerhardt, H. and Carmeliet, P. (2011). Basic and therapeutic aspects of angiogenesis. *Cell* **146**, 873–887.

Risau, W. and Flamme, I. (1995). Vasculogenesis. *Annu. Rev. Cell Dev. Biol.* **11**, 73–91.

Rosenblatt, J., Cramer, L. P., Baum, B. and McGee, K. M. (2004). Myosin II-dependent cortical movement is required for centrosome separation and positioning during mitotic spindle assembly. *Cell* **117**, 361–372.

Sambrook, J. and Russell, D. W. (2006a). Purification of expressed proteins from inclusion bodies. *CSH Protoc* **2006**.

Sambrook, J. and Russell, D. W. (2006b). Plating bacteriophage m13. *CSH Protoc* **2006**.

Sambrook, J. and Russell, D. W. (2006c). Growing bacteriophage m13 in liquid culture. *CSH Protoc* **2006**.

Sauteur, Loïc Aurélien (2015). In vivo analysis of junctional dynamics underlying angiogenic cell behaviors. PhD Thesis.

Sauteur, L., Krudewig, A., Herwig, L., Ehrenfeuchter, N., Lenard, A., Affolter, M. and Belting, H.-G. (2014). Cdh5/VE-cadherin Promotes Endothelial Cell Interface Elongation via Cortical Actin Polymerization during Angiogenic Sprouting. *CellReports* **9**, 504–513.

Shigei, T., Tsuru, H., Ishikawa, N. and Yoshioka, K. (2001). Absence of endothelium in invertebrate blood vessels: significance of endothelium and sympathetic nerve/medial smooth muscle in the vertebrate vascular system. *Jpn. J. Pharmacol.* **87**, 253–260.

Siekmann, A. F. and Lawson, N. D. (2007a). Notch signalling limits angiogenic cell behaviour in developing zebrafish arteries. *Nature* **445**, 781–784.

Siekmann, A. F. and Lawson, N. D. (2007b). Notch signalling limits angiogenic cell behaviour in developing zebrafish arteries. *Nature* **445**, 781–784.

Siekmann, A. F., Affolter, M. and Belting, H.-G. (2013). The tip cell concept 10 years after: New players tune in for a common theme. *Exp Cell Res* **319**, 1255–1263.

Sigurbjörnsdóttir, S., Mathew, R. and Leptin, M. (2014). Molecular mechanisms of de novo lumen formation. *Nat Rev Mol Cell Biol* **15**, 665–676.

Stenmark, H. (2009). Rab GTPases as coordinators of vesicle traffic. *Nat Rev Mol Cell Biol* **10**, 513–525.

Strilić, B., Kucera, T., Eglinger, J., Hughes, M. R., McNagny, K. M., Tsukita, S., Dejana, E., Ferrara, N. and Lammert, E. (2009). The molecular basis of vascular lumen formation in the developing mouse aorta. *Dev. Cell* **17**, 505–515.

Tay, H. G., Ng, Y. W. and Manser, E. (2010). A vertebrate-specific Chp-PAK-PIX pathway maintains E-cadherin at adherens junctions during zebrafish epiboly. *PLoS ONE* **5**, e10125.

Thisse, B., Heyer, V., Lux, A., Alunni, V., Degrave, A., Seiliez, I., Kirchner, J., Parkhill, J.-P. and Thisse, C. (2004). Spatial and temporal expression of the zebrafish genome by large-scale in situ

hybridization screening. *Methods Cell Biol.* **77**, 505–519.

Torres-Vázquez, J., Kamei, M. and Weinstein, B. M. (2003). Molecular distinction between arteries and veins. *Cell and Tissue Research* **314**, 43–59.

Tsarouhas, V., Senti, K.-A., Jayaram, S. A., Tiklová, K., Hemphälä, J., Adler, J. and Samakovlis, C. (2007). Sequential pulses of apical epithelial secretion and endocytosis drive airway maturation in Drosophila. *Dev. Cell* **13**, 214–225.

Ullrich, O., Reinsch, S., Urbé, S., Zerial, M. and Parton, R. G. (1996). Rab11 regulates recycling through the pericentriolar recycling endosome. *J Cell Biol* **135**, 913–924.

Ulrich, F., Krieg, M., Schötz, E.-M., Link, V., Castanon, I., Schnabel, V., Taubenberger, A., Mueller, D., Puech, P.-H. and Heisenberg, C.-P. (2005). Wnt11 functions in gastrulation by controlling cell cohesion through Rab5c and E-cadherin. *Dev. Cell* **9**, 555–564.

Wang, H., Yang, H., Shivalila, C. S., Dawlaty, M. M., Cheng, A. W., Zhang, F. and Jaenisch, R. (2013). One-step generation of mice carrying mutations in multiple genes by CRISPR/Cas-mediated genome engineering. *Cell* **153**, 910–918.

Wener Risau (1997). Mechanisms of angiogenesis. Nature 386/ 17 April

Westerfield, M. (2007). *The Zebrafish Book*.

Wright, L. P. and Philips, M. R. (2006). Thematic review series: lipid posttranslational modifications. CAAX modification and membrane targeting of Ras. *J. Lipid Res.* **47**, 883–891.

Xu, K. and Cleaver, O. (2011). Tubulogenesis during blood vessel formation. *Seminars in Cell & Developmental Biology* **22**, 993–1004.

Yu, J. A., Castranova, D., Pham, V. N. and Weinstein, B. M. (2015). Single-cell analysis of endothelial morphogenesis in vivo. *Development* **142**, 2951–2961.

Yu, W., Shewan, A. M., Brakeman, P., Eastburn, D. J., Datta, A., Bryant, D. M., Fan, Q.-W., Weiss, W. A., Zegers, M. M. P. and

Mostov, K. E. (2008). Involvement of RhoA, ROCK I and myosin II in inverted orientation of epithelial polarity. *EMBO Rep.* **9**, 923–929.

Zeng, G., Taylor, S. M., McColm, J. R., Kappas, N. C., Kearney, J. B., Williams, L. H., Hartnett, M. E. and Bautch, V. L. (2007). Orientation of endothelial cell division is regulated by VEGF signaling during blood vessel formation. *Blood* **109**, 1345–1352.

Zhang, J., Schulze, K. L., Hiesinger, P. R., Suyama, K., Wang, S., Fish, M., Acar, M., Hoskins, R. A., Bellen, H. J. and Scott, M. P. (2007). Thirty-one flavors of Drosophila Rab proteins. *Genetics* **176**, 1307–1322.

Zhang, M., Chen, L., Wang, S. and Wang, T. (2009). Rab7: roles in membrane trafficking and disease. *Biosci. Rep.* **29**, 193–209.